UNDERSTANDING THE QUASI-STATIC THERMO-ELECTRO-MECHANICAL RESPONSE OF PIEZOELECTRIC MATERIALS

BY

JEFFREY MARK GANLEY

B.S., Civil Engineering, University of Minnesota, 1994

M.S., Civil Engineering, University of New Mexico, 1998

DISSERTATION

Submitted in Partial Fulfillment of the
Requirements for the Degree of

**Doctor of Philosophy
Engineering**

The University of New Mexico
Albuquerque, New Mexico

May, 2007

UMI Number: 3268852

INFORMATION TO USERS

The quality of this reproduction is dependent upon the quality of the copy submitted. Broken or indistinct print, colored or poor quality illustrations and photographs, print bleed-through, substandard margins, and improper alignment can adversely affect reproduction.

In the unlikely event that the author did not send a complete manuscript and there are missing pages, these will be noted. Also, if unauthorized copyright material had to be removed, a note will indicate the deletion.

UMI®

UMI Microform 3268852
Copyright 2007 by ProQuest Information and Learning Company.
All rights reserved. This microform edition is protected against unauthorized copying under Title 17, United States Code.

ProQuest Information and Learning Company
300 North Zeeb Road
P.O. Box 1346
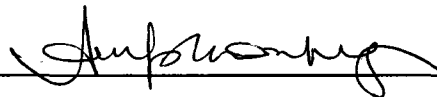Ann Arbor, MI 48106-1346

Jeffrey Mark Ganley
Candidate

Civil Engineering
Department

This dissertation is approved, and it is acceptable in quality
and form for publication on microfilm:

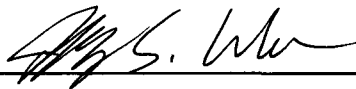*Approved by the Dissertation Committee:*

Dr. Arup K. Maji _____ , Chairperson _____

Dr. Benjamin K. Henderson _____

Dr. Jeffry S. Welsh _____

Dr. Balu Santhanam _____

_____

_____

_____

Accepted: _____
Dean, Graduate School

_____ APR 2 4 2007 _____
Date

DEDICATION

To my amazing wife, Sally, for her love and unwavering support through this long and

sometimes trying process.

iii

ACKNOWLEDGEMENTS

Jeff Ganley

The University of New Mexico

May, 2007

UNDERSTANDING THE QUASI-STATIC THERMO-ELECTRO-MECHANICAL RESPONSE OF PIEZOELECTRIC MATERIALS

BY

JEFFREY MARK GANLEY

ABSTRACT OF DISSERTATION

Submitted in Partial Fulfillment of the
Requirements for the Degree of

**Doctor of Philosophy
Engineering**

The University of New Mexico
Albuquerque, New Mexico

May, 2007

UNDERSTANDING THE QUASI-STATIC THERMO-ELECTRO-MECHANICAL RESPONSE OF PIEZOELECTRIC MATERIALS

By:

Jeffrey Mark Ganley

B.S., Civil Engineering, University of Minnesota, 1994
M.S., Civil Engineering, University of New Mexico, 1998
Ph.D., Engineering, University of New Mexico, 2007

ABSTRACT

Piezoelectricity describes the behavior of a class of materials which exhibit a relationship between mechanical strain and electrical field. Piezoelectric materials can be crystals (e.g. quartz), ceramic (e.g. lead-zirconate-titanate – PZT – the primary focus of the present research), or polymers (e.g. polyvinylidine-fluoride - PVDF). Piezopolymers and piezoceramics offer a significant improvement in piezoelectric properties over naturally occurring piezoelectrics like quartz. In the last five years, research in piezoelectrics has begun to change focus from the more traditional sensor / actuator applications to utilizing piezoelectric materials in energy harvesting applications. The present research will explore the very low frequency response of piezoelectrics, including several energy harvesting applications, as well as the interactions between thermal, mechanical and electrical energy in a thermally driven piezoelectric energy generation system.

In Chapter 1, the history of piezoelectric research and development is given, along with an overview of piezoelectricity for those readers who are not familiar with the topic.

In Chapter 2, current investigations in piezoelectric energy harvesting research are summarized. The present research, namely understanding the quasi-static thermo-electro-mechanical response of piezoelectric materials is also summarized. In addition, two applications: thermal management in a satellite and energy harvesting from a vibrating highway bridge are detailed as motivators for the present research.

Chapter 3 gives a summary of the relevant piezoelectric theory. In addition, electrical circuit theory and thermodynamic heat capacity / heat energy considerations required to complete the present research are given.

Chapter 4 provides a summary of the experimental testing completed during the course of the present research. Significant testing, including determination of the PZT/Aluminum substrate sample time constants, thermal calibration testing and quantification of the voltage resulting from the PZT/Aluminum substrate samples, is detailed and summarized.

In Chapter 5 the research analysis, including variance of the PZT element capacitance with loading condition, is presented. Novel piezoelectric theory associated with the thermally induced planar strain loading condition, along with corroborating test results, are also presented.

Chapter 6 notes the significant results, conclusions and recommendations for future research resulting from the present research, including a system level summary of the 'satellite' and 'bridge' applications.

TABLE OF CONTENTS

x

xi

LIST OF FIGURES

LIST OF TABLES

xvi

CHAPTER 1 - INTRODUCTION

Piezoelectricity describes the behavior of a class of materials which exhibit a relationship between mechanical strain and electrical field. In the last five years, research in piezoelectrics has begun to change focus from the more traditional sensor and actuator applications to utilizing piezoelectric materials as an energy source, harvesting 'waste' energy from various systems (Sodano, 2004). The present research will expand on this growing research field by exploring very low frequency thermally driven energy generation systems utilizing piezoelectric materials.

History

Piezoelectricity was first discovered in 1880 in Paris, France by the brothers Jacques and Pierre Curie. They found that, in certain materials such as quartz and topaz, applied mechanical stress produced electric surface charges. This relationship became known as the (direct) piezoelectric effect. The inverse piezoelectric effect, or mechanical strain due to applied electric field, was first proposed by Lippmann in 1881, and was quickly confirmed experimentally by the Curie brothers (Ballato, 1995).

From the time of their discovery until around 1915, piezoelectric materials were largely ignored and found use mainly as parlor tricks. During World War I, piezoelectric materials were successfully utilized to create sonar devices for the detection of submarines. The success of sonar spurred widespread piezoelectric materials research and development. Several early commercial applications included ultrasonic transducers and piezoelectric quartz crystal resonators for keeping accurate time. The crystal resonators found in almost all wristwatches today rely on the quartz piezoelectric effect

1

to keep accurate time. In the late 1960's, development of high quality, high efficiency, relatively inexpensive piezoceramics spurred another round of active piezoelectric device research and development. The advanced piezoelectric sensors and actuators which are used in piezoelectric energy harvesting research today began their development during this time. Today, piezoelectrics have widespread commercial application in various sound applications (speakers, microphones, etc.), quartz resonators for keeping accurate time, highly precise actuators (~ 1 nm) and ceramic lighters (e.g. gas grill lighters).

Piezoelectricity Overview

Piezoelectricity is formed from the words piezo and electricity. Piezo is derived from the Greek word "piezein", which means "to press tight" or "to squeeze". Electricity rather obviously describes the complimentary electrical behavior of this class of materials. Piezoelectricity thus describes the behavior of a class of materials which exhibit a relationship between mechanical strain and electrical field. As will be shown in Chapter 3, in standard piezoelectric theory (IEEE STD 176-1987) the relationship between mechanical strain and electrical field in a piezoelectric material is assumed linear. Piezoelectric materials produce a high impedance voltage when strained. The piezoelectric effect is also reversible; an applied voltage will produce a mechanical strain in a piezoelectric material.

Quartz is the most common piezoelectric material. As was stated previously, the crystal resonator found in almost all modern wristwatches relies on the resonant piezoelectric behavior of a quartz crystal to keep accurate time. However, quartz and other naturally occurring piezoelectrics have a low coupling factor (i.e. mechanical to

2

electrical conversion efficiency), and are therefore not used in advanced applications, including sensors, actuators and energy harvesting.

Piezoelectric materials can be crystals (e.g. quartz), ceramic (e.g. lead-zirconate-titanate - PZT), or polymers (e.g. polyvinylidine-fluoride - PVDF). Recent research has focused on the production of high quality, large-size single crystal piezoelectric materials, which possess an extremely high electromechanical coupling factor. Currently, single crystal piezoelectrics have been produced on the scale of approximately 1 cm. However, their lack of durability and extremely high cost make them impractical in most applications, including the current research.

Piezoelectric ceramics and polymers are made by initial forming of the material by traditional ceramic or polymer fabrication processes. In this state, the 'Weiss domain' electric dipoles in the material are randomly oriented, resulting in a net zero charge potential. As such, an additional step is required. The material is heated above its Curie point, and then cooled in the presence of a strong electric field ($\sim$ 1 kV/mm). This process, called 'poling', uniformly aligns the electric dipoles in the material with the electric field, and thus sets the macroscopic piezoelectric behavior (Sodano, 2004). Figure 1-1 shows a generalized piezoelectric poling process diagram. As a consequence of the poling process, the piezoelectric material becomes anisotropic. It should be noted that under the strict definition of piezoelectricity (i.e. single material crystal, refer to the Definitions Appendix), piezoceramics and piezopolymers are not actually piezoelectric because they are not single materials. Strictly speaking, they are electrostrictive materials. However, because they exhibit the desired macroscopic piezoelectric behavior, by convention these materials are called piezoelectric.

3
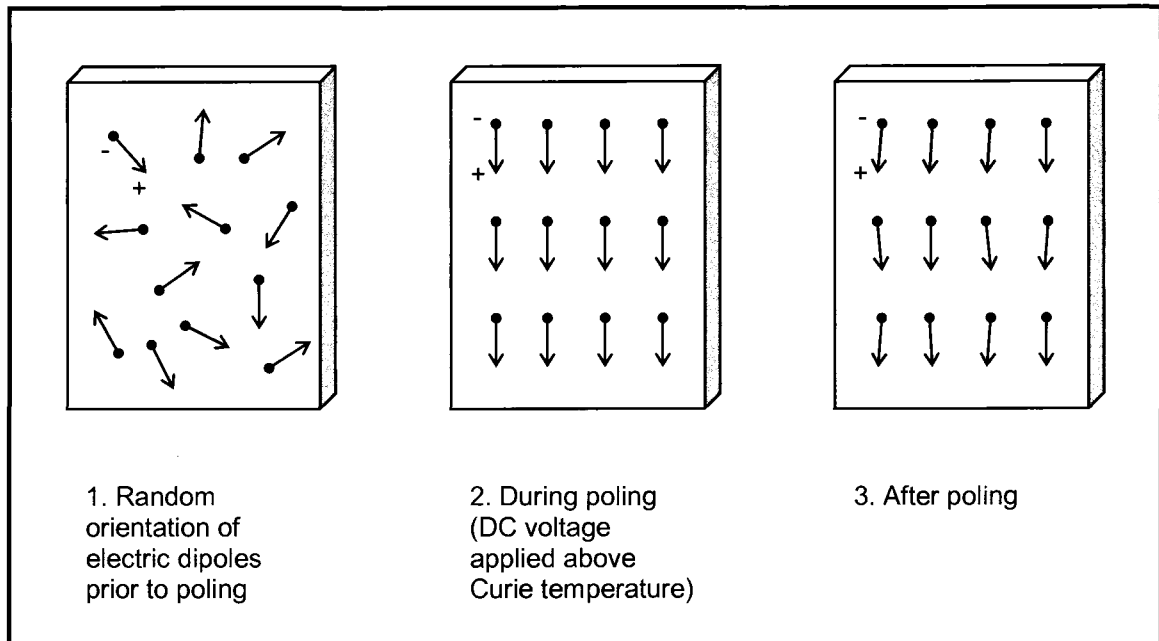
Figure 1-1 – Poling Process Diagram

To physically understand the piezoelectric effect, consider that the dipoles in

Step 3 of Figure 1-1 represent the average location of the (+) and (-) charges in the

piezoelectric material crystal structure. The value of the (+) and (-) charges in the crystal

structure are equal, but the poling process provides a preferred directionality to the

average charge locations. If the poled piezoelectric material is then stretched (or

squeezed) in the vertical direction in Figure 1-1, the (+) and (-) charges are then separated

(or brought closer together). This action represents the definition of electrostatic dipole

potential (i.e. charge separated by a distance), and results in a potential (i.e. voltage

change) between the top and bottom of the element in Step 3 of Figure 1-1.

Next consider the inverse piezoelectric effect, where the top and bottom of the

element in Step 3 of Figure 1-1 are electroded, and an electric potential (i.e. voltage) is

4

applied. In this case a mechanical strain will result. As was the case with the direct

piezoelectric effect, the nature of the strain (tensile or compressive) will depend on the

polarity of the applied voltage. For example, an applied voltage with the positive

terminal on the top of the element in Step 3 of Figure 1-1 will result in a tensile strain,

while a negative terminal on the top of the element in Step 3 of Figure 1-1 will result in a

compressive strain.

Piezoelectric Material Properties

Table 1-1 gives a top level comparison of select average piezoelectric material

properties as presented in the literature.

Table 1-1 – Piezoelectric Material Properties Comparison

Property	Quartz	PVDF	PZT-5H	PMN-PT Single Crystal
Curie Temp. – T_c (°C)	573	110	215	140
Relative Permittivity – $\varepsilon/\varepsilon_0$ (-)	4.5	12	3400	5500
Coupling Coeff. – k_{33} (-)	0.098 (k_{11})	0.12	0.74	0.87
Charge Coeff. – d_{33} (x 10^{-12} C/N)	2.3 (d_{11})	32	600	1600
Density – ρ (x 10^3 kg/m^3)	2.65	1.78	7.7	8.2
Young's Modulus – Y (x 10^{10} Pa)	7.3	0.3	5.5	-

As can be seen in Table 1-1, piezopolymers and piezoceramics offer a significant

improvement in piezoelectric properties over naturally occurring piezoelectrics like

5

quartz. In addition, the single crystal piezoelectric properties of Lead-Magnesium-

Niobate – Lead-Titanate (PMN-PT) greatly exceed those of PVDF and PZT. However,

as was mentioned previously, single crystal piezoelectrics have other impediments to

implementation, namely unit cost, lack of durability and producible size limits.

A representative piezoceramic (PZT-5H) was chosen to illustrate the difference in

properties between the various piezoelectric materials. However, it should be noted that

piezoceramics are available in a wide range of formulations, with the ability to vary their

piezoelectric properties over a wide range. In addition, the piezoelectric charge

coefficient d_{33} was chosen for comparison in Table 1-1. Other charge coefficients may

be used depending on specific application and loading conditions (e.g. d_{31}), but the other

charge coefficients tend to track coarsely with d_{33}, making it a good parameter to use for

first order comparison purposes.

Piezoelectric Energy Harvesting System Diagram

A generalized piezoelectric energy harvesting system diagram and equivalent

quasi-static circuit model is shown in Figure 1-2. The purpose of this diagram is to show

the primary elements of a typical piezoelectric energy harvesting system, and how they

map into an equivalent electrical circuit model. Of special note is the fact that a

piezoelectric material can be modeled electrically as a capacitor, with a high value

resistor in parallel to model the piezoelectric material internal resistance. This electrical

equivalency will be utilized throughout this research to model the piezoelectric elements.

6
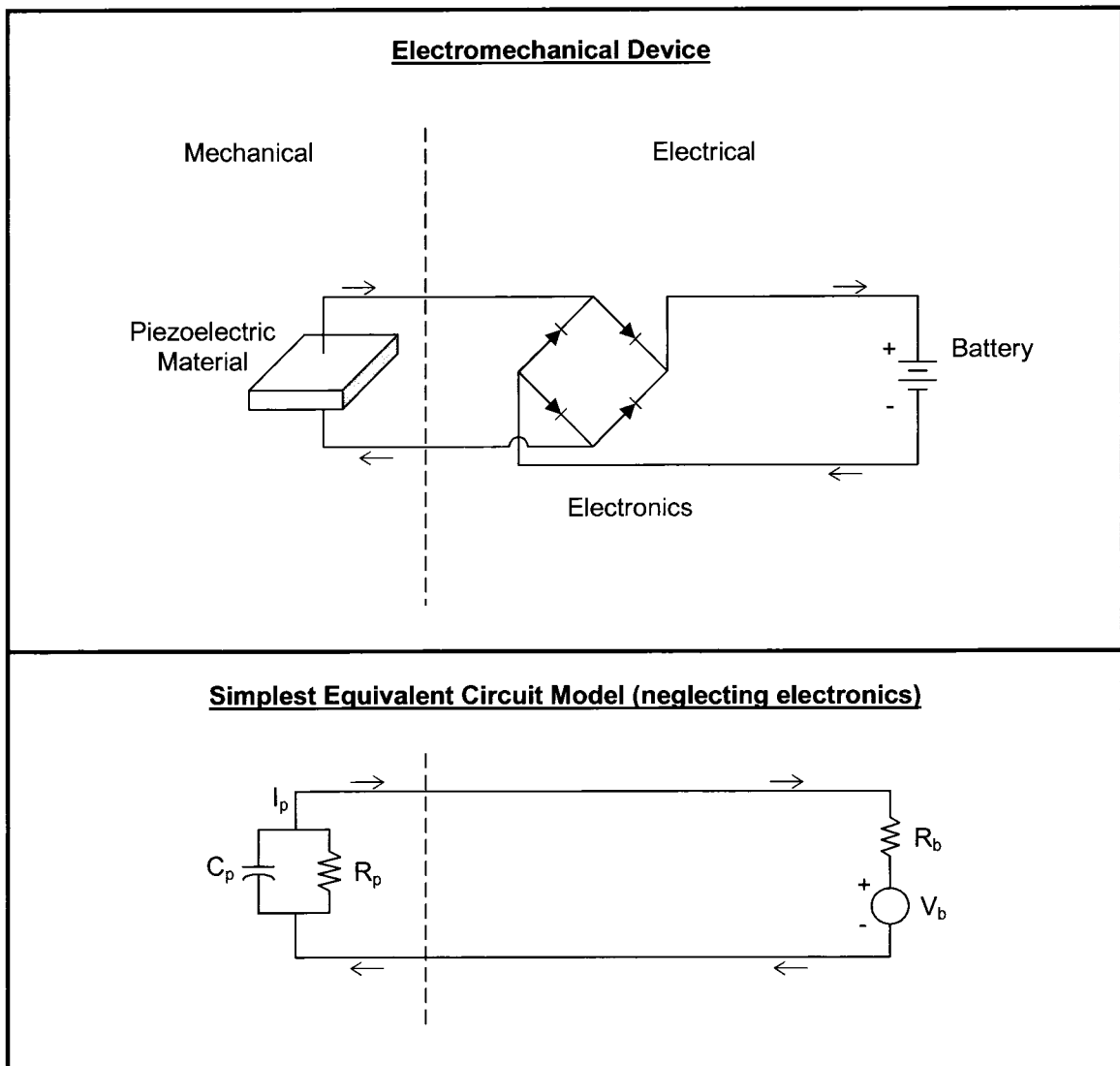
Figure 1-2 – Generalized Piezoelectric Energy Harvesting System Diagram and Equivalent Quasi-Static Circuit Model

As can be seen in Figure 1-2, a piezoelectric energy harvesting system is comprised of three primary elements: the piezoelectric material, the conditioning/charge electronics, and the battery or energy storage device. The energy storage system is typically a commercial off the shelf (COTS) capacitor/super-capacitor or traditional rechargeable lithium-ion (Li-ion) or nickel-cadmium (Ni-Cd) battery. The charge

7

electronics can vary significantly, from very simple to very complex, depending on the application. In general, the charge electronics complexity is driven by the desire to maximize the stored energy by optimizing the energy capture from the piezoelectric element.

The various components of a piezoelectric energy harvesting system (the piezoelectric material, the conditioning/charge electronics, and the battery or energy storage device) have been extensively studied in the literature. As will be discussed in greater detail in Chapter 2, the present research will focus almost exclusively on the piezoelectric element portion of the energy harvesting system. The charge electronics and the energy storage components are not the focus of the present research.

CHAPTER 2 – BACKGROUND / LITERATURE SURVEY / PRESENT RESEARCH

In this chapter, the background and existing state of the art in piezoelectric energy harvesting are summarized. Next, the contributions of the present research to the field of piezoelectric energy harvesting are presented.

Background

Piezoelectric materials have found extensive use in many high frequency applications, including simple applications like electric buzzers and quartz resonators for timekeeping, as well as more advanced applications like precision sensors and actuators. In all of these cases, the piezoelectric material is utilized in a high frequency application (> 1 kHz). Piezoelectric materials have also found use in certain applications that could be considered low frequency, such as gas ignition lighters (e.g. a gas grill igniter). However, in these applications the time duration of force application on the piezoelectric is very limited in duration (i.e. impact), and the duration of material straining is on the same order as the high frequency applications discussed above. In the last five years, research in piezoelectrics has begun to change focus from the more traditional sensor and actuator applications to utilizing piezoelectric materials as an energy source, harvesting energy from various systems.

9

Literature Survey

Recent advances in the fields of micro-electro-mechanical systems (MEMS) and electronics miniaturization allow for the use of practical very low power electronic devices. This in turn has led to the investigation of the potential of piezoelectric materials, among other methods, to harvest energy from the environment to power these electronic devices in personal computing and distributed sensing applications (Sodano, 2004). For example, the Defense Advanced Research Projects Agency (DARPA) recently funded work to look at harvesting energy from the heel strike in a soldier's boot (Steyn, 2003), and the Massachusetts Institute of Technology (MIT) Media Laboratory is investigating the feasibility of human powered (e.g. thermal, respiration, walking, etc.) personal computing (Shenck, 2001). In these applications, the available power source is a human, and the power that has been effectively extracted is on the order of milli-watts. Unfortunately, this is not sufficient (by approximately an order of magnitude) to make the above mentioned systems feasible.

Other areas of significant piezoelectric energy harvesting application research include the harvesting of power from stream/river eddy currents (Taylor, 2001), and distributed sensor network device power scavenging on systems like bridges, buildings, etc. (Ayers, 2003). In spite of the fact that these are for large scale applications like buildings and rivers, the proposed energy harvesting devices are small, effectively resulting in a small scale application. In the piezoelectric energy harvesting field, research to date has focused primarily on small scale, high frequency applications utilizing advanced piezoceramics and piezopolymers (Sodano, 2003).

10

In addition to the above application specific piezoelectric energy harvesting research areas, extensive research has also focused on optimization of the power conditioning electronics used to rectify the piezoelectric voltage into an energy storage device (rechargeable battery or capacitor) (Guan, 2004; Le, 2003; Lesieutre, 2004; and Park, 2001). This work seeks to optimize the electrical energy captured as the piezoelectric device goes through cyclic loading, regardless of the specific energy source. Significant research effort has also been focused on the understanding the piezoelectric energy harvesting mechanisms and supporting theories. These research efforts have ranged from precise quantification and supporting theory development for high frequency piezoelectric energy harvesting devices (Keawboonchuay, 2004 and Roundy, 2004), to understanding the system level efficiencies for piezoelectric systems (Goldfarb, 1999; Richards, 2004; and Vujic, 2002).

In summary, the existing investigations into energy harvesting utilizing piezoelectric devices have focused primarily on high frequency and/or small scale applications. Due to the conceptual novelty of the present research (i.e. low frequency thermal and large scale applications), no conceptually similar existing literature was identified that could be meaningfully leveraged in the present research. However, technical literature in support of the present research theoretical development and testing was located, and is referenced as applicable throughout this document.

Present Research

The present research will expand on the current state of the art in piezoelectric energy harvesting by examining very low frequency force applications (down to quasi-

11

static conditions), and large scale (i.e. higher total energy input) applications. In addition, the present research will define and quantify the complex relationship between thermal / mechanical strain and electrical output in piezoelectric devices under thermally induced straining. This research is motivated by two potential applications: a bridge and a satellite application, which are discussed in detail in the following sections.

Bridge Application

A typical piezoelectric energy harvesting civil engineering application, such as a bridge deflecting due to a vehicle traversing the span, is shown in Figure 2-1. In this application, the frequency of vibration will be low (< 5 Hz), but the total available energy will be significantly higher than that available from previously studied human powered systems.
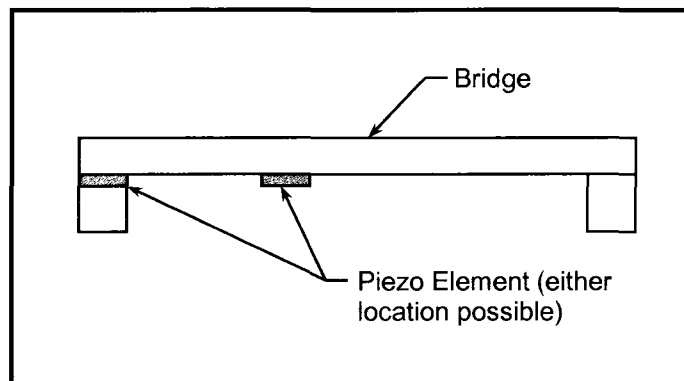
Figure 2-1 – Bridge Application

A human powered piezoelectric energy harvesting system utilizing a heel strike device can generate approximately 0.5 W (Shenck, 2001 and Starner, 1996), which

12

assumes a 70 kg person displacing a piezoelectric device by 1 cm at 1.5 Hz. Scaling this example linearly to the bridge example to get a first order estimate of power generation capability, the average vehicle (averaging passenger cars and semi-tractors) is approximately 2500 kg/axle and displaces the bridge at mid-span by 4 cm, with a frequency of vibration on the order of 2 Hz. Thus,

- Human – 70 kg * 9.81 m/s^2 * 0.01 m * 1.5 Hz = 10.3 W

- Bridge – 2500 kg/axle * 9.81 m/s^2 * 0.04 m * 2 Hz = 1962 W

- Relative Power Ratio (i.e. ratio of available energy) = 1962 W / 10.3 W = 190

- Bridge Application Scaled Power = 190 * 0.5 W = 95 W

As can be seen above, the first order approximation for the energy production capability in a typical civil engineering application results in a usable amount of power (~ 95 Watts). It is important to note that the previous calculations are not meant as an accurate representation of a specific system, but simply as an order of magnitude estimation to motivate the current research. The energy generation capability comparison given above is extremely conservative in that the piezoelectric element is assumed to be the same size in the bridge application as in the shoe application. The available mounting area on a bridge is 10 – 100 times this value, which would lead to an estimated power output of 950 – 9500 Watts – a very useful amount of power. As an implementation example, a bridge energy harvesting system could be used to light a remote bridge which is far from the power grid. In addition, one of the consequences of the energy harvesting

13

process is that it removes energy from the bridge system, thus necessarily increasing structural damping and potentially reducing long term deleterious effects.

The bridge application allows for multiple piezoelectric configurations / loading conditions (Reference Figure 2-1). Two likely configurations could be PVDF for the bridge underside (larger deflections), and PZT at abutments (smaller deflections, but higher loads). In addition, the large scale associated with a bridge application provides for a more favorable system level current/voltage output. Piezoelectric materials are inherently high voltage, low current devices, which makes matching of the battery storage and other electrical circuit component parameters difficult in small scale systems (Reference Figure 1-2). However, this can be easily corrected in a bridge application by placing multiple elements in parallel electrically to get a higher current with the same voltage.

Satellite Application

To date, the predominant piezoelectric energy harvesting mechanism explored has been mechanical vibration. This has been primarily driven by the application of interest – small terrestrial electronic devices. Unfortunately, for a satellite on-orbit, the mechanical disturbances due to vibration are very low to non-existent. The on-orbit environment for a satellite is quiescent, with the only mechanical disturbances coming from internal functions. This typically represents a poor source of available energy. However, a significant source of available energy in a satellite application is the sun, with an average flux of 1350 W/m^2 (Wertz, 1999). In fact, the primary (almost exclusive) mode of power generation for near Earth satellites is photovoltaic solar cells/panels. In

14

the present research, piezoelectric materials will be explored as a power augmentation / thermal dissipation source for Earth orbiting satellites, utilizing the coefficient of thermal expansion of substrate materials to mechanically strain piezoelectric materials, thus generating electrical energy.
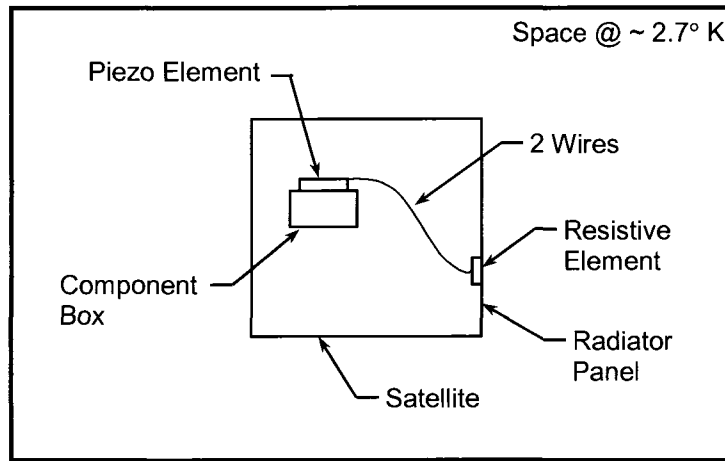
Figure 2-2 – Satellite Application

The satellite application could involve multiple configurations, including backing a solar panel with piezoelectric material to recover additional energy from the sun currently lost to heat, and/or running the piezoelectric voltage to a battery for recovery. Alternatively (Reference Figure 2-2), piezoelectric materials can be placed on component boxes within the satellite and used to transfer heat energy to a resistor on the satellite radiator panel. An interesting aspect of the satellite application configuration is that the piezoelectric element generates a direct current (DC) voltage on both heating and cooling from the temperature at which it is applied. The voltage is opposite in sign depending on heating or cooling, but is nonetheless a usable voltage in both directions.

15

Summary

The 'bridge' and 'satellite' applications discussed above share a common foundation in terms of fundamental research elements. Thus, to explore the 'bridge' and 'satellite' applications, the present research will focus on two areas that have not been extensively studied in the literature. First, the present research will explore the low frequency (< 5 Hz) behavior of piezoelectric materials with an eye toward large scale applications. As was stated previously, almost all piezoelectric energy harvesting research to date has occurred in the >1 kHz domain and/or at small scales. Second, the present research will characterize the electromechanical behavior of select piezoceramic/substrate elements under thermal loading.

Contribution of the Present Research

The present research will expand on the existing knowledge base in the field of piezoelectric energy harvesting by exploring the very low frequency thermo-electro-mechanical response of piezoelectrics, including two potential energy harvesting applications: thermal management in a near Earth orbiting satellite and energy harvesting from a vibrating highway bridge.

Significant theoretical development and laboratory research contributions of the present research are as follows:

1. *Demonstration that piezoceramics and piezopolymers are viable in very low frequency (< 0.01 Hz) energy harvesting applications.*

16

2. *The challenges and significant variables associated with low frequency piezoelectric testing were explored, quantified and to a significant extent resolved.*

3. *Quantification of the piezoelectric element capacitance changes both from a free state to a bonded state, and as the bonded piezoelectric element is heated or cooled; including development of the applicable theory.*

4. *Determination of the component and system level energy conversion efficiencies associated with a piezoceramic bonded to an aluminum (Al) substrate sample test setup.*

5. *Theoretical development to describe the strain plus pyroelectric induced voltage in a PZT element due to a thermally induced planar strain loading condition, as well as the thermally induced planar strain electromechanical coupling factor.*

17

CHAPTER 3 – THEORY

The present research into the thermo-electro-mechanical response of piezoelectric materials is fairly broad in scope, and therefore requires a theoretical foundation in piezoelectricity, as well as elements of electric circuit theory and thermodynamics. The applicable theory in each of these areas required to complete the present research is given in this chapter.

Piezoelectricity

The piezoelectric constitutive relations can be applied to all classes of piezoelectric materials (crystals, piezoceramics and piezopolymers). Because the piezoceramics and piezopolymers have such a marked increase in capability and applicability for energy harvesting applications, and are thus the focus of the present research, the derivations presented here will be on the constitutive relations as applicable to these materials.

Piezoelectric Crystal Classes

As was stated previously, piezoceramics and piezopolymers are not true single crystal piezoelectrics. Therefore, the crystal class assignment for these materials is most correctly thought of as a similarity, or 'behaves like', as opposed to a true classification. For the specific materials under study in the present research, the crystal classes are given in Table 3-1 below (Ballato, 1995).

18

Table 3-1 – Crystal Classifications for Select Piezoelectric Materials

Piezoelectric Material	Crystal Class
Lead-Zirconate-Titanate (PZT-5A)	6mm
Lead-Zirconate-Titanate (PZT-5H)	6mm
Polyvinylidine-fluoride (PVDF)*	mm2

*Note – PVDF can take on the properties of different crystal classes depending on the poling method utilized in its manufacture, but mm2 is the most common crystal class.

For the purpose of this research, the crystal classifications are important only in that they define the piezoelectric matrices in Equations 3-11a and 3-11b. Readers with a further interest in crystal classes, and how they relate to piezoelectricity and other electrical properties, are encouraged to reference the Institute of Electrical and Electronics Engineers (IEEE) Standard on Piezoelectricity, IEEE STD 176-1987, which contains a thorough treatment on the subject.

It should be noted that crystal classes 6mm and mm2 are pyroelectric in addition to being piezoelectric. As will be seen in Chapter 4, because the present research involves thermal loading of a piezoelectric element, the pyroelectric nature of the piezoelectric material will contribute to the overall electrical response.

Material Axes Definition

The piezoelectric effect involves a relationship between mechanical and electrical properties within the piezoelectric material. For the purpose of developing the piezoelectric constitutive relations, the relationship between mechanical and electrical

19

properties is assumed to be linear. This assumption is true for voltages, strains and temperatures within the pre-defined operating range of the various piezoceramics and piezopolymers. However, it is well known that the piezoelectric relationship is not linear outside of this range. As a practical matter, the piezoelectric materials tend to suffer performance degradation when operated in this non-linear regime. As such, it is not practical to design piezoelectric systems for use in the non-linear regime. Regardless, care must be taken to apply the linear relations appropriately.

A prerequisite to defining constitutive relations for the piezoelectric effect is establishing the material axes convention to be used. Piezoceramics and piezopolymers are made by a process of poling, followed by application of electrodes, which provides an electrical connection to the piezoelectric element. By convention, the poling axis of the material is the 3 axis, with the 1 and 2 axes forming a right handed coordinate system as shown in Figure 3-1.
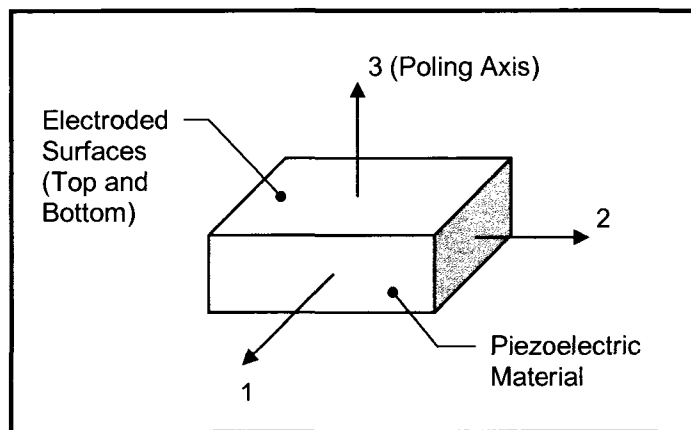
Figure 3-1 – Piezoelectric Material Axes Definition

20

Mechanical Properties

For the purpose of developing mechanical constitutive relations, the piezoelectric material is assumed to behave in a linear elastic manner. Further, the stress components are defined in Figure 3-2.
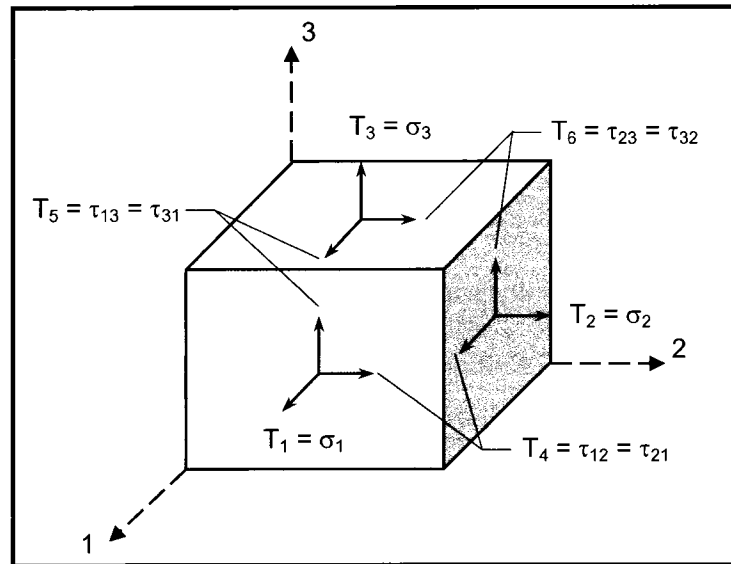
Figure 3-2 – Stress Component Definitions

The stress-strain relationship for a linear elastic piezoelectric material is given in Equation 3-1.

$$\{T\} = [c] \cdot \{S\} \qquad \text{(Equation 3-1)}$$

Or:

$$\begin{Bmatrix} T_1 \\ T_2 \\ T_3 \\ T_4 \\ T_5 \\ T_6 \end{Bmatrix} = \begin{bmatrix} c_{11} & c_{12} & c_{13} & c_{14} & c_{15} & c_{16} \\ c_{21} & c_{22} & c_{23} & c_{24} & c_{25} & c_{26} \\ c_{31} & c_{32} & c_{33} & c_{34} & c_{35} & c_{36} \\ c_{41} & c_{42} & c_{43} & c_{44} & c_{45} & c_{46} \\ c_{51} & c_{52} & c_{53} & c_{54} & c_{55} & c_{56} \\ c_{61} & c_{62} & c_{63} & c_{64} & c_{65} & c_{66} \end{bmatrix} \cdot \begin{Bmatrix} S_1 \\ S_2 \\ S_3 \\ S_4 \\ S_5 \\ S_6 \end{Bmatrix} \qquad \text{(Equation 3-1)}$$

Where:

$\{T\}$ = Stress tensor (6x1) (pascal, Pa = N/m^2)

$[c]$ = Stiffness matrix (6x6) (pascal, Pa = N/m^2)

$\{S\}$ = Strain tensor (6x1) (meter/meter, m/m, dimensionless)

Alternatively, Equation 3-1 can be expressed as:

$$\{S\} = [s] \cdot \{T\} \qquad \text{(Equation 3-2)}$$

Or:

$$\begin{Bmatrix} S_1 \\ S_2 \\ S_3 \\ S_4 \\ S_5 \\ S_6 \end{Bmatrix} = \begin{bmatrix} s_{11} & s_{12} & s_{13} & s_{14} & s_{15} & s_{16} \\ s_{21} & s_{22} & s_{23} & s_{24} & s_{25} & s_{26} \\ s_{31} & s_{32} & s_{33} & s_{34} & s_{35} & s_{36} \\ s_{41} & s_{42} & s_{43} & s_{44} & s_{45} & s_{46} \\ s_{51} & s_{52} & s_{53} & s_{54} & s_{55} & s_{56} \\ s_{61} & s_{62} & s_{63} & s_{64} & s_{65} & s_{66} \end{bmatrix} \cdot \begin{Bmatrix} T_1 \\ T_2 \\ T_3 \\ T_4 \\ T_5 \\ T_6 \end{Bmatrix} \qquad \text{(Equation 3-2)}$$

22

With:

$$[s] = [c]^{-1} \qquad \qquad \qquad \text{(Equation 3-3)}$$

Where:

$[s]$ = Compliance matrix (6x6) (meter^2/newton, m^2/N)

In a piezoelectric material, the stiffness and compliance matrices differ under constant electric field (i.e. short circuit) vs. constant electric displacement (i.e. open circuit) conditions. As such, the [c] and [s] matrices are defined with the following superscripts:

$[c^E]$ = Stiffness matrix – constant electric field / short circuit

$[c^D]$ = Stiffness matrix – constant electric displacement / open circuit

$[s^E]$ = Compliance matrix – constant electric field / short circuit

$[s^D]$ = Compliance matrix – constant electric displacement / open circuit

For the most general anisotropic linear elastic material, and assuming small strains, the coefficients of Equation 3-1 have $c_{ij} = c_{ji}$ (Boresi, 1993), thus Equation 3-1 takes the following form:

23

$$\begin{Bmatrix} T_1 \\ T_2 \\ T_3 \\ T_4 \\ T_5 \\ T_6 \end{Bmatrix} = \begin{bmatrix} c_{11} & c_{12} & c_{13} & c_{14} & c_{15} & c_{16} \\ c_{12} & c_{22} & c_{23} & c_{24} & c_{25} & c_{26} \\ c_{13} & c_{23} & c_{33} & c_{34} & c_{35} & c_{36} \\ c_{14} & c_{24} & c_{34} & c_{44} & c_{45} & c_{46} \\ c_{15} & c_{25} & c_{35} & c_{45} & c_{55} & c_{56} \\ c_{16} & c_{26} & c_{36} & c_{46} & c_{56} & c_{66} \end{bmatrix} \cdot \begin{Bmatrix} S_1 \\ S_2 \\ S_3 \\ S_4 \\ S_5 \\ S_6 \end{Bmatrix} \qquad \text{(Equation 3-1a)}$$

Which contains 21 independent coefficients. Similarly, Equation 3-2 takes the following form, also with 21 independent coefficients:

$$\begin{Bmatrix} S_1 \\ S_2 \\ S_3 \\ S_4 \\ S_5 \\ S_6 \end{Bmatrix} = \begin{bmatrix} s_{11} & s_{12} & s_{13} & s_{14} & s_{15} & s_{16} \\ s_{12} & s_{22} & s_{23} & s_{24} & s_{25} & s_{26} \\ s_{13} & s_{23} & s_{33} & s_{34} & s_{35} & s_{36} \\ s_{14} & s_{24} & s_{34} & s_{44} & s_{45} & s_{46} \\ s_{15} & s_{25} & s_{35} & s_{45} & s_{55} & s_{56} \\ s_{16} & s_{26} & s_{36} & s_{46} & s_{56} & s_{66} \end{bmatrix} \cdot \begin{Bmatrix} T_1 \\ T_2 \\ T_3 \\ T_4 \\ T_5 \\ T_6 \end{Bmatrix} \qquad \text{(Equation 3-2a)}$$

From IEEE Std. 176-1987, for lead-zirconate-titanate (PZT), due to symmetries and lack of coupling of certain stress/strain pairs associated with the crystal structure (crystal class - 6mm), Equation 3-1 reduces to the following (with 5 independent coefficients):

$$\begin{Bmatrix} T_1 \\ T_2 \\ T_3 \\ T_4 \\ T_5 \\ T_6 \end{Bmatrix} = \begin{bmatrix} c_{11} & c_{12} & c_{13} & 0 & 0 & 0 \\ c_{12} & c_{11} & c_{13} & 0 & 0 & 0 \\ c_{13} & c_{13} & c_{33} & 0 & 0 & 0 \\ 0 & 0 & 0 & c_{44} & 0 & 0 \\ 0 & 0 & 0 & 0 & c_{44} & 0 \\ 0 & 0 & 0 & 0 & 0 & c_{66} = \dfrac{c_{11} - c_{12}}{2} \end{bmatrix} \cdot \begin{Bmatrix} S_1 \\ S_2 \\ S_3 \\ S_4 \\ S_5 \\ S_6 \end{Bmatrix} \qquad \text{(Equation 3-1b)}$$

24

In the language of solid mechanics, the form of Equation 3-1b results because PZT is an orthotropic material. Similarly, for PZT, Equation 3-2 takes the following form (also with 5 independent coefficients):

$$
\begin{Bmatrix} S_1 \\ S_2 \\ S_3 \\ S_4 \\ S_5 \\ S_6 \end{Bmatrix} = \begin{bmatrix} s_{11} & s_{12} & s_{13} & 0 & 0 & 0 \\ s_{12} & s_{11} & s_{13} & 0 & 0 & 0 \\ s_{13} & s_{13} & s_{33} & 0 & 0 & 0 \\ 0 & 0 & 0 & s_{44} & 0 & 0 \\ 0 & 0 & 0 & 0 & s_{44} & 0 \\ 0 & 0 & 0 & 0 & 0 & s_{66} = 2(s_{11} - s_{12}) \end{bmatrix} \cdot \begin{Bmatrix} T_1 \\ T_2 \\ T_3 \\ T_4 \\ T_5 \\ T_6 \end{Bmatrix}
$$ (Equation 3-2b)

Again from IEEE Std. 176-1987, for polyvinylidine-fluoride (PVDF), due to symmetries and lack of coupling of certain stress/strain pairs associated with the crystal structure (crystal class - mm2), Equation 3-1 reduces to the following (with 9 independent coefficients):

$$
\begin{Bmatrix} T_1 \\ T_2 \\ T_3 \\ T_4 \\ T_5 \\ T_6 \end{Bmatrix} = \begin{bmatrix} c_{11} & c_{12} & c_{13} & 0 & 0 & 0 \\ c_{12} & c_{22} & c_{23} & 0 & 0 & 0 \\ c_{13} & c_{23} & c_{33} & 0 & 0 & 0 \\ 0 & 0 & 0 & c_{44} & 0 & 0 \\ 0 & 0 & 0 & 0 & c_{55} & 0 \\ 0 & 0 & 0 & 0 & 0 & c_{66} \end{bmatrix} \cdot \begin{Bmatrix} S_1 \\ S_2 \\ S_3 \\ S_4 \\ S_5 \\ S_6 \end{Bmatrix}
$$ (Equation 3-1c)

As in the case of PZT, the form of Equation 3-1c results because PVDF is also an orthotropic material. Similarly, for PVDF, Equation 3-2 takes the following form (also with 9 independent coefficients):

25

$$\begin{Bmatrix} S_1 \\ S_2 \\ S_3 \\ S_4 \\ S_5 \\ S_6 \end{Bmatrix} = \begin{bmatrix} s_{11} & s_{12} & s_{13} & 0 & 0 & 0 \\ s_{12} & s_{22} & s_{23} & 0 & 0 & 0 \\ s_{13} & s_{23} & s_{33} & 0 & 0 & 0 \\ 0 & 0 & 0 & s_{44} & 0 & 0 \\ 0 & 0 & 0 & 0 & s_{55} & 0 \\ 0 & 0 & 0 & 0 & 0 & s_{66} \end{bmatrix} \cdot \begin{Bmatrix} T_1 \\ T_2 \\ T_3 \\ T_4 \\ T_5 \\ T_6 \end{Bmatrix}$$

(Equation 3-2c)

Electrical Properties

The electrical properties of interest in a piezoelectric material are the electric field (E), and the electric displacement (D). This relationship is given in Equation 3-4.

$$\{D\} = [\varepsilon] \cdot \{E\}$$

(Equation 3-4)

Or:

$$\begin{Bmatrix} D_1 \\ D_2 \\ D_3 \end{Bmatrix} = \begin{bmatrix} \varepsilon_{11} & \varepsilon_{12} & \varepsilon_{13} \\ \varepsilon_{21} & \varepsilon_{22} & \varepsilon_{23} \\ \varepsilon_{31} & \varepsilon_{32} & \varepsilon_{33} \end{bmatrix} \cdot \begin{Bmatrix} E_1 \\ E_2 \\ E_3 \end{Bmatrix}$$

(Equation 3-4)

Where:

$\{D\}$ = Electric displacement tensor (3x1) (coulomb/meter^2, C/m^2)

$[\varepsilon]$ = Permittivity matrix (3x3) (farad/meter, F/m)

$\{E\}$ = Electric field tensor (3x1) (volt/meter, V/m)

26

Alternatively, Equation 3-4 can be expressed as:

$$\{E\} = [\beta] \cdot \{D\} \qquad \text{(Equation 3-5)}$$

Or:

$$\begin{Bmatrix} E_1 \\ E_2 \\ E_3 \end{Bmatrix} = \begin{bmatrix} \beta_{11} & \beta_{12} & \beta_{13} \\ \beta_{21} & \beta_{22} & \beta_{23} \\ \beta_{31} & \beta_{32} & \beta_{33} \end{bmatrix} \cdot \begin{Bmatrix} D_1 \\ D_2 \\ D_3 \end{Bmatrix} \qquad \text{(Equation 3-5)}$$

With:

$$[\beta] = [\varepsilon]^{-1} \qquad \text{(Equation 3-6)}$$

Where:

$[\beta]$ = Impermeability matrix (3x3) (meter/farad, m/F)

Similar to the stress/strain relations above, in a piezoelectric material, the permittivity and impermeability matrices differ under constant stress (i.e. mechanically free) or constant strain (i.e. mechanically clamped) conditions. As such, the $[\varepsilon]$ and $[\beta]$ matrices are defined with the following superscripts:

27

$[\varepsilon^T]$ = Permittivity matrix – constant stress / mechanically free

$[\varepsilon^S]$ = Permittivity matrix – constant strain / mechanically clamped

$[\beta^T]$ = Impermeability matrix – constant stress / mechanically free

$[\beta^S]$ = Impermeability matrix – constant strain / mechanically clamped

For lead-zirconate-titanate (PZT), Equation 3-4 reduces to the following (with 2 independent coefficients):

$$
\begin{Bmatrix} D_1 \\ D_2 \\ D_3 \end{Bmatrix} = \begin{bmatrix} \varepsilon_{11} & 0 & 0 \\ 0 & \varepsilon_{22} = \varepsilon_{11} & 0 \\ 0 & 0 & \varepsilon_{33} \end{bmatrix} \cdot \begin{Bmatrix} E_1 \\ E_2 \\ E_3 \end{Bmatrix}
\qquad \text{(Equation 3-4a)}
$$

Similarly, for lead-zirconate-titanate (PZT), Equation 3-5 takes the following form (also with 2 independent coefficients):

$$
\begin{Bmatrix} E_1 \\ E_2 \\ E_3 \end{Bmatrix} = \begin{bmatrix} \beta_{11} & 0 & 0 \\ 0 & \beta_{22} = \beta_{11} & 0 \\ 0 & 0 & \beta_{33} \end{bmatrix} \cdot \begin{Bmatrix} D_1 \\ D_2 \\ D_3 \end{Bmatrix}
\qquad \text{(Equation 3-5a)}
$$

For polyvinylidine-fluoride (PVDF), Equation 3-4 reduces to the following (with 3 independent coefficients):

$$
\begin{Bmatrix} D_1 \\ D_2 \\ D_3 \end{Bmatrix} = \begin{bmatrix} \varepsilon_{11} & 0 & 0 \\ 0 & \varepsilon_{22} & 0 \\ 0 & 0 & \varepsilon_{33} \end{bmatrix} \cdot \begin{Bmatrix} E_1 \\ E_2 \\ E_3 \end{Bmatrix}
\qquad \text{(Equation 3-4b)}
$$

28

Similarly, for polyvinylidine-fluoride (PVDF), Equation 3-5 takes the following form, also with 3 independent coefficients:

$$\begin{Bmatrix} E_1 \\ E_2 \\ E_3 \end{Bmatrix} = \begin{bmatrix} \beta_{11} & 0 & 0 \\ 0 & \beta_{22} & 0 \\ 0 & 0 & \beta_{33} \end{bmatrix} \cdot \begin{Bmatrix} D_1 \\ D_2 \\ D_3 \end{Bmatrix} \qquad \text{(Equation 3-5b)}$$

Piezoelectric Properties

The piezoelectric matrices linearly relate the mechanical and electrical properties defined in Equations 3-1 through 3-3 and 3-4 through 3-6, respectively. Because, in the most general form, the electrical relationship is defined by 3 quantities and the mechanical relationship by 6 quantities, the piezoelectric matrices are 3x6 in size. The piezoelectric relationship is expressed by four sets of two equations (given as Equations 3-7 through 3-10 below), depending on the specific application. The four sets of equations are not independent, and can therefore be derived from one another.

$$\{S\} = [s^E] \cdot \{T\} + [d]' \cdot \{E\} \qquad \text{(Equation 3-7a)}$$

$$\{D\} = [d] \cdot \{T\} + [\varepsilon^T] \cdot \{E\} \qquad \text{(Equation 3-7b)}$$

$$\{S\} = [s^D] \cdot \{T\} + [g]' \cdot \{D\} \qquad \text{(Equation 3-8a)}$$

$$\{E\} = -[g] \cdot \{T\} + [\beta^T] \cdot \{D\} \qquad \text{(Equation 3-8b)}$$

29

$${T} = [c^E] \cdot {S} - [e]' \cdot {E}$$ (Equation 3-9a)

$${D} = [e] \cdot {S} + [\varepsilon^S] \cdot {E}$$ (Equation 3-9b)

$${T} = [c^D] \cdot {S} - [h]' \cdot {D}$$ (Equation 3-10a)

$${E} = -[h] \cdot {S} + [\beta^S] \cdot {D}$$ (Equation 3-10b)

Where:

[d] = Piezoelectric matrix (3x6) (meter/Volt, m/V = C/N)

[g] = Piezoelectric matrix (3x6) (meter^2/ coulomb, m^2/C = (m·V)/N)

[e] = Piezoelectric matrix (3x6) (coulomb/meter^2, C/m^2 = N/(m·V))

[h] = Piezoelectric matrix (3x6) (volt/meter, V/m = N/C)

In Equations 3-7 through 3-10 the matrix transpose of [x] is defined as [x]', instead of the more traditional [x]^t or [x]^T. For clarity, in the present work the superscript T is reserved for the constant stress definition of the permittivity ([ε^T]) and impermeability ([β^T]) matrices.

It should be noted that the linear assumptions given in Equations 3-7 through 3-10 are not applicable for piezoceramic and piezopolymer materials at high electrical or mechanical loading, nor at elevated temperatures (near the Curie point of the material). Care must be taken during testing to ensure that the linear assumptions stated above are valid in order for them to be used.

30

The piezoelectric matrices [d], [g], [e] and [h] are all of the same size (3x6) and take the same general form. For example, the general form of the [d] matrix is as follows:

$$[d] = \begin{bmatrix} d_{11} & d_{12} & d_{13} & d_{14} & d_{15} & d_{16} \\ d_{21} & d_{22} & d_{23} & d_{24} & d_{25} & d_{26} \\ d_{31} & d_{32} & d_{33} & d_{34} & d_{35} & d_{36} \end{bmatrix}$$
(Equation 3-11)

With the [g], [e] and [h] matrices having the same form, but not the same term values. For example, simply change the d_{ij} terms to g_{ij} terms in Equation 3-11 to obtain the form of the [g] matrix.

The following terms are all used for d_{ij} in the literature: charge coefficient, which seems to be the most popular; charge constant; strain constant; charge density/stress; piezoelectric strain/field coefficient; and piezoelectric constant, which is used in IEEE STD 176-1987. In this document, the IEEE STD 176-1987 nomenclature is followed (i.e. piezoelectric matrix and piezoelectric constant) to describe d_{ij}. In addition, in the literature two equivalent sets of units are used for d_{ij}:

$$\frac{meter}{Volt} = \frac{Coulomb}{Newton}$$

For lead-zirconate-titanate (PZT), Equation 3-11 reduces to the following (with 3 independent coefficients):

31

$$[d] = \begin{bmatrix} 0 & 0 & 0 & 0 & d_{15} & 0 \\ 0 & 0 & 0 & d_{15} & 0 & 0 \\ d_{31} & d_{31} & d_{33} & 0 & 0 & 0 \end{bmatrix}$$
(Equation 3-11a)

For polyvinylidine-fluoride (PVDF), Equation 3-11 reduces to the following (with 5 independent coefficients):

$$[d] = \begin{bmatrix} 0 & 0 & 0 & 0 & d_{15} & 0 \\ 0 & 0 & 0 & d_{24} & 0 & 0 \\ d_{31} & d_{32} & d_{33} & 0 & 0 & 0 \end{bmatrix}$$
(Equation 3-11b)

Piezoelectric material energy conversion efficiencies are often expressed through the use of a non-dimensional piezoelectric electromechanical coupling factor (k), which can be expressed as the ratio of usable energy divided by total energy input into a piezoelectric device. Because a piezoelectric is reversible, the electromechanical coupling factor can be expressed for both the mechanical to electrical conversion and the electrical to mechanical conversion as follows (from "Piezoelectric Ceramics Properties and Applications," Morgan Electro Ceramics):

$$k^2 = \frac{\text{mechanical energy converted to electrical charge}}{\text{mechanical energy input}}$$
(Equation 3-12a)

Alternatively:

32

$$k^2 = \frac{\text{electrical energy converted to mechanical displ.}}{\text{electrical energy input}} \qquad \text{(Equation 3-12b)}$$

Where Equations 3-12a and 3-12b are numerically equal if the piezoelectric

material behavior is assumed linear, which is the case in standard piezoelectric theory.

Care should be exercised in applying Equations 3-12a and 3-12b because, in fact,

piezoelectric materials are known to behave in a non-linear fashion at high electrical or

mechanical loading, as well as having a non-linear electro-mechanical response as a

function of temperature. In addition, the piezoelectric energy harvesting system will not

behave in a lossless fashion to the extent that the real system components do not behave

as idealized electrical components (i.e. capacitors, resistors, conductors, etc.)

The quasi-static (to include static) piezoelectric electromechanical coupling

factors can be expressed as follows:

$$k_{33} = \frac{d_{33}}{\sqrt{\varepsilon_{33}^{T} \cdot s_{33}^{E}}} \;;\; \text{(1D stress state } T_3, T_{1,2,4,5,6} = 0) \qquad \text{(Equation 3-13)}$$

$$k_{31} = \frac{d_{31}}{\sqrt{\varepsilon_{33}^{T} \cdot s_{11}^{E}}} \;;\; \text{(1D stress state } T_1, T_{2,3,4,5,6} = 0) \qquad \text{(Equation 3-14)}$$

$$k_{p} = \frac{\sqrt{2} \cdot d_{31}}{\sqrt{\varepsilon_{33}^{T} \cdot \left(s_{11}^{E} + s_{12}^{E}\right)}} \;;\; \text{(2D stress state } T_1, T_2, T_{3,4,5,6} = 0) \qquad \text{(Equation 3-15)}$$

33

$$k_t = \frac{e_{33}}{\sqrt{c_{33}^D \cdot \varepsilon_{33}^S}} \ ; (1\text{D strain state } S_3, S_{1,2,4,5,6} = 0) \qquad \text{(Equation 3-16)}$$

$$k_{15} = \frac{e_{15}}{\sqrt{c_{55}^D \cdot \varepsilon_{11}^S}} \ ; (1\text{D strain state } S_5, S_{1,2,3,4,6} = 0) \qquad \text{(Equation 3-17)}$$

Where:

k_{33} = Longitudinal Coupling Factor (Rods, unitless)

k_{31} = Transverse Coupling Factor (Plates, unitless)

k_p = Planar Coupling Factor (Thin Disks, unitless)

k_t = Thickness Coupling Factor (Laterally Clamped, unitless)

k_{15} = Shear Coupling Factor (Shear Plates, unitless)

As can be seen from the restrictions given in Equations 3-13 through 3-17 (e.g. 1D stress state T_3 in Equation 3-13), the piezoelectric coupling factors apply to a very specific material shape and orientation, as well as electrical and mechanical loading configuration, in order to achieve the specific value of (k).

The piezoelectric electromechanical coupling factors (k) also define the relationship between the stiffness and compliance matrices at constant electric field and displacement, and the permittivity and impermeability matrices at constant stress and strain, as follows (from "Piezoelectric Ceramics Properties and Applications," Morgan Electro Ceramics):

34

$$[c^D] \cdot (1\text{-}k^2) = [c^E] \qquad\qquad\qquad \text{(Equation 3-18)}$$

$$[s^E] \cdot (1\text{-}k^2) = [s^D] \qquad\qquad\qquad \text{(Equation 3-19)}$$

$$[\varepsilon^T] \cdot (1\text{-}k^2) = [\varepsilon^S] \qquad\qquad\qquad \text{(Equation 3-20)}$$

$$[\beta^S] \cdot (1\text{-}k^2) = [\beta^T] \qquad\qquad\qquad \text{(Equation 3-21)}$$

Energy in Deflecting a Piezoelectric Linear Elastic Material

To be able to quantify the system level mechanical to electrical conversion efficiency of a piezoelectric/substrate element, the energy required to mechanically strain a piezoelectric material must first be defined. In considering the most general case, the energy in straining the linear elastic material in Figure 3-3 is represented by the shaded area under the curve in Figure 3-3.
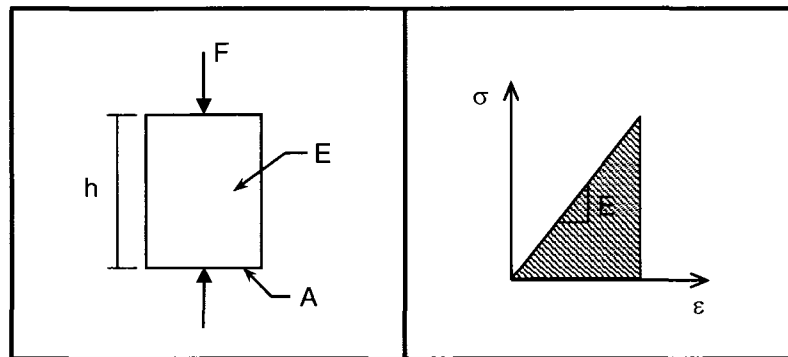
Figure 3-3 – Energy in Straining a Linear Elastic Material

35

Energy = Shaded area under the curve in Figure 3-3 = $\int \sigma \cdot d\varepsilon = \frac{1}{2} \cdot \sigma \cdot \varepsilon$

Including volume in the previous energy equation:

$$Energy = \frac{1}{2} \cdot V \cdot \sigma \cdot \varepsilon = \frac{1}{2} \cdot V \cdot \sigma^2 \cdot s$$

Where:

V = Volume (m^3)

ε = Strain (m/m)

σ = Stress (N/m^2)

s = Compliance (m^2/N)

From this basis, and modifying the symbols which represent the terms to match the piezoelectric nomenclature, the energy in straining a piezoelectric linear elastic material is given in Equation 3-22.

$$E = \frac{1}{2} \cdot V \cdot s \cdot T^2 \qquad \text{(Equation 3-22)}$$

Where:

E = Energy (J = N·m)

36

V = Volume (m^3)

s = Compliance (m^2/N) (s^D or s^E, depending on open or short circuit condition)

$T = \sigma$ = Stress (N/m^2)

Mechanical / Electrical Energy Distribution in a Mechanically Strained Piezo Element

Next, take Equation 3-22 and consider the simplifying case of a 1-D stress state due to an applied force in a long thin bar of piezoelectric material under an open circuit piezoelectric condition. Equation 3-22 then becomes Equation 3-23 below:

$$W_{TOT} = \frac{1}{2} \cdot V \cdot s_{33}^{D} \cdot T_{3}^{2}$$
(Equation 3-23)

In Equation 3-23 above, the energy term has been represented by (W_{TOT}) instead of (E) in order to eliminate confusion with the electric field (E). Combining Equations 3-12a and 3-23:

$$W_{ELEC} = \frac{1}{2} \cdot V \cdot k^{2} \cdot s_{33}^{D} \cdot T_{3}^{2}$$
(Equation 3-24)

Or, because electric + mechanical = total:

$$W_{MECH} = \frac{1}{2} \cdot V \cdot (1 - k^{2}) \cdot s_{33}^{D} \cdot T_{3}^{2}$$
(Equation 3-25)

37

The mechanical / electrical energy distribution due to mechanically straining a piezoelectric element given above is similar in form for other loading and circuit conditions, with the appropriate substitutions for the (s) and (k) terms.

Piezoelectric Energy Conversion for One Complete Loading Cycle

The energy conversion in a piezoelectric element for one complete loading cycle is as follows:

$$W_{ELEC}(\text{for one complete cycle}) = W_{ELEC}(\text{force application}) + W_{ELEC}(\text{rebound})$$

$$W_{ELEC}(\text{force application}) = W_{TOT} \cdot k_{33}^2$$

$$W_{ELEC}(\text{rebound}) = [W_{TOT} \cdot (1 - k_{33}^2)] \cdot k_{33}^2 = W_{TOT} \cdot (k_{33}^2 - k_{33}^4)$$

$$W_{ELEC}(\text{one cycle}) = W_{TOT} \cdot k_{33}^2 + W_{TOT} \cdot (k_{33}^2 - k_{33}^4)$$

$$W_{ELEC}(\text{one cycle}) = W_{TOT} \cdot (2 \cdot k_{33}^2 - k_{33}^4) \qquad \text{(Equation 3-26)}$$

As can be seen in Equation 3-26, when considering the total system level piezoelectric energy conversion, it is important to consider the rebound energy, as it contributes significantly to the overall energy conversion efficiency.

38

Electrical Circuit Theory

The piezoelectric elements under study in the present research can be modeled as idealized RC circuits. The fundamentals of RC circuit theory are given below.

RC Circuits

For the idealized RC circuit shown in Figure 3-4, the time constant is expressed by the following equation (Dorf, 1993):

$$V_c(t) = V_c(0) \cdot e^{-t/RC}$$ (Equation 3-27)

Where:

Initial Circuit Voltage, $V_c(0) = V_0$

Time Constant, $t_c = R \cdot C$
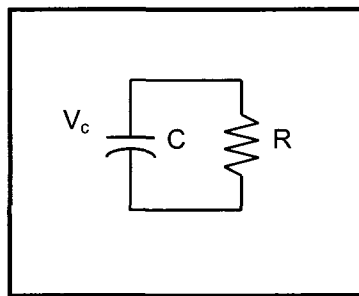
Figure 3-4 – Idealized RC Circuit

39

The voltage decay for the idealized RC circuit in Figure 3-4 is given in Figure 3-5 (Grossman, 1986).

Voltage Decay in a RC Circuit
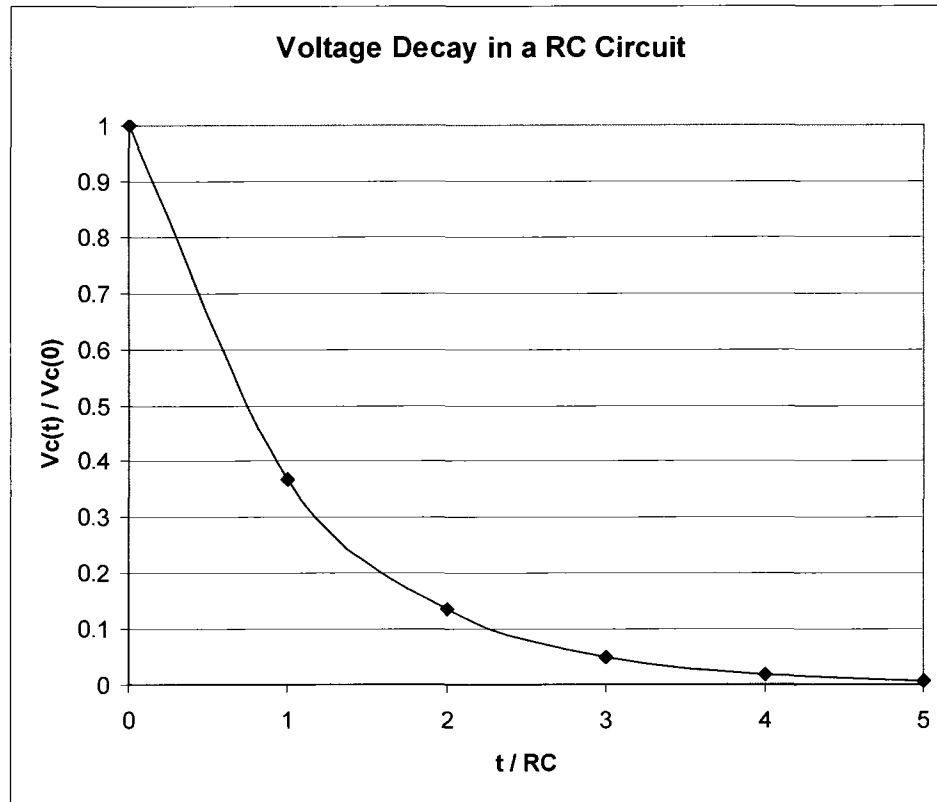
Figure 3-5 – Voltage Decay in a RC Circuit

The voltage decay as a function of time in a RC circuit will be utilized to quantify the internal resistance losses in the piezoelectric elements in Chapter 4, which behave as idealized RC circuits.

40

Thermodynamic Considerations

Heat Energy / Specific Heat Capacity

As part of the system level energy balance in Chapter 5, the heat energy input into the aluminum substrate and PZT-5A3 samples can be determined from their heat capacity as follows (Ohanian, 1989):

$$E = c_p \cdot V \cdot \rho \cdot \Delta T \qquad \text{(Equation 3-28)}$$

Where:

E = Heat Energy into Material (J)

c_p = Heat Capacity (J/kg·°C)

V = Volume (m^3)

ρ = Density (kg/m^3)

ΔT = Temperature Change in Material (°C)

Equation 3-28 will be utilized in Chapter 5 to calculate the thermal energy inputs into the aluminum substrate and PZT-5A3 element. These inputs are required to calculate the conversion efficiency of the PZT/Al elements.

41

CHAPTER 4 – SUMMARY OF EXPERIMENTS

This chapter provides a summary of the relevant laboratory testing which was conducted in the course of the present research.

PZT-5A3 Piezoceramic Sample Properties

The piezoelectric material that was used in the present research was Morgan Electro-Ceramics PZT-5A3 piezoceramic. The research samples all came from the same lot, which was purchased by the Air Force Research Laboratory (AFRL). A picture of a representative PZT-5A3 sample bonded to the aluminum substrate is given in Figure 4-1 below.
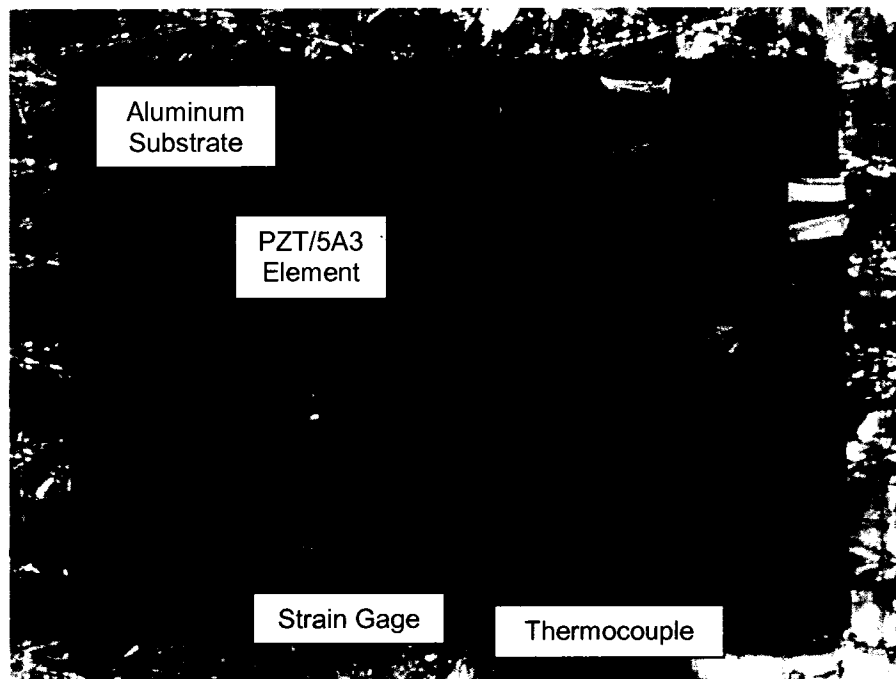
Figure 4-1 – Picture of Morgan Electro-Ceramics PZT-5A3 Sample Bonded to Aluminum Substrate

42

The relevant properties for the PZT-5A3 samples that were used in the present research are given below. Typical properties for PZT-5A3 as reported by the manufacturer (Morgan Electro-Ceramics) are given in Table 4-1.

- Size: 6.35 cm (2.5 in) wide x 3.81 cm (1.5 in) tall x 0.0254 cm (0.01 in) thick
- Finished with electroded surfaces – no leads
- 33 direction is through thickness (i.e. 0.0254 cm direction)
- Piezoelectric properties (Reference Table 4-1)

Table 4-1 – Morgan Electro-Ceramics PZT-5A3 Typical Properties

Property	Symbol	Unit	PZT-5A3†
Relative Permittivity	ε_{r33}^{T}	-	1700
	ε_{r11}^{T}	-	1730
Coupling Factors	k_p	-	0.60
	k_{15}	-	0.69
	k_{31}	-	0.34
	k_{33}	-	0.71
Piezoelectric Constants	d_{33}	$\times 10^{-12}$ C/N (or m/V)	374
	d_{31}	$\times 10^{-12}$ C/N (or m/V)	-171
	d_h	$\times 10^{-12}$ C/N (or m/V)	32
	d_{15}	$\times 10^{-12}$ C/N (or m/V)	585
	g_{33}	$\times 10^{-3}$ V·m/N	24.8

43

Property	Symbol	Unit	PZT-5A3†
	g_{31}	$\times 10^{-3}$ V·m/N	-11.4
	g_h	$\times 10^{-3}$ V·m/N	2
	g_{15}	$\times 10^{-3}$ V·m/N	38.2
Mechanical Compliance	s_{11}^{E}	$\times 10^{-12}$ m^2/N	16.4
	s_{33}^{E}	$\times 10^{-12}$ m^2/N	18.8
	s_{12}^{E}	$\times 10^{-12}$ m^2/N	-5.74
	s_{13}^{E}	$\times 10^{-12}$ m^2/N	-7.22
	s_{44}^{E}	$\times 10^{-12}$ m^2/N	47.5
Mechanical Stiffness	c_{11}^{E}	$\times 10^{10}$ N/m^2	6.1
	c_{33}^{E}	$\times 10^{10}$ N/m^2	5.3
	c_{11}^{D}	$\times 10^{10}$ N/m^2	6.9
	c_{33}^{D}	$\times 10^{10}$ N/m^2	10.6
Density	ρ	kg/m^3	7700
Poisson's Ratio	ν	-	0.3
Curie Temperature	T_c	°C	365

†Source – Mogan Electro-Ceramics Web Site (http://www.morganelectroceramics.com),
"Typical Values of Morgan Electro-Ceramics Navy Type II Piezoelectric Ceramics"

It is important to differentiate between PZT-5A3 sample property values as
reported in the literature (Table 4-1), which are specific to the samples that were used in

the present research, and PZT-5A sample property values (Table 4-2), which one would

expect to be close to the 5A3 values, but not necessarily exact.

Table 4-2 – Morgan Electro-Ceramics PZT-5A Typical Properties

Property	Symbol	Unit	PZT-5A*
Volume Resistivity	ρ	$\Omega\cdot$m (at 25 °C)	$>10^{11}$
	ρ	$\Omega\cdot$m (at 100 °C)	10^{11}
Time Constant	t_c	sec. (at 25 °C)	>2000
	t_c	sec. (at 100 °C)	1800
Piezoelectric Constants	h_{31}	$\times 10^8$ V/m	-7.3
	h_{33}	$\times 10^8$ V/m	21.5
Mechanical Stiffness	c_{11}^D	$\times 10^{10}$ N/m^2	12.6
	c_{12}^D	$\times 10^{10}$ N/m^2	8.09
Coefficient of Thermal Expansion	α	$\times 10^{-6}$ / °C	1.4

*Source – Morgan Technical Publication TP-226.

Aluminum Substrate Properties

The aluminum substrate to which the PZT-5A3 samples were bonded is 6061-T6

rolled aluminum. The individual substrate parts were 10.16 cm (4 in) long by 7.62 cm

(3 in) wide by 0.3175 cm (0.125 in) thick. The edges of each substrate part were broken

and the top of each part was lightly sandblasted to facilitate bonding of the PZT element.

The aluminum substrates that were used in the present research all came from the same

45

rolled sheet, which was purchased by the Air Force Research Laboratory. A picture of an aluminum substrate with a PZT-5A3 sample bonded to the top is given in Figure 4-1.

Preliminary Testing

Preliminary testing was first performed to accomplish three objectives:

1. To gain a visceral understanding of the piezoelectric material behavior.

2. To eliminate, to the maximum extent possible, initial test setup errors associated with the testing program.

3. To understand the limitations associated with the Air Force Research Laboratory / Space Vehicles Directorate (AFRL/VS) Building 472 testing facilities and capabilities as they relate to piezoelectric materials.

The following is a listing of preliminary testing that was completed under the present research. Each test, along with the test results, as appropriate, is explained in the following sections.

1. Verification of the PZT-5A3 internal resistance (R), capacitance (C) and time constant properties.

2. Verification of the PZT-5A3 / Fluke 87 III digital multi-meter (DMM) system circuit properties.

3. Varying the electrical lead attachment conditions to the PZT-5A3 elements to ensure the element is not damaged during the process.

46

4. Verification and calibration of the thermocouples and thermometers.

5. Verification of the bonding process between the PZT-5A3 sample and the
    aluminum substrate.

Determination of PZT-5A3 Sample Natural Time Constant

To be able to use piezoelectric materials in a quasi-static loading condition, the
natural time constant (i.e. the time constant associated with internal piezoelectric element
resistance) for the element must be verified to be significantly greater than the frequency
of the applied loading. If this were not the case, the energy gained through loading in
each cycle would be lost to internal resistance before it can be effectively captured.
Referring to Chapter 3, the time constant (t_c) equals the element internal resistance (R)
multiplied by the element capacitance (C).

PZT-5A3 Element Theoretical Resistance

The theoretical PZT-5A3 element resistance is given by the following equation:

$$R = \frac{\rho \cdot T}{L \cdot W}$$
(Equation 4-1)

Where:

R = Element Resistance (Ω)

ρ = Volume Resistivity ($\Omega \cdot$cm)

47

T = Element Thickness (cm)

L = Element Length (cm)

W = Element Width (cm)

For the PZT-5A3 elements of the present research:

$$R = \frac{\rho \cdot T}{L \cdot W}$$

$$= \frac{1 \cdot 10^{11} \Omega \cdot m \times \dfrac{100cm}{1m} \times 0.0254cm}{6.35cm \times 3.81cm}$$

$$= 1.05 \cdot 10^{10} \Omega$$

Thus, for the PZT-5A3 elements, the theoretical calculated internal resistance was 10.5 GΩ.

PZT-5A3 Element Measured Resistance

The PZT-5A3 element resistance was measured using a 3M-701 Megohmeter, which is typically used to verify the performance of electrostatic discharge (ESD) mats, floors, etc. The high value resistance measurements were accomplished per the 3M-701 Megohmeter User's Manual, which requires a battery and continuity check prior to each series of tests. These checks were accomplished successfully. Table 4-3 contains the results of the 3M-701 Megohmeter high resistance measurements on the PZT-5A3 samples.

48

Table 4-3 – Measured Resistance for PZT-5A3 Samples

Sample Number	10 V Test Resistance* (Ω)	100 V Test Resistance* (Ω)
1	9.5×10^9	1×10^{10}
2	9.8×10^9	9.7×10^9
3	9.8×10^9	9.5×10^9
4	9.8×10^9	9.8×10^9
5	1×10^{10}	9.5×10^9
6	1×10^{10}	9.2×10^9
7	9.8×10^9	9.7×10^9
8	1×10^{10}	9.8×10^9
Average	9.84×10^9	9.65×10^9

*Note – Measurements were taken after 15 seconds per the 3M-701 Megohmeter User's Manual. The measurements were somewhat noisy ($\sim 2 \times 10^9$ Ω), and the standard deviation of the data set was 0.218×10^9 Ω.

From the above testing, the overall average measured resistance for the PZT-5A3 samples was 9.74×10^9 Ω. This agrees well with the theoretical calculated value of 10.5×10^9 Ω from the previous section.

PZT-5A3 Element Theoretical Capacitance

The PZT-5A3 element capacitance can be calculated theoretically using the following general equation for a capacitor:

49

$$C = \frac{\varepsilon_0 \cdot \varepsilon_r \cdot A}{t}$$ (Equation 4-2)

Thus, for the PZT-5A3 elements in the present research:

$$C = \frac{\varepsilon_0 \cdot \varepsilon_r \cdot A}{t}$$

$$= \frac{8.8542 \times 10^{-12} F/m \cdot 1700 \cdot (0.0635m \cdot 0.0381m)}{0.000254m}$$

$$= 1.4 \times 10^{-7} F$$

$$= 0.14 \mu F$$

Where:

ε_0 = Permittivity of Free Space (F/m)

ε_r = Relative Permittivity (Constant stress loading condition) (unitless)

A = Element Area (Perpendicular to poling direction) (m^2)

t = Element Thickness (m)

PZT-5A3 Element Measured Capacitance

The capacitance for the same 8 PZT-5A3 samples from the previous resistance measurements were measured using a Fluke 87 III DMM.

50

Table 4-4 – Measured Capacitance for PZT-5A3 Samples

Sample Number	Capacitance (µF)
1	0.179
2	0.177
3	0.174
4	0.176
5	0.179
6	0.173
7	0.175
8	0.176
Average	0.176

Thus, the average measured capacitance for the PZT-5A3 samples was 0.176 µF, with a standard deviation of 0.002 µF. The average measured capacitance is comparable to the calculated value of 0.14 µF using manufacturer's data from the previous section. In Chapter 5, further analysis shows that the manufacturer's data for the PZT-5A3 samples under predicts the element capacitance, and the measured value above is correct for the samples in the present research.

PZT-5A3 Element Time Constant

In summary, the theoretical and measured values for both resistance and capacitance of the PZT-5A3 samples were in good agreement, and yielded an acceptably

51

high time constant. Using the measured values for PZT-5A3 sample resistance and capacitance, the time constant was as follows:

$$t_c = R \cdot C = 9.7125 \times 10^9 \, \Omega \cdot 0.176125 \times 10^{-6} \, F = 1711 \, \text{sec} = 28.5 \, \text{min}$$

This large natural time constant verifies that piezo elements can be used effectively in quasi-static loading conditions. Further, the high time constant verifies that the PZT-5A3 elements can be used with confidence in the present research.

PVDF Time Constant Analysis

The time constant for PVDF was calculated to verify that it is sufficiently large to support quasi-static loading conditions. The following analysis was based on the MSI sensors data sheet (refer to Appendix A) for PVDF film.

- Volume Resistivity: $> 10^{13} \, \Omega \cdot m$

- Capacitance: $= 380 \, pF/cm^2$ for 28 μm thick sample

- Assume: 1 cm x 1 cm x 28 μm thick sample

PVDF Element Resistance:

$$R = \frac{\rho \cdot T}{L \cdot W} \qquad\qquad \text{(Equation 4-1)}$$

52

$$= \frac{1 \times 10^{13} \, \Omega \cdot m \cdot 28 \times 10^{-6} m}{0.01m \cdot 0.01m}$$

$$= 2.8 \times 10^{12} \, \Omega$$

PVDF Element Capacitance:

$$C = \frac{\varepsilon_0 \cdot \varepsilon_r \cdot A}{t} \qquad \text{(Equation 4-2)}$$

$$= \frac{110 \times 10^{-12} \, F/m \cdot 0.01m \cdot 0.01m}{28 \times 10^{-6} m}$$

$$= 393 \, pF$$

PVDF Element Time Constant:

$$t_c = R \cdot C$$

$$= 2.8 \times 10^{12} \, \Omega \cdot 393 \times 10^{-12} \, F$$

$$= 1100 \text{ sec.} = 18.33 \text{ min.}$$

A time constant of greater than 18 minutes is sufficiently large for PVDF to be used effectively in quasi-static loading conditions.

Generalized Piezo Time Constant

The above time constant analysis was generalized and abbreviated as follows:

53

$$t_c = R \cdot C$$

$$= \frac{\rho \cdot T}{A} \cdot \frac{\varepsilon_0 \cdot \varepsilon_r \cdot A}{T}$$

$$= \rho \cdot \varepsilon_0 \cdot \varepsilon_r$$

$$= \rho \cdot \varepsilon$$

So that the time constant could be expressed as follows:

$$t_c = \rho \cdot \varepsilon \qquad\qquad \text{(Equation 4-3)}$$

Where:

Time Constant – t_c (sec)

Element Resistance – R (Ω)

Element Capacitance – C (F)

Volume Resistivity – ρ ($\Omega \cdot$cm or $\Omega \cdot$m)

Element Thickness – T (cm or m)

Element Area – A (cm^2 or m^2)

Permittivity – ε (F/m)

Relative Permittivity – ε_r (unitless)

Permittivity of Free Space – ε_0 (= 8.8542 x 10^{-12} F/m)

54

Equation 4-3 represents a simplification of the time constant expression for PZT-5A3, or more generally for any piezoelectric material, which will be utilized later.

PZT-5A3 / Fluke 87 III DMM System Circuit Properties

The next test in the preliminary test sequence was to verify the circuit properties of the combined PZT-5A3 sample and Fluke 87 III DMM. It was noted during the previous testing that the time constant for the PZT-5A3 / Fluke 87 III DMM system was much lower than the natural time constant for the PZT-5A3. Once the time constant for the PZT-5A3 was verified, this left only significant participation of the DMM in the test measurements as the possible source of the time constant reduction. The DMM participation was calculated in the PZT-5A3 / Fluke 87 III DMM time constant analysis below.

PZT-5A3 Sample Properties (from previous testing):

- $R_P = 9.7 \times 10^9 \ \Omega$

- $C_P = 0.176 \times 10^{-6} \ F$

Fluke 87 III DMM voltage measurement properties (from the Fluke 87 III User's Manual):

- $R_D = 10 \times 10^6 \ \Omega$ (voltage measurement mode)

- $C_D = 100 \times 10^{-12} \ F$

55

The circuit model for the PZT-5A3 element / Fluke 87 III DMM system is shown in Figure 4-2 below.
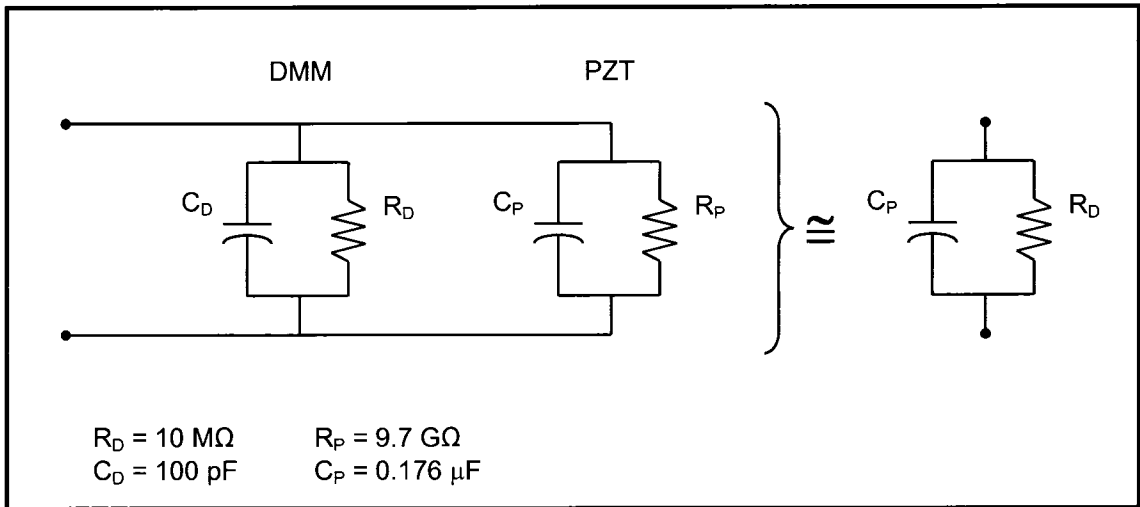
Figure 4-2 – Circuit Model of PZT-5A3 Element and Fluke 87 III DMM

Next, the PZT-5A3 element / Fluke 87 III DMM circuit equivalent capacitance (C_E) and resistance (R_E) were calculated:

$$C_E = C_P + C_D$$

$$= 0.176 \times 10^{-6} F + 100 \times 10^{-12} F$$

$$= 0.1761 \times 10^{-6} F$$

$$R_E = \frac{R_P \cdot R_D}{R_P + R_D}$$

$$= \frac{9.7 \times 10^9 \Omega \cdot 10 \times 10^6 \Omega}{9.7 \times 10^9 \Omega + 10 \times 10^6 \Omega}$$

56

$$= 9.99 \times 10^6 \, \Omega$$

The PZT-5A3 element / Fluke 87 III DMM equivalent circuit model is shown in Figure 4-3 below.
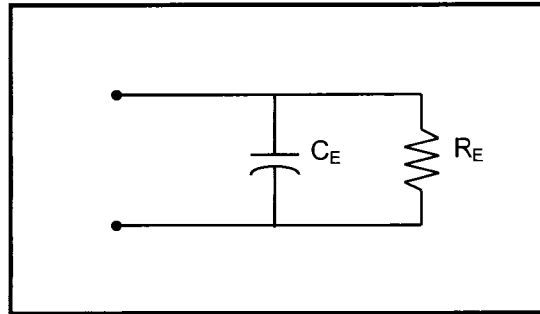
Figure 4-3 – Equivalent Circuit Model of PZT-5A3 Element and Fluke 87 III DMM

The time constant (t_c) for the equivalent PZT-5A3 element / Fluke 87 III DMM circuit is calculated below:

$$t_c = C_E \cdot R_E$$

$$= 0.1761 \times 10^{-6} F \cdot 9.99 \times 10^6 \, \Omega$$

$$= 1.76 \, \text{sec}$$

As is shown in the above analysis, because of the high internal resistance of the piezoceramic elements, the measurement device (in this case the Fluke 87 III DMM) played a significant role in the test setup. Instead of being a passive element whose

57

contribution could be ignored, the DMM lowered the time constant from almost a half-hour to less than 2 seconds. This result is significant, and must be properly accounted for in all testing of this nature with piezoelectrics, as they all tend to have high internal resistances.

PZT-5A3 Electrical Lead Attachment

Several tests were run to determine the best way to attach electrical lead wires to the PZT-5A3 samples. There were concerns about the thickness of the lead wire attachment solder bead, and that the soldering process could damage the PZT sample. Initial testing of the capacitance before and after bonding of the lead wires led to the following conclusions:

1. Care should be taken to prevent solder flux from bridging the top and bottom of the PZT-5A3 element. When this happened, the capacitance measurements varied significantly (both lower and higher values). Cleaning the flux from the PZT element with alcohol and lint free wipes resolved this issue.

2. PZT-5A3 sample #4 was deliberately broken at approximately 2/3 of its length to see if this changed the measured capacitance. According to Equation 4-2, the capacitance should go down due to the reduced surface area. However, this was not what occurred. Instead, the measured capacitance increased. It is believed that this increase was due to PZT damage at the fracture site.

3. Long duration soldering of the PZT-5A3 sample with a soldering iron set at 710° F (376.7° C) didn't result in a change in the measured capacitance. Thus, it

58

is not likely that heat from the soldering iron during a typical lead attachment solder causes damage or de-poling.

Thermometer and Thermocouple Calibration and Verification

To support the research primary testing, the thermocouples and thermometers used in the research were calibrated and verified over the expected test temperature range ($30°$ F – $150°$ F, $-1.1°$ C – $65.6°$ C) before use. Table 4-5 below gives a summary of the various temperatures, meters tested, and results of the initial verification testing.

Temperatures:

- Glass of water and ice - with mostly ice (calibrated, $32°$ F / $0°$ C)

- Optical table surface in lab (room temperature, not calibrated, but stable)

- Heater setup with bare Al block (not calibrated, targeting $150°$ F / $65.6°$ C)

- Boiling water (calibrated, $\sim 212°$ F / $100°$ C, dependent on barometric pressure & elevation – see corrections following Table 4-5)

Thermometers:

- Grey Craftsman Professional 82357

- Red Craftsman 82309

- Omega HH12A Serial #600709, (#1), AFWL EMAS #A051122

- Omega HH12A Serial #600713, (#2), AFWL EMAS #A051123

59

Table 4-5 – Thermometer Variation Measurements

Thermometer*	Reading in Glass of Ice / Water (32° F / 0° C)	Reading on Optical Table Metal Surface (Room Temp.)	Reading on Al Block on Heaters (~ 150° F / 65.6° C)	Reading in Boiling Water** (~ 202° F / 94.4° C)
Grey Craftsman Professional 82357	31.3° F / -0.4° C	69.1° F / 20.6° C	150.2° F / 65.7° C	201.4° F / 94.1° C
Red Craftsman 82309	31° F / -0.6° C	68° F / 20.0° C	148° F / 64.4° C	199° F / 92.8° C
Omega HH12A #1, Ch. #1	30.9° F / -0.6° C	69.4° F / 20.8° C	149.9° F / 65.5° C	202° F / 94.4° C
Omega HH12A #1, Ch. #2	30.9° F / -0.6° C	69.6° F / 20.9° C	150.0° F / 65.6° C	202° F / 94.4° C
Omega HH12A #2, Ch. #1	32.5° F / 0.3° C	71.0° F / 21.7° C	151.7° F / 66.5° C	203° F / 95.0° C
Omega HH12A #2, Ch. #2	32.6° F / 0.3° C	71.1° F / 21.7° C	151.6° F / 66.4° C	204° F / 95.6° C

*All tests summarized in this table use Omega TC #1 as the measurement device.

**The boiling point of water is dependent on atmospheric pressure and elevation. The following is a summary of the appropriate atmospheric pressure and elevation corrections at the time of the testing:

Atmospheric Pressure Correction:

- Barometric pressure at the time of the test = 29.71 in. Hg. (100,610 Pa)

  (from Weather Channel, www.weather.com, for ABQ Sunport)

- Boiling point = 49.161 * Ln (in. Hg.) + 44.932 (from Biggreenegg.com)

  = 49.161 * Ln (29.71) + 44.932

  = 211.6° F (99.8° C) (Δ = -0.4° F)

Altitude Correction:

- Altitude = 5355 feet (ABQ Sunport runway elevation)

- Pressure (in. Hg.) = 29.921 * [1 - 6.8753×10-6 * Altitude(feet)] ^ 5.2559

  = 29.921 * (1 - 6.8753×10-6 * 5355) ^ 5.2559

  = 24.567 In. Hg. (83,193 Pa)

- Boiling point of water (°F) = 49.161 * ln (in. Hg.) + 44.932

  = 49.161 * ln (24.567) + 44.932

  = 202.3° F (94.6° C)

61

Atmospheric Pressure and Altitude Correction:

- Boiling point of water (°F) = 202.3° F – 0.4° F

$$= 201.9° F (94.4° C)$$

Check of Type K Thermocouples

Next, each of the type K thermocouples used in the present research were tested in the same cup of ice water using the same digital multimeter (the Craftsman 82357) to determine the inherent variation in the type K thermocouples. The results of this testing are given in Table 4-6 below.

Table 4-6 – Type K Thermocouple Variation Measurements

Thermocouple	Reading in Glass of Ice / Water (32° F / 0° C)	Reading on Optical Table Metal Surface (Room Temp.)
Omega #1	31.6° F / -0.2° C	70.3° F / 21.3° C
Omega #2	31.6° F / -0.2° C	70.1° F / 21.2° C
Omega #3	31.6° F / -0.2° C	70.4° F / 21.3° C
Omega #4	31.6° F / -0.2° C	70.2° F / 21.2° C
Lab #1	31.4° F / -0.3° C	70.4° F / 21.3° C
Lab #3	31.4° F / -0.3° C	70.5° F / 21.4° C
Lab #4	31.4° F / -0.3° C	70.5° F / 21.4° C
Ertco Mercury Thermometer	0.3° C	20.3° C

62

Results of Initial Thermocouple and Thermometer Verification Testing

The results of the thermocouple and thermometer verification testing were as follows:

1. Referencing Table 4-6, the thermocouple lots (i.e. Omega leads and Lab leads) tended to give the same readings. This was shown by the fact that the standard deviation for the thermocouple lots (taken separately) in ice water in Table 4-6 was zero.

2. The standard deviation on the optical table readings (considering all of the thermocouples) was 0.14° F (0.08° C).

3. Referencing Table 4-5, the Craftsman 82309 thermometer (DMM) wasn't used further – it was definitely biased 1 - 3° F (0.6 - 1.7° C) low.

4. Referencing Table 4-5, all of the meters exhibited a definite bias (low or high), depending on their calibration set point, inherent device bias, and natural variation from test to test, but they tracked very well over the working temperature range (30 – 150° F, -1.1 – 65.6° C).

5. For all subsequent temperature data collection, Omega HH12A #600713 (#2), AFWL EMAS #A051123, and Omega thermocouples #3 and #4 were used. Prior to collecting temperature data, a calibration on the Omega HH12A, and Omega thermocouples #3 and #4 was completed (reference the next section).

63

Based on the results of the previous thermocouple and thermometer testing,

Omega HH12A #600713 (#2) thermometer, and Omega thermocouples #3 and #4 were

selected for calibration and use in subsequent testing. The thermometer/thermocouple

calibration used the following reference temperatures:

1. Glass of Ice/Water (mostly ice)

2. Boiling Water

Table 4-7 – Thermometer / Thermocouple Calibration Measurements

Meter	Thermocouple Channel	Ice Water* (°F / °C)	Boiling Water** (°F / °C)
Omega HH12A #600713, AFWL EMAS #A051123	Ch. 1	32.0 / 0.0	203 / 95.0
	Ch. 2	32.0 / 0.0	203 / 95.1

Notes:

*Omega HH12A was calibrated using the front face trip pot adjustment to give exactly

32.0° F / 0.0° C in glass of ice & water.

** The boiling point of water is dependent on atmospheric pressure and elevation. The

following is a summary of the appropriate atmospheric pressure and elevation corrections

at the time of the testing:

64

Atmospheric Pressure Correction:

- Barometric pressure at the time of the test = 29.64 in. Hg. (100,373 Pa)

  (from Weather Channel, www.weather.com, for ABQ Sunport)

- Boiling point = 49.161 * Ln (in. Hg.) + 44.932 (from Biggreenegg.com)

  $= 49.161 * Ln (29.64) + 44.932$

  $= 211.54° \text{ F } (99.74° \text{ C}) (\Delta = -0.46° \text{ F})$

Altitude Correction:

- Altitude = 5355 feet (ABQ Sunport runway elevation)

- Pressure (in. Hg.) = $29.921 * [1 - 6.8753 \times 10^{-6} * \text{Altitude(feet)}] \wedge 5.2559$

  $= 29.921 * (1 - 6.8753 \times 10^{-6} * 5355) \wedge 5.2559$

  $= 24.567 \text{ In. Hg. } (83,193 \text{ Pa})$

- Boiling point of water (°F) = 49.161 * ln (in. Hg.) + 44.932

  $= 49.161 * \ln (24.567) + 44.932$

  $= 202.3° \text{ F } (94.6° \text{ C})$

65

Atmospheric Pressure and Altitude Correction:

- Boiling point of water (°F) = 202.3° F − 0.46° F

$$= 201.8° F (94.3° C)$$

Thus, calibration of the Omega HH12A #600713 (#2) thermometer, and Omega thermocouples #3 and #4 at freezing resulted in a 1.2° F (0.7° C) error at the boiling point of water.

Verification of PZT-5A3 Sample to Al Substrate Bonding Process

In order to achieve strain transfer from the aluminum substrate to the PZT, the two were bonded (i.e. glued) together. There are several important trades to note in the bonding process: First, the glue (in the final satellite application, not in the specific test setup of the present research) should be electrically insulative (i.e. can't ground); and second, the bond line should be as thin as possible (to transmit strain), but thick enough to maintain electrical isolation and support the bottom side PZT electrical contact (between the bottom of the PZT and the aluminum) in the final assembly. Options for accomplishing the electrical contact included a copper tab or soldering of fanned out lead wire. The most likely optimal solution to satisfy these requirements would be to purchase COTS PZT packages with leads and kapton tape outer packaging. However, this was not required for the present research, primarily because electrical isolation was not required.

66

Three different glues (Plastic Fusion, M-Bond 200, and Superglue) were tested to determine their compatibility with the above requirements, as well as the requirements associated with the overall test configuration, most notably strain to failure capability, thermal operating range, and ease of use. During the course of this testing the capacitance and resistance of the PZT element were verified both pre and post bond. Several practical recommendations were noted during this practice bonding:

1. If silver paste is used for the PZT electrical contacts, care should be taken to prevent the silver paste from flowing to bridge the top/bottom of the PZT element.

2. Tape should be used (and removed after glue cure) along the edge of the PZT sample to prevent glue from bridging the top and bottom of the PZT element.

3. Plastic Fusion adhesive adheres to kapton tape much better than the Teflon tape.

4. Superglue is a remarkably good electrical insulator – even in a thin bond line. If used, it needs to be kept off of the copper tabs during bonding.

5. The copper tape adhesive in not sufficient to get a good, reliable electrical bond. However, the resistance with silver paste goes down to an acceptable level once the silver paste sets (~1 Ω after 30 minutes; 0.8 Ω after 5 days). Soldering is definitely a more reliable solution if a thin enough solder joint can be achieved.

During the process of bonding the PZT-5A3 sample to the aluminum substrate, the PZT-5A3 sample capacitance dropped from ~ 0.176 μF to ~ 0.134 μF. Initially, this was incorrectly assumed to be the result of damage to the PZT during bonding. However, it was later discovered that this was a natural consequence of the change in the

PZT boundary condition from a mechanically free condition to more of a mechanically clamped condition. This results in a change in the ε_r term in Equation 4-2 (i.e. from ε_r^T to a value approaching ε_r^S). The change in PZT element capacitance with bonding phenomenon is discussed in detail in Chapter 5, Section "Capacitance Changes in PZT-5A3 Elements with Bonding".

In addition, it was also discovered during the course of this testing that the PZT capacitance measurements made with the Fluke 87 III DMM tend to be higher than those measured with the Hewlett Packard (HP) 4261A LCR meter. This was due to damping losses in the HP 4261A LCR meter. For this reason, the Fluke 87 III DMM capacitance measurements are more accurate, and were therefore used for subsequent analysis and testing.

The results of the preliminary bonding testing were that the Plastic Fusion worked best in the PZT/Al bonding application, primarily because it provided a slightly thicker bond line, which supported the PZT bottom side electrical contact while maintaining excellent strain transfer. The M-Bond 200 and Superglue had good bond and strain transfer, and could likely be used successfully in combination with kapton tape and a sufficiently thin PZT bottom side electrical contact.

Thermal Calibration of Strain Gages and PZT-5A3/Al Samples

In order to be able to accurately quantify the actual strains in the aluminum substrate and PZT-5A3 sample during heating or cooling, separate testing was first performed to calibrate the strain gage outputs to the actual strains in the PZT/Al samples (reference Vishay Measurements Group Tech Notes #TN-513-1 and #TN-504-1). As

68

will be seen later in this section, for proper baselining of the strain measurements, it is

important that the strain gages are applied to the aluminum and PZT at room temperature

(~ 70° F / 21.1° C), which was done. It is also important that the heating (or cooling) of

the PZT-5A3 sample bonded to the aluminum substrate testing is accomplished with the

same strain gage lot, 6061-T6 Al substrate and PZT-5A3 samples, or portions of the

strain gage calibration test will need to be redone. This duplication of the calibration

testing was not required in the present research because all of the above items remained

the same throughout the testing sequence.

Thermal Calibration of Strain Gages and PZT-5A3/Al Samples Test Setup

A diagram of the thermal calibration of the strain gages to the aluminum substrate

and PZT-5A3 samples test setup is shown in Figure 4-4.

69
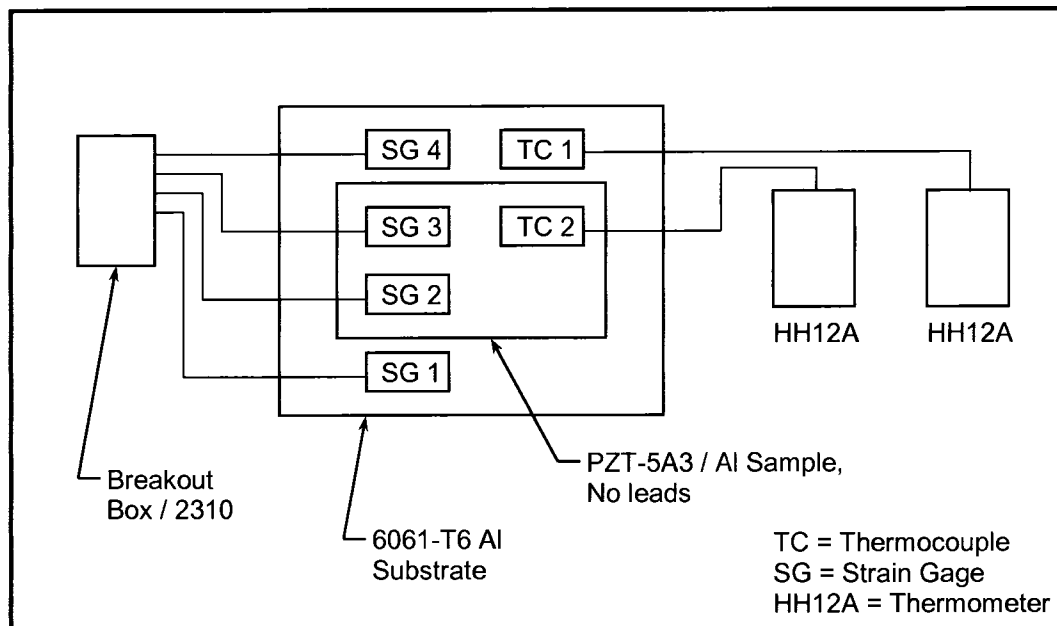
Figure 4-4 – Thermal Calibration of Strain Gages and PZT-5A3 / Aluminum Samples Test Setup

Referencing Figure 4-4, the following is a more complete description of the test components:

- Strain Gage #1, (SG 1) / 350.3 Ω/ Box Ch. 1 / 2310 Ch. 1 / on Al

- Strain Gage #2, (SG 2) / 350.2 Ω/ Box Ch. 2 / 2310 Ch. 2 / on PZT

- Strain Gage #3, (SG 3) / 350.2 Ω/ Box Ch. 3 / 2310 Ch. 3 / on PZT

- Strain Gage #4, (SG 4) / 350.3 Ω/ Box Ch. 5 / 2310 Ch. 4 / on Al

- Thermocouple #1, (TC 1) / on Al / Omega TC #3 / HH12A #600713, Ch. 1

- Thermocouple #2, (TC 2) / on PZT / Omega TC #4 / HH12A #600709, Ch. 1

70

Utilizing the test setup in Figure 4-4, four tests were performed: two tests from 70° F (21.1° C) to 150° F (65.6° C), and a second set of two tests from 70° F (21.1° C) to 30° F (-1.1° C), while capturing the 4 strain gage and thermocouple readings at 5° F (2.8° C) increments. This provided all of the required data to evaluate the repeatability of the test setup (assuming the two data sets from the two pairs of similar tests matched well), and to thermally calibrate the strain gage outputs to actual strains in the aluminum substrate and PZT-5A3 samples during heating or cooling.
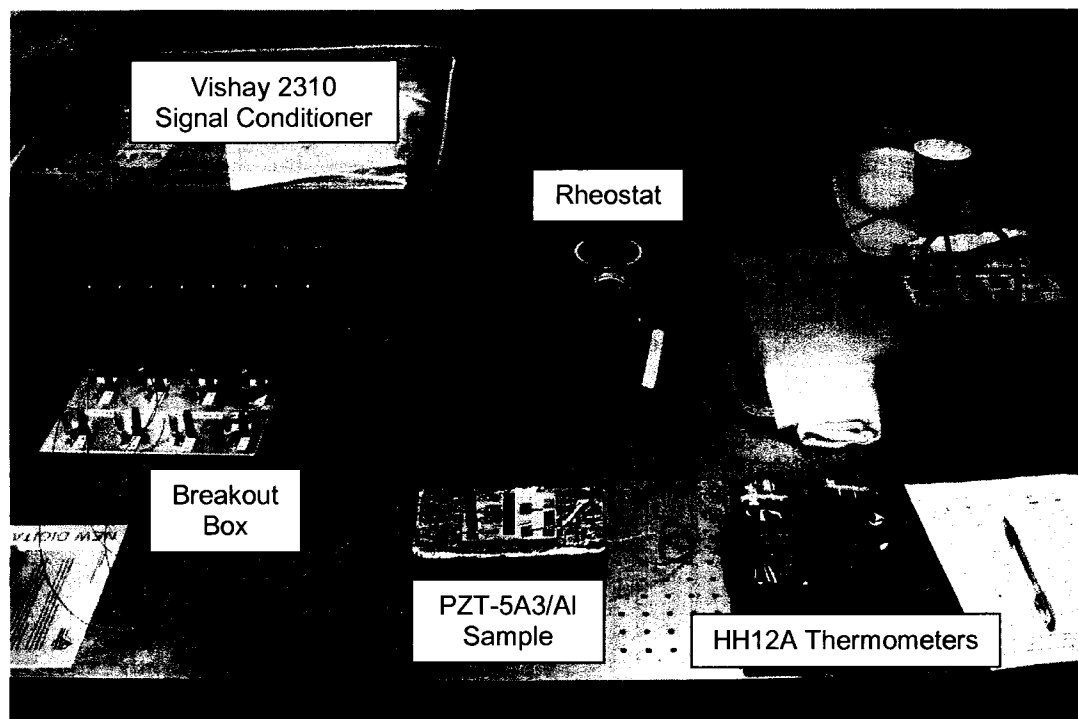
Figure 4-5 – Picture of Thermal Calibration of Strain Gages and PZT-5A3/Al Samples Heating Test Setup

71

- Test Date: 5/8/06

- Begin Test: 3:08 PM

- End Test: 5:20 PM

Table 4-8 – Thermal Calibration Data Capture – Heating #1 from 70° F (21.1° C) – 150° F (65.6° C)

Nominal Temp (°F / °C)	SG 1, on Al (με)	SG 2, on PZT (με)	SG 3, on PZT (με)	SG 4, on Al (με)	TC 1, on Al (°F / °C)	TC 2, on PZT (°F / °C)
70 / 21.1	0	0	0	0	71.7 / 22.1	70.5 / 21.4
75 / 23.9	1	-28	-32	2	75.1 / 23.9	73.9 / 23.3
80 / 26.7	2	-80	-85	2	80.1 / 26.7	78.8 / 26.0
85 / 29.4	2	-131	-136	3	85.1 / 29.5	83.8 / 28.8
90 / 32.2	2	-183	-187	3	90.1 / 32.3	88.7 / 31.5
95 / 35	2	-238	-241	4	95.1 / 35.1	93.6 / 34.2
100 / 37.8	1	-290	-293	3	100.1 / 37.8	98.4 / 36.9
105 / 40.6	0	-343	-346	3	105.1 / 40.6	103.4 / 39.7
110 / 43.3	0	-394	-395	2	110.1 / 43.4	108.1 / 42.3
115 / 46.1	-1	-445	-446	1	115.1 / 46.2	113.2 / 45.1
120 / 48.9	-3	-497	-498	0	120.1 / 48.9	118.1 / 47.8
125 / 51.7	-4	-547	-550	-1	125.1 / 51.7	123.1 / 50.6
130 / 54.4	-7	-598	-602	-2	130.1 / 54.5	128.0 / 53.3
135 / 57.2	-10	-657	-660	-4	135.1 / 57.3	132.9 / 56.1

72

Nominal Temp (°F / °C)	SG 1, on Al (με)	SG 2, on PZT (με)	SG 3, on PZT (με)	SG 4, on Al (με)	TC 1, on Al (°F / °C)	TC 2, on PZT (°F / °C)
140 / 60	-13	-709	-711	-6	140.1 / 60.1	137.8 / 58.8
145 / 62.8	-16	-762	-766	-7	145.1 / 62.8	142.8 / 61.6
150 / 65.6	-18	-814	-816	-8	150.1 / 65.6	147.5 / 64.2
Back to 70	-3	66	68	2	72.2 / 22.3	71.0 / 21.7

Notes:

1. A plastic Tupperware cover was utilized to limit the effect of the building air conditioning on the PZT/Al sample.

2. Heating of the PZT/Al sample was accomplished using the heater / rheostat setup shown in Figure 4-5. The rheostat setting was adjusted slowly to allow the sample to come to equilibrium at each of the 5° F (2.8° C) test data capture increments.

Thermal Calibration Data Capture – Cooling #1 from 70°F (21.1°C) – 30°F (-1.1°C)

- Test Date: 5/9/06

- Begin Test: 8:15 AM

- End Test: 9:00 AM

73

Table 4-9 – Thermal Calibration Data Capture – Cooling #1 from 70° F (21.1° C) – 30° F (-1.1° C)

Nominal Temp (°F / °C)	SG 1, on Al (με)	SG 2, on PZT (με)	SG 3, on PZT (με)	SG 4, on Al (με)	TC 1, on Al (°F / °C)	TC 2, on PZT (°F / °C)
70 / 21.1	0	0	0	0	70.4 / 21.3	69.4 / 20.8
65 / 18.3	0	38	43	3	65.4 / 18.6	64.5 / 18.1
60 / 15.6	-1	92	96	1	60.4 / 15.8	59.9 / 15.5
55 / 12.8	-3	145	147	-1	55.4 / 13	55.0 / 12.8
50 / 10	-6	213	203	-1	50.4 / 10.2	50.0 / 10
45 / 7.2	-9	255	248	-6	45.4 / 7.4	45.3 / 7.4
40 / 4.4	-12	303	295	-9	40.4 / 4.7	40.4 / 4.7
35 / 1.7	-16	305	294	-15	35.4 / 1.9	35.8 / 2.1
30 / -1.1	-22	307	298	-21	30.4 / -0.9	31.0 / -0.6
Back to 70	1	-85	-74	0	70.4 / 21.3	69.3 / 20.7

Notes:

1. Cooling of the PZT/Al sample was accomplished using an aluminum block from a freezer as shown in Figures 4-6 and 4-7. Variable quantities of rags and bubble wrap were used to control the cooling rate of the PZT/Al sample to achieve more or less steady state 5° F (2.8° C) data capture points.

74

Figure 4-6 – Thermal Calibration Cooling Test Configuration
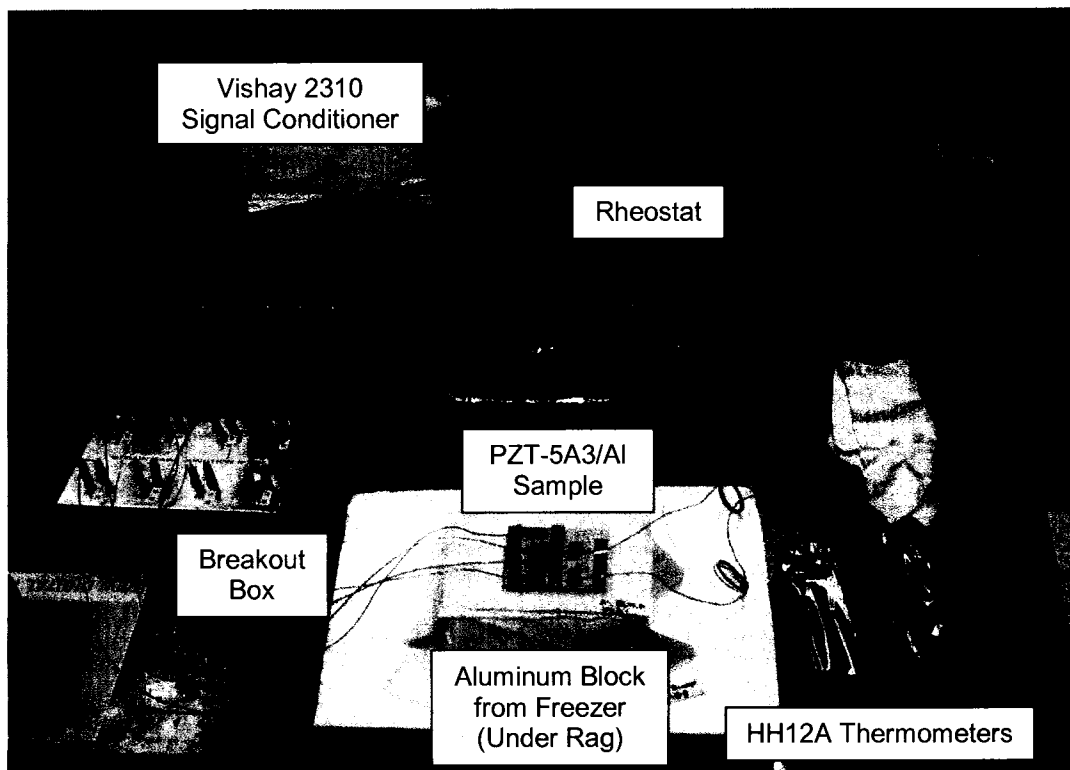
Figure 4-7 – Picture of Thermal Calibration of Strain Gages and PZT-5A3/Al

Samples Cooling Test Setup

75

- Test Date: 5/9/06

- Begin Test: 2:50 PM

- End Test: 5:20 PM

Table 4-10 – Thermal Calibration Data Capture – Heating #2 from 70° F (21.1° C) – 150° F (65.6° C)

Nominal Temp (°F / °C)	SG 1, on Al (με)	SG 2, on PZT (με)	SG 3, on PZT (με)	SG 4, on Al (με)	TC 1, on Al (°F / °C)	TC 2, on PZT (°F / °C)
70 / 21.1	0	0	0	0	69.8 / 21.0	68.7 / 20.4
75 / 23.9	1	-46	-59	2	75.0 / 23.9	73.8 / 23.2
80 / 26.7	2	-99	-110	3	80.0 / 26.7	78.8 / 26.0
85 / 29.4	2	-151	-163	3	85.0 / 29.4	83.6 / 28.7
90 / 32.2	2	-204	-214	3	90.0 / 32.2	88.5 / 31.4
95 / 35	1	-258	-268	3	95.0 / 35.0	93.5 / 34.2
100 / 37.8	1	-310	-320	3	100.0 / 37.8	98.4 / 36.9
105 / 40.6	0	-366	-374	2	105.0 / 40.6	103.3 / 39.6
110 / 43.3	0	-416	-426	1	110.0 / 43.3	108.1 / 42.3
115 / 46.1	-1	-470	-479	1	115.0 / 46.1	113.2 / 45.1
120 / 48.9	-3	-522	-531	0	120.0 / 48.9	118.1 / 47.8
125 / 51.7	-5	-566	-575	-1	125.0 / 51.7	123.0 / 50.6
130 / 54.4	-6	-623	-630	-2	130.0 / 54.4	127.6 / 53.1
135 / 57.2	-8	-673	-681	-3	135.0 / 57.2	132.7 / 55.9

76

Nominal Temp (°F / °C)	SG 1, on Al (με)	SG 2, on PZT (με)	SG 3, on PZT (με)	SG 4, on Al (με)	TC 1, on Al (°F / °C)	TC 2, on PZT (°F / °C)
140 / 60	-9	-715	-725	-4	140.0 / 60.0	137.2 / 58.4
145 / 62.8	-10	-769	-776	-5	145.0 / 62.8	142.5 / 61.4
150 / 65.6	-12	-827	-832	-6	150.0 / 65.6	147.4 / 64.1
Back to 70	2	63	58	-5	70.7 / 21.5	69.2 / 20.7

Notes:

1. A plastic Tupperware cover was utilized to limit the effect of the building air conditioning on the PZT/Al sample.

2. Heating of the PZT/Al sample was accomplished using the heater / rheostat setup shown in Figure 4-5. The rheostat setting was adjusted slowly to allow the sample to come to equilibrium at each of the 5° F (2.8° C) test data capture increments.

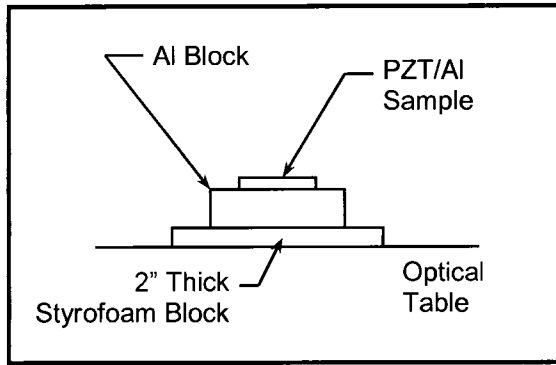*Thermal Calibration Data Capture – Cooling #2 from 70 °F (21.1 °C) – 30 °F (-1.1 °C)*

- Test Date: 5/10/06

- Begin Test: 2:00 PM

- End Test: 2:45 PM

Table 4-11 – Thermal Calibration Data Capture – Cooling #2 from 70° F (21.1° C) – 30° F (-1.1° C)

Nominal Temp (°F / °C)	SG 1, on Al (με)	SG 2, on PZT (με)	SG 3, on PZT (με)	SG 4, on Al (με)	TC 1, on Al (°F / °C)	TC 2, on PZT (°F / °C)
70 / 21.1	0	0	0	0	70.0 / 21.1	69.0 / 20.6
65 / 18.3	0	36	39	0	65.0 / 18.3	64.1 / 17.8
60 / 15.6	-2	91	92	0	60.0 / 15.6	59.3 / 15.2
55 / 12.8	-4	146	146	-3	55.0 / 12.8	54.3 / 12.4
50 / 10	-7	211	200	-8	50.0 / 10	49.6 / 9.8
45 / 7.2	-9	256	245	-12	45.0 / 7.2	44.9 / 7.2
40 / 4.4	-13	311	295	-18	40.0 / 4.4	39.9 / 4.4
35 / 1.7	-18	332	313	-23	35.0 / 1.7	35.1 / 1.7
30 / -1.1	-23	344	329	-29	30.0 / -1.1	30.3 / -0.9
Back to 70	0	-49	-49	-3	70.0 / 21.1	68.9 / 20.5

Notes:

1. Cooling of the PZT/Al sample was accomplished using an aluminum block from a freezer as shown in Figures 4-6 and 4-7. Variable quantities of rags and bubble wrap were used to control the cooling rate of the PZT/Al sample to achieve more or less steady state 5° F (2.8° C) data capture points.

Thermal Calibration Strain Gage Data Check

As was mentioned previously, the above four data sets are sufficient to perform a valid strain gage thermal calibration only if the data sets are in good agreement. To

78

check this, the four thermal calibration data captures were plotted on a single graph. The extent to which the resulting eight strain gage data sets fall on two curves (one for the aluminum gages, and a second for the PZT gages) gives their level of agreement.
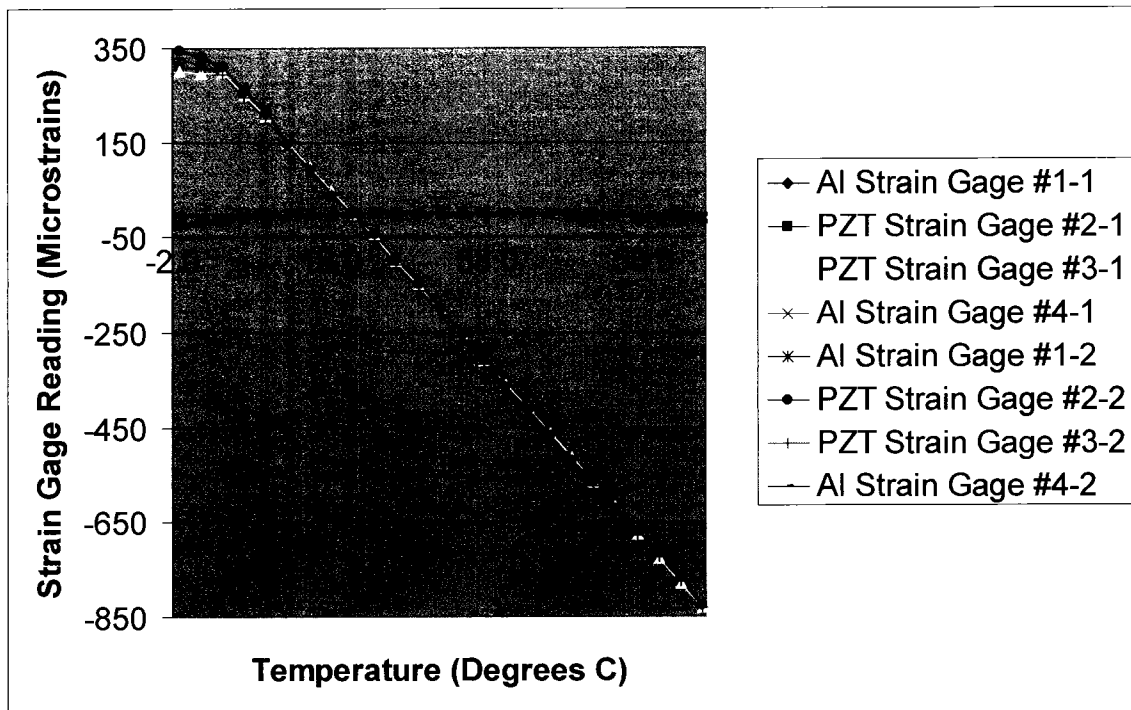
Figure 4-8 – Plot of All Thermal Calibration Strain Gage Data

As can be seen in Figure 4-8 above, with the exception of the PZT data near $0°$ C, the data sets do indeed fall on two curves. The precise reason for the PZT behavior near $0°$ C is not known, but is believed to be due to a non-linear and variable change in the PZT CTE at that temperature. To avoid the PZT behavior and associated uncertainty in the CTE data near freezing, the comparative analysis in Chapter 5 considers only heating cases from room temperature (i.e. 21.1 – 51.7° C). As such, the analysis can proceed with confidence to the strain gage thermal calibration in the next section.

79

<u>Strain Gage Calibration</u>

Using the above data, the strain gages were calibrated through a detailed step-by-step process (given below) such that the strain gage readings were converted to an actual strain in either the aluminum substrate or the PZT-5A3 sample.

1. Take the average aluminum strain gage readings from the testing in the previous section for the temperature range from 30° F (-1.1° C) to 150° F (65.6° C).

2. Utilize MIL-HDBK-5H Figure 3.6.2.0, "Effect of Temperature on the Physical Properties of 6061 Aluminum Alloy", which gives the precise coefficient of thermal expansion (CTE) for 6061 aluminum over the test temperature range, to calculate the Al 6061-T6 thermal (i.e. CTE) strain.

3. Subtract the average aluminum strain gage readings (1) from the Al 6061-T6 CTE strain (2) for each 5° F (2.8° C) temperature increment. This value is the strain gage thermal strain. The corresponding strain gage CTE for each temperature increment can then be calculated by dividing the strain gage thermal strain by the ΔT from the specific temperature increment to 70° F (21.1° C).

4. Take the average PZT-5A3 strain gage readings from the testing in the previous section for the temperature range from 30° F (-1.1° C) to 150° F (65.6° C).

5. Add the average PZT-5A3 strain gage readings (4) to the strain gage thermal strain (3) for each 5° F (2.8° C) temperature increment. This value is the PZT-5A3 thermal strain. The corresponding PZT-5A3 CTE for each temperature increment can then be calculated by dividing the PZT-5A3 thermal strain by the ΔT from the specific temperature increment to 70° F (21.1° C).

80

The preceding procedure represents a complex methodology by which the strain gage output values from the testing were converted to the actual strains in the substrate to which they are bonded (i.e. either aluminum or PZT). This high level of effort was required given the only known thermal behavior was that of the 6061 aluminum substrate as defined in MIL-HDBK-5H. From that baseline, the precise thermal behavior of the strain gages and PZT-5A3 samples was then determined. This thermal behavior data will be used in subsequent sections to precisely correlate the voltage outputs of the PZT-5A3 to a known strain level in both the PZT-5A3 and the aluminum substrate. The results of the above calibration testing/analysis are given in Figures 4-9 and 4-10.
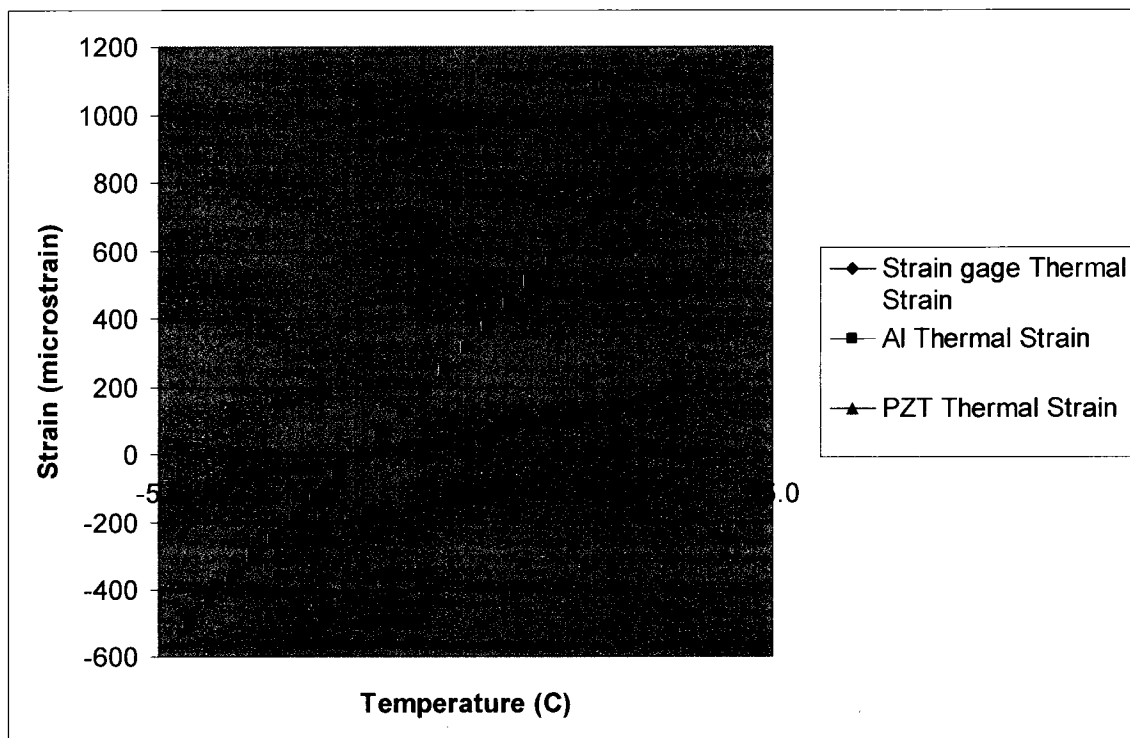
Figure 4-9 – Thermal Calibration Testing Thermal Strains

81

As can be seen in Figure 4-9, the CTE of the strain gages and the 6061-T6 aluminum were almost identical. This is by design, as the type of Vishay strain gages used (type 13) are designed to match the CTE of aluminum. In addition, the CTE for the strain gages and the PZT-5A3 were calculated from the data in Figure 4-9, and are given in Figure 4-10.
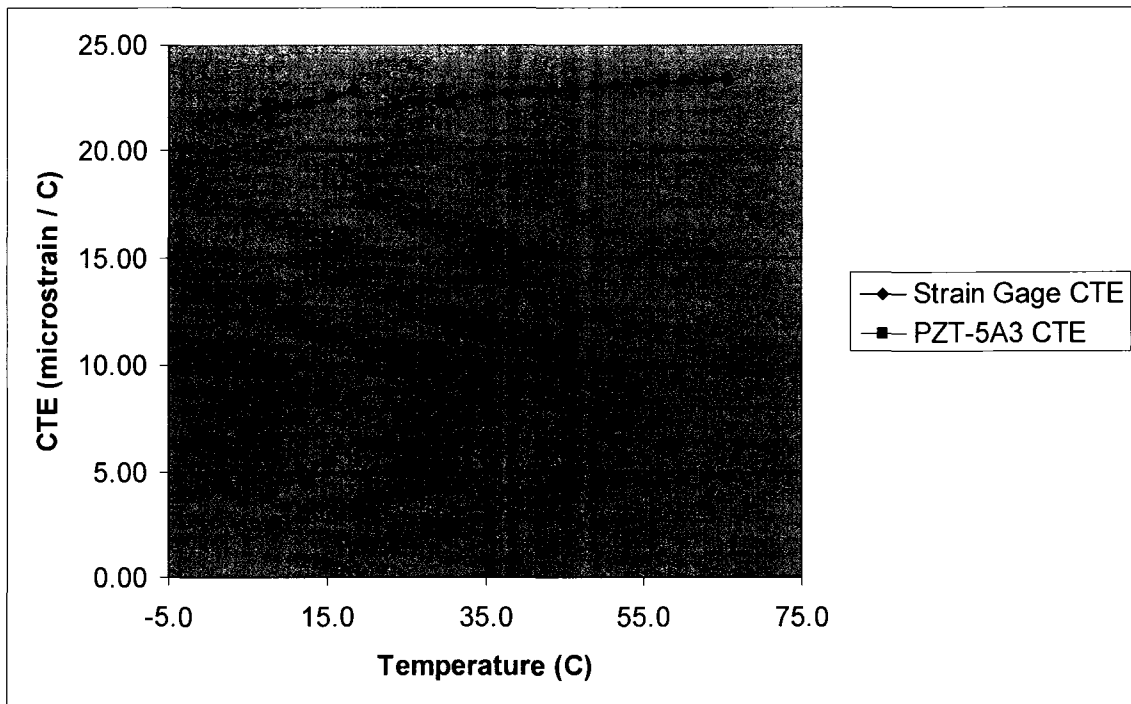
Figure 4-10 – CTE for Vishay Strain Gages and PZT-5A3

In Figure 4-10, the apparent CTE for both aluminum and PZT-5A3 diverges near 70° F (21.1° C). This is the result of the CTE calculation sensitivity to the denominator (i.e. reference temperature – 70° F), and does not represent a true trend.

82

Heating (or Cooling) of PZT-5A3 Sample Bonded to Al Substrate

As was stated previously, the primary test for the present research is the heating

(or cooling) of a PZT-5A3 sample bonded to an aluminum substrate. This type of testing

explores both the low frequency and thermo-electro-mechanical behavior of the

piezoelectric material, which are the focus of the present research.

Closed Circuit Test Setup

The heating/cooling of the PZT-5A3/Al samples began with a series of closed

circuit (on the PZT-5A3 / DMM voltage measurement circuit) tests, which are described

in the following sections, and shown in Figures 4-11 and 4-12.
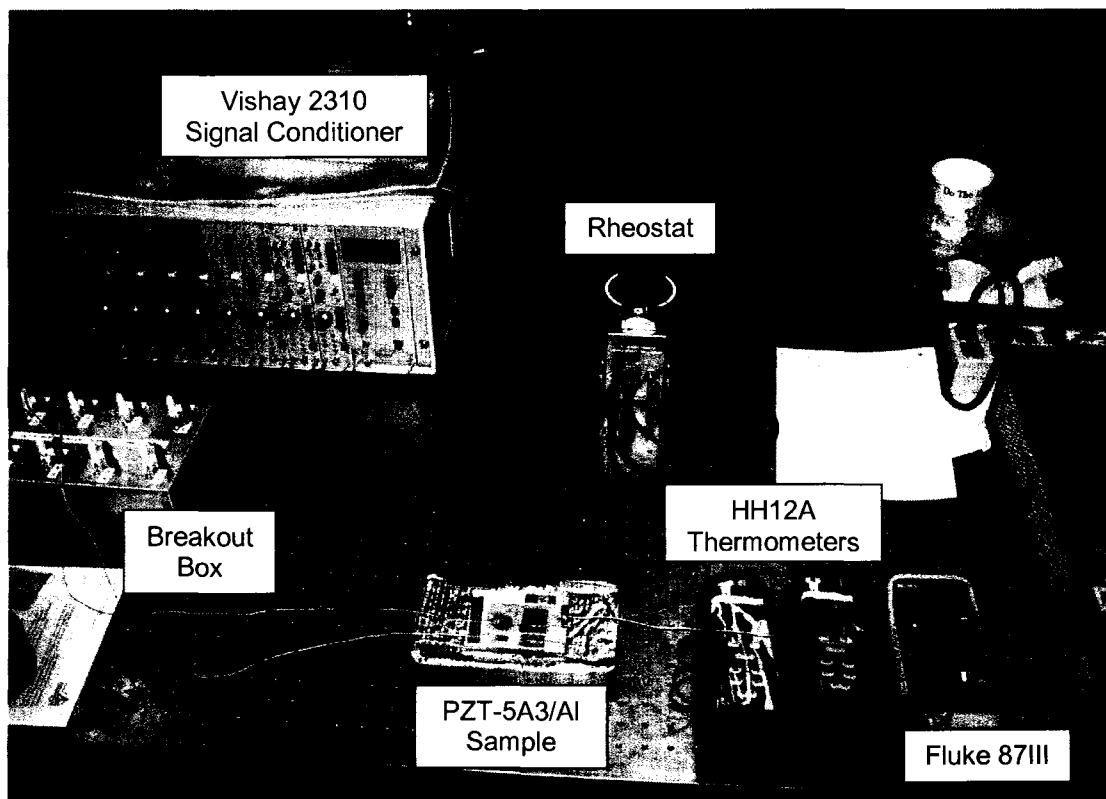
Figure 4-11 – Picture of Closed Circuit Heating or Cooling of PZT/Al Test Setup

83
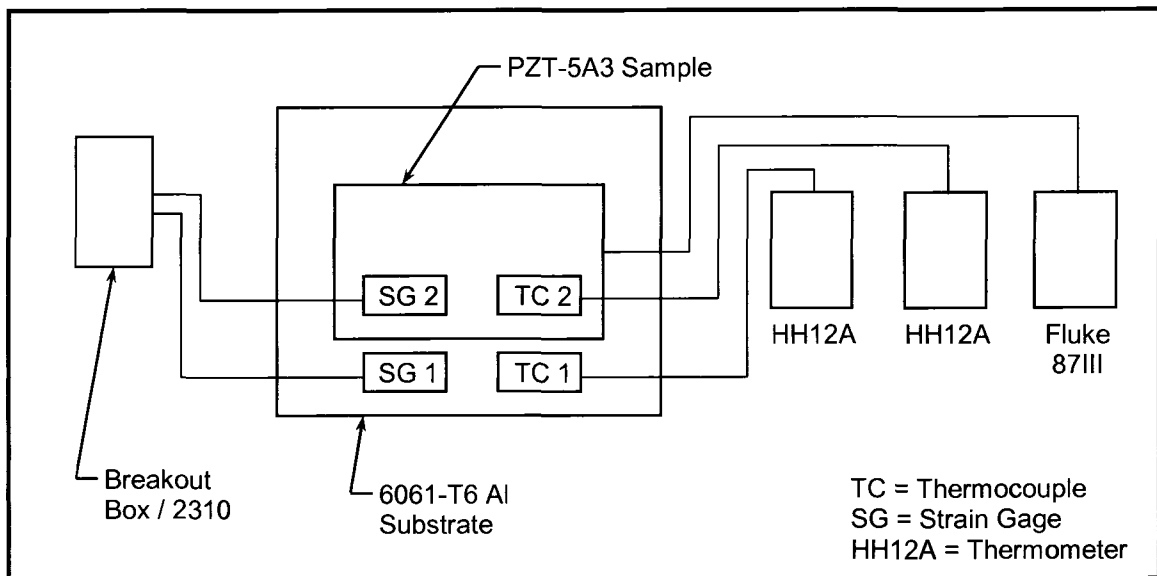
Figure 4-12 – Closed Circuit Heating or Cooling of PZT/Al Test Configuration

In Figure 4-12, the following is a more complete description of select test components:

- Strain Gage #1, (SG 1) / 350.4 Ω / Box Ch. 1 / 2310 Ch. 1 / on Al

- Strain Gage #2, (SG 2) / 350.4 Ω / Box Ch. 2 / 2310 Ch. 2 / on PZT-5A3

- Thermocouple #1, (TC 1) / on Al / Omega TC #3 / HH12A #600713, Ch. 1

- Thermocouple #2, (TC 2) / on PZT-5A3 / Omega TC #4 / HH12A #600709, Ch. 1

- PZT leads to voltage reading on Fluke 87 III DMM

- Strain Gage bonding temperatures $\cong$ 70° F (21.1° C, room temperature)

84

Parts List

The following is a complete parts list for the heating/cooling of PZT/Al samples

test configuration given in Figure 4-12 above.

- PZT-5A3 samples (3.81 cm x 6.35 cm x 0.0254 cm)

- Al Substrate – 6061-T651 (0.3175 cm thick)

- Type K thermocouples (alumel/chrome, ~0.04 mV/°C) - with the standard yellow

  lead adapter attached

- Copper electrical tape (for copper tabs)

- Power Strip – Tripp Lite Isobar Ultra 8 diagnostic surge suppressor

- Green fiberglass insulation block

- 2 x 750 Ω resistive heaters

- Rheostat – Staco Energy Products type 3PNJ20IA

  o Input = 120 V, 50/60 Hz AC

  o Output = 0 – 140 V DC, 2 A, 0.28 kVA

- PZT Adhesive – Super Glue Corp. "Plastic Fusion", P/N 15277

  o Working time = 8 minutes

  o Handling time = 30 minutes

  o Temperature range = -40° F (-40° C) – 250° F (121.1° C)

  o Strength = 3500 psi

- Strain Gages – Vishay Micro-Measurements CEA-13-250UW-350

  o Lot #A59AF815, Batch VF335022

  o Resistance = 350.0 ± 0.3% Ω

85

- o Gage Factor = 2.110 ± 0.5%

- Strain Gage Adhesive – Vishay M-Bond 200 Adhesive

  - o Installation procedure: B-127-14

  - o 60,000 με capability

  - o Operating temperature range: -25° F (-31.7° C) – 150° F (65.6° C)

Closed Circuit Heating Test

Table 4-12 below gives the test results of the closed circuit heating of a PZT-5A3 sample bonded to an aluminum substrate. What is meant by closed circuit is that the Fluke 87 III DMM was recording the voltage output from the PZT-5A3 sample continuously throughout the test. This data (Table 4-12), as well as the rapid heating (Table 4-13) and rapid cooling (Table 4-14) data will be used to attempt to quantify the time constant in the PZT-5A3 / Fluke 87 III DMM system.

Table 4-12 – Closed Circuit Heating of PZT/Al Sample

Time	SG 1, on Al (με)	SG 2, on PZT (με)	TC 1, on Al (°F / °C)	TC 2, on PZT (°F / °C)	PZT Voltage (V)
3:37:00	0	0	70.7 / 21.5	69.7 / 20.9	-0.020
3:38:00	0	0	72.0 / 22.2	70.7 / 21.5	-0.37
3:39:00	-3	-3	74.8 / 23.8	73.6 / 23.1	-0.49
3:40:00	-6	-7	78.6 / 25.9	76.9 / 24.9	-0.56
3:41:00	-9	-9	82.2 / 27.9	80.6 / 27.0	-0.65
3:42:00	-10	-11	85.9 / 29.9	84.2 / 29.0	-0.65

86

Time	SG 1, on Al ($\mu\varepsilon$)	SG 2, on PZT ($\mu\varepsilon$)	TC 1, on Al (°F / °C)	TC 2, on PZT (°F / °C)	PZT Voltage (V)
3:43:00	-14	-14	89.2 / 31.8	87.3 / 30.7	-0.65
3:44:00	-16	-16	92.4 / 33.6	90.2 / 32.3	-0.70
3:45:00	-18	-19	95.4 / 35.2	93.2 / 34.0	-0.65
3:46:00	-20	-21	98.2 / 36.8	95.8 / 35.4	-0.65
3:47:00	-23	-23	100.9 / 38.3	98.4 / 36.9	-0.59
3:48:00	-26	-26	103.4 / 39.7	100.9 / 38.3	-0.57
3:49:00	-28	-29	105.9 / 41.1	103.4 / 39.7	-0.52
3:50:00	-30	-32	107.7 / 42.1	105.0 / 40.6	-0.52
3:51:00	-31	-34	110.0 / 43.3	106.9 / 41.6	-0.48
3:52:00	-33	-39	112.0 / 44.4	109.0 / 42.8	-0.35*
3:53:00	-32	-42	112.4 / 44.7	109.5 / 43.1	0.08
3:54:00	-29	-39	111.1 / 43.9	108.3 / 42.4	0.22
3:55:00	-27	-36	109.2 / 42.9	106.3 / 41.3	0.27
3:56:00	-23	-33	107.1 / 41.7	104.6 / 40.3	0.29
3:57:00	-21	-29	105.2 / 40.7	102.4 / 39.1	0.30
3:58:00	-19	-25	103.4 / 39.7	100.5 / 38.1	0.30
3:59:00	-16	-23	101.3 / 38.5	98.9 / 37.2	0.29
4:00:00	-14	-20	99.8 / 37.7	97.3 / 36.3	0.26
4:01:00	2	-8	85.3 / 29.6	83.8 / 28.8	1.72[†]
4:02:00	4	1	77.6 / 25.3	76.3 / 24.6	0.68
4:03:00	5	3	75.0 / 23.9	73.9 / 23.3	0.34
4:04:00	5	4	74.0 / 23.3	72.8 / 22.7	0.21

87

Time	SG 1, on Al ($\mu\varepsilon$)	SG 2, on PZT ($\mu\varepsilon$)	TC 1, on Al (°F / °C)	TC 2, on PZT (°F / °C)	PZT Voltage (V)
4:05:00	6	5	73.3 / 22.9	72.2 / 22.3	0.13
4:06:00	6	5	72.8 / 22.7	71.8 / 22.1	0.09
4:07:00	6	6	72.6 / 22.6	71.4 / 21.9	0.06
4:15:00	7	8	71.0 / 21.7	70.0 / 21.1	0.001

Notes:

1. Prior to the start of the test, the heat was turned on, and the rheostat was set to the 5th dot (heaters not preheated).

* The heat was turned off at approximately 3:51:50, and subsequent reading taken approximately 10 seconds after heat turnoff.

† The PZT/Al sample was placed on the optical table at approximately 4:00:50; the PZT measured voltage went up to 2+ volts immediately after the sample was placed on the optical table.

Closed Circuit Rapid Heating Test

Table 4-13 gives the results of the closed circuit rapid heating of a PZT-5A3 sample bonded to an aluminum substrate test. What is meant by closed circuit is that the Fluke 87 III DMM was recording the voltage output from the PZT-5A3 sample continuously throughout the test. For this test, the rheostat was set to the 6th dot and the heater temperature was measured at 160° F (71.1° C). In agreement with previous

88

testing, the temperature drop to the aluminum sample (at equilibrium) was ~145° F

(62.8° C).

Table 4-13 – Closed Circuit Rapid Heating of PZT/Al Sample

Time	SG 1, on Al (με)	SG 2, on PZT (με)	TC 1, on Al (°F / °C)	TC 2, on PZT (°F / °C)	PZT Voltage (V)
9:49:00	0	0	70.6 / 21.4	69.6 / 20.9	-0.014
9:54:00	-59	-91	133.6 / 56.4	129.4 / 54.1	-0.46
9:56:00	-65	-130	139.4 / 59.7	135.0 / 57.2	-0.25
9:56:50	-	-	-	-	6.6
9:58:30	0	-58	84.0 / 28.9	82.3 / 27.9	1.34
10:05:00	3	-50	73.2 / 22.9	72.0 / 22.2	0.08

Notes:

1. The sample was placed on the optical table for cool down at 9:56:30.

2. Observed a 4-5° F (2.2-2.8° C) ΔT on heating between TC #1 and TC #2.

3. The PZT voltage peaked at approximately -5 V after the sample was initially placed on the heaters.

Closed Circuit Rapid Cooling Test

Table 4-14 gives the results of the closed circuit rapid cooling of a PZT-5A3 sample bonded to an aluminum substrate test. As before, what is meant by closed circuit is that the Fluke 87 III DMM was recording the voltage output from the PZT-5A3 sample continuously throughout the test. For this test, the sample was placed on an aluminum

89

block from the freezer with 1 rag between the sample and aluminum block to slow the cooling rate enough to be able to take readings.

Table 4-14 – Closed Circuit Rapid Cooling of PZT/Al Sample

Time	SG 1, on Al (με)	SG 2, on PZT (με)	TC 1, on Al (°F / °C)	TC 2, on PZT (°F / °C)	PZT Voltage (V)
3:31:00	0	0	69.7 / 20.9	68.7 / 20.4	-0.018
3:33:00	3	0	51.3 / 10.7	51.4 / 10.8	1.24
3:35:00	-1	-5	40.8 / 4.9	40.8 / 4.9	0.61
3:37:00	-4	-9	35.5 / 1.9	36.2 / 2.3	0.16
3:42:00	-8	-11	31.6 / -0.2	32.0 / 0.0	0.026
3:44:35	-9	-13	60.5 / 15.8	59.3 / 15.2	-0.62*
3:46:00	-9	-16	65.0 / 18.3	63.9 / 17.7	-0.31
3:50:00	-9	-19	70.8 / 21.6	69.6 / 20.9	-0.06

Notes:

1. The sample was placed on the table for cool down at 3:43:10.

2. The maximum voltage post placement on the Al block = +1.92 V at ~3:32:00.

3. The maximum voltage post placement on the optical table = -0.62 V at 3:44:35.

4. With no rag the maximum PZT voltage = +6.3 V at ~15 sec. after placement on the aluminum block.

90

Quantification of Time Constant Losses in Piezo Circuit

At the conclusion of the closed circuit heating/cooling of the PZT/Al sample testing, it was noted that a significant amount of electrical energy was being lost to the internal resistor in the Fluke 87 III DMM during the test. This result was expected based on the preliminary testing. However, what was learned from this testing was that the energy loss due to this effect would be very difficult to quantify with enough precision to be able to effectively measure the conversion efficiency of the PZT, which is the ultimate goal of the present research. For this reason, another test configuration was required. Unfortunately, none of the commercially available voltage measurement devices surveyed had a high enough internal measurement resistance to be effective in this application. For this reason, a high value resistor was added in series to the test setup PZT / DMM voltage measurement circuit shown in Figure 4-12. In addition, subsequent heating and cooling testing was run open circuit to minimize the voltage bleed off to the DMM, and thus enable accurate quantification of the electrical energy (i.e. voltage) generated by the PZT-5A3 sample.

Comparing the time constants for the PZT-5A3 sample open circuit, PZT-5A3 sample and Fluke 87 III in voltage mode, and PZT-5A3 sample and Fluke 87 III in voltage mode, plus a 950 MΩ resistor in series:

PZT-5A3 Sample Open Circuit

- $R = 9.7 \times 10^{9} \ \Omega$

- $C = 0.132 \times 10^{-6} \ F$

91

- $t = R \cdot C = 1280$ sec $= 21.3$ minutes

PZT-5A3 Sample and Fluke 87 III (Voltage Mode)

- $R \cong 10 \times 10^6 \ \Omega$

- $C = 0.132 \times 10^{-6}$ F

- $t = R \cdot C = 1.32$ sec

PZT-5A3 Sample, Fluke 87 III (Voltage Mode), and 950 MΩ Resistor

- $R = 874 \times 10^6 \ \Omega$

- $C = 0.132 \times 10^{-6}$ F

- $t = R \cdot C = 115.4$ sec $= 1.93$ minutes

In comparing the above time constants, the PZT / DMM time constant was only 1.32 seconds. This did not provide enough time to get a reliable voltage measurement. However, the 950 MΩ resistor in series provided a sufficiently large time constant (~ 2 minutes) to collect a voltage reading at the conclusion of an open circuit test without losing a significant amount of voltage. More importantly, because the time constant is large (~ 2 minutes) compared to the Fluke 87 III DMM settling time (i.e. time required for the Fluke 87 III DMM to obtain a reliable voltage reading, which was approximately equal to 1 second), reliable voltage readings were subsequently obtained.

Test Setup with 950 MΩ Resistor in Series

As was stated in the previous section, a high value resistor was added in series to the Fluke 87 III DMM voltage measurement circuit to be able to reliably and accurately quantify the voltage from the PZT-5A3 sample during testing without losing a significant (and very difficult to accurately quantify) voltage to the measurement device. The resistor used was a #MOX1125J-1000M-ND Thick Film, 1000 MΩ nominal resistance, 1.5 Watt, 5% resistor with a measured resistance = 950 MΩ (measured using the 3M-701 Megohmeter).

Figure 4-13 below shows the electrical circuit model of the PZT /DMM circuit from Figure 4-12 (with the 950 MΩ resistor added). Using the electrical configuration shown in Figure 4-13, the 950 MΩ resistor was added to enable the accurate quantification the PZT-5A3 voltage output by increasing the PZT voltage measurement circuit time constant.
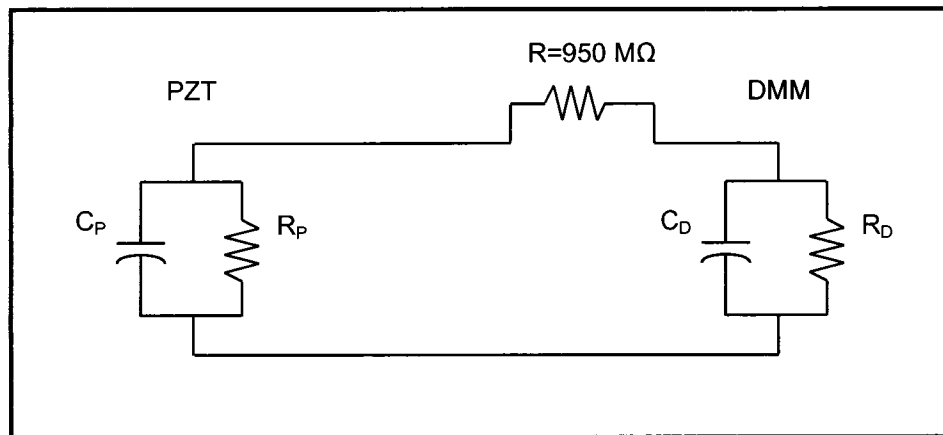
Figure 4-13 – Electrical Model of PZT-5A3 / 950 MΩ Resistor Test Setup

93

Test to Determine Voltage and Polarity of PZT-5A3 Sample Strain and Pyroelectric Terms

The purpose of this testing was to quantify the voltage and polarity (+,-) on both the pyroelectric and pyroelectric plus thermal strain induced PZT-5A3 terms.

Test Setup to Determine Voltage and Polarity of PZT-5A3 Pyroelectric Term

- Sample Capacitance = 0.176 μF

- Lead Orientation:

    o Dot side of PZT to COM/Black on Fluke 87 III DMM

    o Other (non-dot) side of PZT to V/Red on Fluke 87 III DMM
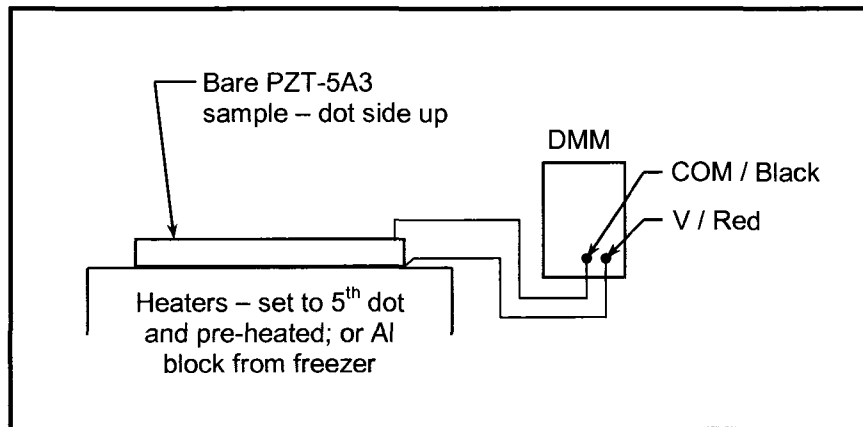
Figure 4-14 – Test Setup to Determine Voltage and Polarity of PZT-5A3 Pyroelectric Term

94

- Measurements (open circuit during all heating and cooling phases – voltage bled to zero in between):

  o Heating from room temperature (RT) to ~100° F (37.8° C) → - V

  o Cooling from ~100° F (37.8° C) to RT → + V

  o Cooling from RT to ~35° F (1.7° C) → + V

  o Heating from ~35° F (1.7° C) to RT → - V

In addition to the above results, three other samples were tested with the same qualitative results. When the lead orientation in Figure 4-14 was reversed, the reverse polarity (+,-) was obtained, as expected.

Next, the 950 MΩ resistor was added in series to the "Com" leg in Figure 4-14, and the bare PZT-5A3 sample was heated multiple times from ~70° F (21.1° C) to ~125° F (51.7° C), and the pyroelectrically induced voltage recorded.

Table 4-15 – PZT-5A3 Pyroelectric Voltage Measurements

Time	TC 2, on PZT (°F / °C)	PZT Voltage (V)	Notes
10:32:00	67.7 / 19.8	-0.002	
10:33:00	137.5 / 58.6	-1.23	
10:38:00	68.6 / 20.3	0.000	1 minute
10:39:00	130.4 / 54.7	-1.27	5th dot
10:43:00	68.4 / 20.2	0.002	No cover
10:44:00	122.0 / 50.0	-1.16	Preheated

95

Time	TC 2, on PZT (°F / °C)	PZT Voltage (V)	Notes
10:53:00	68.7 / 20.4	-0.001	Average PZT Voltage / ΔT = 1.15 V / 55° F (30.6° C)
10:54:00	116.6 / 47.0	-1.10	
11:02:00	68.8 / 20.4	-0.001	
11:03:00	119.0 / 48.3	-1.145	
11:09:00	68.9 / 20.5	0.002	
11:10:00	122.8 / 50.4	-1.07	

Notes:

1. Thermocouple #2 (TC 2) was the same thermocouple test setup as in the strain gage thermal calibration testing (i.e. Omega T.C. #4 and HH12A #600709, Ch. 1).

2. The Fluke 87 III DMM circuit was open during heating.

It is important to note that the voltage readings as reported by the Fluke 87 III DMM are off by a significant factor when the 950 MΩ resistor was added in series (Reference Table 4-15). This is best illustrated by referencing the circuit diagram for the PZT / DMM / 950 MΩ resistor system (Figure 4-13). The Fluke 87 III DMM is designed to read voltage on circuits where the circuit resistance is significantly less than the Fluke 87 III DMM measurement circuit resistance ($R_D = 10$ MΩ). However, in the present research, the circuit resistance was actually much higher (R = 950 MΩ) than the Fluke 87 III DMM measurement circuit resistance. To account for this, the voltage reading from the Fluke 87 III DMM in Table 4-15 should be multiplied by 960 MΩ / 10 MΩ = 96.

96

Referencing Figure 4-13, the PZT-5A3 element resistance (R_P) is not included in the Fluke voltage measurement correction given above. This is because the PZT-5A3 element resistance was too large to register on the Fluke 87 III DMM voltage test circuit, which is only capable of measuring resistances up to approximately 1 GΩ. This behavior was confirmed during preliminary testing when the Fluke was unable to provide a resistance measurement for the PZT-5A3 samples. In addition, the Fluke was later hooked up to the 950 MΩ resistor and PZT-5A3 element in series, and again could not provide a resistance measurement.

Test Setup to Determine Voltage and Polarity of PZT-5A3 Thermal Strain Plus Pyroelectric Term

- $C = 0.132 \times 10^{-6}$ F (HP 4261A); 0.136×10^{-6} F (Fluke 87 III); (both taken at ~ 70° F / 21.1° C)

- R = 1-2 GΩ (3M-701); 1-7 GΩ post testing

- Lead Orientation:

  o Dot side of PZT to COM/Black on Fluke 87 III DMM

  o Other (non-dot) side of PZT to V/Red on Fluke 87 III DMM

97
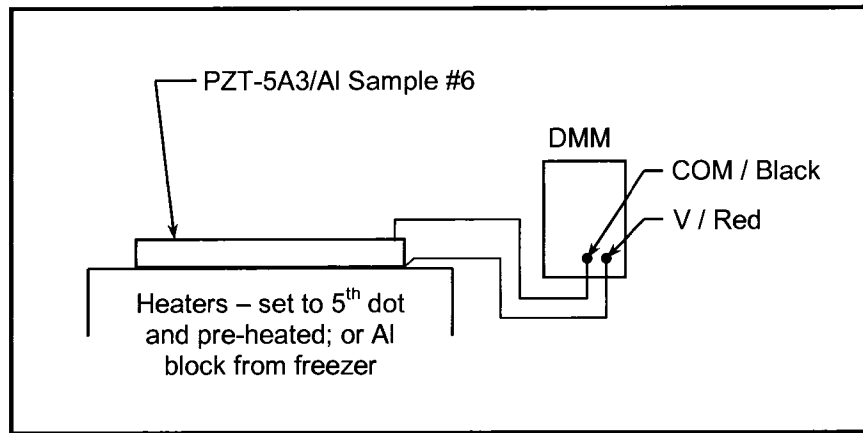
Figure 4-15 – Test Setup to Determine Voltage and Polarity of PZT-5A3 Thermal Strain Plus Pyroelectric Term

- Measurements (open circuit during all heating and cooling phases – voltage bled to zero in between):

  o Heating from RT to ~100° F (37.8° C) → - V

  o Cooling from ~100° F (37.8° C) to RT → + V

  o Cooling from RT to ~35° F (1.7° C) → + V

  o Heating from ~35° F (1.7° C) to RT → - V

Next, as in the bare PZT sample testing, the 950 MΩ resistor was added in series to the "Com" leg in Figure 4-15, and the PZT-5A3/Al sample was heated multiple times from ~70° F (21.1° C) to ~125° F (51.7° C), and the pyroelectric plus thermal strain induced voltage recorded.

98

Table 4-16 – PZT-5A3 Pyroelectric Plus Thermal Strain Voltage Measurements

Time	TC 1, on Al (°F / °C)	TC 2, on PZT (°F / °C)	PZT Voltage (V)	Notes
9:08:00	69.6 / 20.9	68.5 / 20.3	-0.002	10 minutes 5th dot No cover Preheated Average PZT Voltage / ΔT = 1.69 V / 55° F (30.6° C)
9:18:00	124.5 / 51.4	121.5 / 49.7	-1.66	
9:27:00	70.3 / 21.3	69.2 / 20.7	-0.004	
9:37:00	127.5 / 53.1	124.2 / 51.2	-1.69	
9:46:00	70.6 / 21.4	69.5 / 20.8	0.001	
9:56:00	127.9 / 53.3	125.4 / 51.9	-1.69	
10:17:00	70.4 / 21.3	69.3 / 20.7	0.000	5 minutes 5.5th dot No cover Preheated Average PZT Voltage / ΔT = 2.37 V / 55° F (30.6° C)
10:22:00	127.1 / 52.8	124.8 / 51.6	-2.39	
10:32:00	70.6 / 21.4	69.5 / 20.8	-0.002	
10:37:00	127.1 / 52.8	124.5 / 51.4	-2.37	
10:47:00	70.4 / 21.3	69.4 / 20.8	-0.004	
10:52:00	127.6 / 53.1	124.4 / 51.3	-2.38	
3:05:00	70.0 / 21.1	69.0 / 20.6	-0.002	130 sec. 6.7th dot Rag cover Preheated Average PZT Voltage / ΔT = 2.64 V / 55° F (30.6° C)
3:07:10	124.9 / 51.6	121.9 / 49.9	-2.52	
3:13:00	70.0 / 21.1	68.9 / 20.5	-0.002	
3:15:10	124.3 / 51.3	121.0 / 49.4	-2.40	
3:22:00	70.3 / 21.3	69.2 / 20.7	-0.002	
3:24:10	129.0 / 53.9	124.0 / 51.1	-2.66	
3:30:00	70.1 / 21.2	69.1 / 20.6	-0.004	
3:32:10	129.7 / 54.3	125.7 / 52.1	-2.76	
3:39:00	70.3 / 21.3	69.3 / 20.7	-0.002	

99

Time	TC 1, on Al (°F / °C)	TC 2, on PZT (°F / °C)	PZT Voltage (V)	Notes
3:41:10	131.4 / 55.2	127.2 / 52.9	-2.84	
3:57:00	70.1 / 21.2	69.1 / 20.6	-0.002	1 minute 7.5th dot No cover Preheated Average PZT Voltage / ΔT = 3.25 V / 55° F (30.6° C)
3:58:00	126.3 / 52.4	120.6 / 49.2	-3.04	
4:05:00	70.0 / 21.1	69.9 / 21.1	-0.002	
4:06:00	128.7 / 53.7	121.4 / 49.7	-3.12	
4:12:00	70.0 / 21.1	68.9 / 20.5	-0.001	
4:13:00	128.6 / 53.7	121.2 / 49.6	-3.03	

Notes:

1. The thermocouple setup for this test was the same as in the strain gage thermal calibration testing (i.e. TC 1 - Omega TC #3 and HH12A #600713, Ch. 1, and TC 2 - Omega T.C. #4 and HH12A #600709, Ch. 1).

2. The Fluke 87 III DMM circuit was open during heating.

3. The Fluke 87 III DMM PZT-5A3 reported voltage was off by a factor of 96 due to the 950 MΩ resistor in series. This was due to the 950 + 10 = 960 MΩ test resistance vs. the 10 MΩ test circuit resistance internal to the Fluke 87 III DMM.

The data from this section will be used in the next chapter to calculate the pyroelectric and piezoelectric voltage contributions of the PZT-5A3 element during heating of the PZT-5A3/Al sample from room temperature to 125° F (51.7° C).

100

CHAPTER 5 – ANALYSIS

In Chapter 4, a summary of the pertinent testing in the present research was presented. In this chapter, data analysis of the testing is presented.

Capacitance Changes in PZT-5A3 Elements with Bonding

It was noted during the preliminary testing that the capacitance of the PZT-5A3 sample is reduced as the element goes from an un-bonded to a bonded state. This was initially incorrectly assumed to be the result of PZT damage or adhesive bridging from the top face to the bottom face of the element during the bonding process. As is shown below, the capacitance change is in fact the result of a change in the mechanical boundary condition of the PZT element during bonding. Because the element is piezoelectric (i.e. has mechanical / electrical coupling), the change in the mechanical boundary condition manifests itself in an element electrical property change as well. This change in PZT-5A3 element electrical property (i.e. capacitance) with changes in mechanical boundary condition is given quantitatively in the following pages.

Table 5-1 gives a summary of the pre and post bond capacitance measurements for the PZT-5A3 elements in the present research.

Table 5-1 – PZT-5A3 Sample Capacitance Measurements

	Sample 1 (Fluke 87 III)	Sample 4 (Fluke 87 III)	Sample 5 (Fluke 87 III)	Sample 6 (HP 4261A)	Sample 7 (HP 4261A)	Average
C (pre-bond)	0.167 μF	0.179 μF	0.176 μF	0.167 μF	0.166 μF	0.171 μF
C (post-bond)	0.134 μF	0.139 μF	0.134 μF	0.132 μF	0.134 μF	0.135 μF

As was also noted previously, the HP 4261A capacitance measurements have dissipation factor losses, and thus an artificially low capacitance measurement reading. For this reason, the Fluke 87 III DMM readings are more accurate.

The capacitance of the PZT-5A3 elements in the present research can be accurately expressed by the general equation of a capacitor from Chapter 4:

$$C = \frac{\varepsilon_0 \cdot \varepsilon_r \cdot A}{t}$$
(Equation 4-2)

Where, for the PZT-5A3 elements:

$A = 0.0635 \text{ m} \cdot 0.0381 \text{ m} = 2.4194 \times 10^{-3} \text{ m}^2$

$t = 0.000254 \text{ m}$

$\varepsilon_0 = 8.8542 \times 10^{-12} \text{ F/m}$

The above equation will now be used to calculate the PZT-5A3 element capacitance for different boundary conditions.

102

Constant Stress (Mechanically Free) Capacitance $(\varepsilon_{r_{33}}^{T})$

$$\varepsilon_{r_{33}}^{T} = 1700 \ \text{(literature)}$$

$$C = \frac{\varepsilon_0 \cdot \varepsilon_r \cdot A}{t} \qquad\qquad \text{(Equation 4-2)}$$

$$= \frac{8.8542 \times 10^{-12} \dfrac{F}{m} \cdot 1700 \cdot 2.4194 \times 10^{-3} m^2}{0.000254m}$$

$$= 0.143 \times 10^{-6} F$$

Constant Strain (Mechanically Clamped) Capacitance $(\varepsilon_{r_{33}}^{S})$

$$\varepsilon_{r_{33}}^{S} = 830 \ \text{(literature)}$$

$$C = \frac{\varepsilon_0 \cdot \varepsilon_r \cdot A}{t} \qquad\qquad \text{(Equation 4-2)}$$

$$= \frac{8.8542 \times 10^{-12} \dfrac{F}{m} \cdot 830 \cdot 2.4194 \times 10^{-3} m^2}{0.000254m}$$

$$= 0.070 \times 10^{-6} F$$

$$\varepsilon_{33}^{S} = 7.349 \times 10^{-9} \frac{F}{m}$$

103

$$\beta_{33}^{S} = 1.3607 \times 10^{8} \frac{m}{F}$$

Calculation of Mechanically Free (Constant Stress) ε_r Based on PZT-5A3

Capacitance Measurements

The following is a calculation of the mechanically free (i.e. constant stress) ε_r^T for the PZT-5A3 samples based on the measured element capacitance during testing.

$$C = \frac{\varepsilon_0 \cdot \varepsilon_r \cdot A}{t} \qquad \text{(Equation 4-2)}$$

$$0.176\mu F = \frac{8.8542 \times 10^{-12} \frac{F}{m} \cdot \varepsilon_{r_{33}}^{T} \cdot 2.4194 \times 10^{-3} m^2}{0.000254m}$$

$$\varepsilon_{r_{33}}^{T} = 2087$$

$$\varepsilon_{33}^{T} = 1.8479 \times 10^{-8} \frac{F}{m}$$

$$\beta_{33}^{T} = 5.4116 \times 10^{7} \frac{m}{F}$$

104

Calculation of ε_r for PZT-5A3 Samples Bonded to Aluminum

The following is a calculation of ε_r for the PZT-5A3 samples when bonded to the aluminum substrate based on the measured element capacitance during testing.

$$C = \frac{\varepsilon_0 \cdot \varepsilon_r \cdot A}{t} \qquad \text{(Equation 4-2)}$$

$$0.134 \mu F = \frac{8.8542 \times 10^{-12} \frac{F}{m} \cdot \varepsilon_r \cdot 2.4194 \times 10^{-3} m^2}{0.000254 m}$$

$$\varepsilon_r = 1589$$

$$\varepsilon_{33} = 1.4069 \times 10^{-8} \frac{F}{m}$$

$$\beta_{33} = 7.1077 \times 10^{7} \frac{m}{F}$$

The above calculation for the permittivity of the PZT-5A3 samples bonded to the aluminum substrate is applicable (and based on readings taken) at room temperature ($\sim 70^\circ$ F / 21.1° C). It is not necessarily applicable during the active heating or cooling phase of the PZT-5A3/Al sample, as will be discussed in the next section.

105

Capacitance of PZT-5A3 Samples During Heating and Cooling Phases

To determine the capacitance of the PZT-5A3/Al samples during the heating and cooling phases, both the Fluke 87 III DMM and HP 4261A LCR Meter were monitored continuously during active heating and cooling of the samples. During this testing bare PZT-5A3 samples were placed on the heater setup in Figure 4-11 with the rheostat set to the 5th dot, then placed on the optical table to cool the sample back to room temperature. The results of this testing show that the capacitance measurements vary significantly during active heating and cooling of the samples:

On Table – Pre-Heat (70 °F / 21.1 °C)

- C = 0.131 μF (HP 4261A)
- C = 0.135 μF (Fluke 87 III)

During Heating (70-133 °F / 21.1-56.1 °C)

- C = 0.165 μF (HP 4261A)
- C = 0.176 μF (Fluke 87 III)
  - Rose to these values at 133° F / 56.1° C

During Cooling (133-70 °F / 56.1-21.1 °C)

- C = 0.07 μF (HP 4261A)

106

- C = 0.07 μF (Fluke 87 III)

  o Achieved these values during peak cooling rate (just after the sample was placed on the optical table)

Post Cooling (72.5 °F / 22.5 °C)

- C = 0.134 μF (HP 4261A)
- C = 0.138 μF (Fluke 87 III)

When the capacitance measurements above are compared to the theoretical limiting values (reference the previous section "Capacitance Changes in PZT-5A3 Elements with Bonding"), the following results are obtained:

- During heating the PZT-5A3 sample (bonded to the aluminum substrate) is mechanically free (i.e. plane stress condition).
- During cooling the PZT-5A3 sample (bonded to the aluminum substrate) is mechanically clamped (i.e. plane strain condition).
- At steady state at 70° F / 21.1° C, the PZT-5A3 sample (bonded to the aluminum substrate) is somewhere between mechanically free and mechanically clamped (i.e. partially constrained).

As a clarification to the above results, the actual PZT-5A3 element boundary condition is dependent on the heating or cooling rate. However, in the present

107

configuration only 'mild' heating is required to obtain a plane stress condition, while significant cooling rates are required to fully realize a plane strain condition. It is believed that this is because of the inherently 'free' condition of the bonded PZT-5A3 sample in the 3 direction. To achieve a clamped condition on cooling, the strain rates in the 1 and 2 directions must be sufficiently high to effectively clamp the 3 direction via Poisson effects. The reverse is not true for the heating condition, and thus comparatively lower heating rates produce a true mechanically free condition. The above results, which are restated in the "Results" section at the end of this document, are logical in retrospect, but have not been previously noted in the literature.

Calculation of PZT-5A3 Pyroelectric Coefficient Using Measured Capacitances and Pyroelectric Test Voltage Data

The pyroelectric coefficient for PZT-5A is equal to 0.02×10^{-6} Coul/cm$^2 \cdot$°C (Morgan Electro Ceramics TP-226). There is no pyroelectric coefficient value quoted in the literature specifically for PZT-5A3. However, using the measured capacitances and pyroelectric test voltage data collected previously, a pyroelectric coefficient for the PZT-5A3 elements in the present research can be calculated.

$$\begin{Bmatrix} E_1 \\ E_2 \\ E_3 \end{Bmatrix} = \begin{bmatrix} \beta_{11} & 0 & 0 \\ 0 & \beta_{22} = \beta_{11} & 0 \\ 0 & 0 & \beta_{33} \end{bmatrix} \cdot \begin{Bmatrix} D_1 \\ D_2 \\ D_3 \end{Bmatrix} \qquad \text{(Equation 3-5a)}$$

Where:

108

$$E_3 = \beta_{33} \cdot D_3$$

Expanding on the above to consider voltage:

$$V_3 = E_3 \cdot t = t \cdot \beta_{33} \cdot D_3 \qquad\qquad\qquad \text{(Equation 5-1)}$$

Where, for the PZT-5A3 samples and test data:

t = thickness = 0.000254 m

V_3 = measured voltage due to 55° F (30.6° C) ΔT (i.e. 125-70° F) = 112 V

β_{33} = 5.4116×10^7 m/F (value during sample heating)

Substituting the test values into Equation 5-1:

$$112 \text{ V} = 0.000254 \text{ m} \cdot 5.4116\times10^7 \text{ m/F} \cdot D_3$$

Rearranging:

$$D_3 = 8.1481\times10^{-3} \text{ Coul/m}^2 \text{ (for 55° F / 30.6° C } \Delta T\text{)}$$

Also, the pyroelectric coefficient multiplied by the temperature change equals the electric displacement, or:

109

(Pyroelectric coefficient) · 55° F · 5/9 °C/°F· 1×10^4 cm^2/m^2 = D$_3$ = 8.1481×10^{-3} Coul/m^2

Rearranging:

Pyroelectric coefficient = 2.67×10^{-8} Coul/cm^2·°C = 0.0267×10^{-6} Coul/cm^2·°C

Thus, the pyroelectric coefficient for PZT-5A given in the literature (Morgan Electro Ceramics TP-226) is 0.02×10^{-6} Coul/cm^2·°C, while the pyroelectric coefficient for PZT-5A3 calculated from the present testing is 0.0267×10^{-6} Coul/cm^2·°C. These values are in very good agreement, with a slight difference in values, as expected, since one describes the general class of PZT-5A, and the other is a specific sub-type (i.e. PZT-5A3). It is difficult to make conclusive comparative statements about the above values for the pyroelectric coefficient since very little data (i.e. one source) exists for PZT-5A, and no sources exist for PZT-5A3. However, the good agreement in pyroelectric coefficient values obtained suggests that the test methodology used is sound.

Energy Balance of PZT-5A3/Al Samples

The following is a summary of the energy balance calculation for a PZT-5A3 sample bonded to an aluminum substrate (Reference Figure 4-1), and heated from room temperature (70° F / 21.1° C) to 125° F (51.7° C). These data will be used to calculate

110

the energy transfer efficiencies between the thermal, mechanical and electrical states in the PZT-5A3/Al samples of the present research.

PZT-5A3 Sample Properties

Below is a summary of the properties for the PZT-5A3 samples pertinent to the energy balance calculations.

- Volume = V = 0.0635 m (L) · 0.0381 m (W) · 0.000254 m (T)

$$= 6.145 \times 10^{-7} \text{ m}^3$$

- Capacitance = C = 0.134×10^{-6} F (RT post bond measured value)

PZT-5A3/Al Substrate Sample Strain Test Data

Table 5-2 provides a summary of the PZT-5A3/Al sample strain data from all of the relevant testing in the present research.

Table 5-2 – PZT-5A3/Al Sample Strain Measurements

Test	Δ Time (sec)	Δ PZT Strain (με)	Δ Forced PZT Strain (με)	ΔT (in PZT) (°F / °C)	Open or Closed Circuit
5/23/06 Initial Testing / Hot Data #1	840	437.52	340.68	37.2 / 20.7	Closed
5/23/06 Initial Testing / Hot Data #2	300	678.16	522.5	59.8 / 33.2	Closed

111

Test	Δ Time (sec)	Δ PZT Strain (με)	Δ Forced PZT Strain (με)	ΔT (in PZT) (°F / °C)	Open or Closed Circuit
7/3/06 1GΩ Resistor Testing / Test 1	600	616.82	472.09	55.6 / 30.9	Open
7/3/06 1GΩ Resistor Testing / Test 2	600	603.34	460.44	54.9 / 30.5	Open
Average to get 125-70° F = 55° F (30.6 °C) ΔT	-	605	462	55 / 30.6	Based on Open*

*Note: the 5/23/06 testing is closed circuit, which has a different element compliance (s^D). The average value in Table 5-2 above is based on the open circuit testing only, as open circuit is the basis of the following energy balance analysis.

PZT-5A3/Al Sample RC Circuit Analysis

The governing piezoelectric equations presented in Chapter 3 neglect internal PZT voltage losses due to element internal resistance. This is a valid assumption for a relatively fast (< 1 second) loading cycle. However, when the load cycle is slower, as in the present research, PZT voltage losses due to element internal resistance must be taken into account. To quantify the internal PZT resistance voltage losses, data was taken at various load cycle times from 10 minutes to 60 seconds. In each case, the ΔT was 55° F (30.6° C) (Reference Chapter 4, "Test Setup to Determine Voltage and Polarity of PZT-5A3 Strain Plus Pyroelectric Term" Section). This allows for the construction of a RC decay curve similar to Figure 3-5 – Voltage Decay in a RC Circuit.
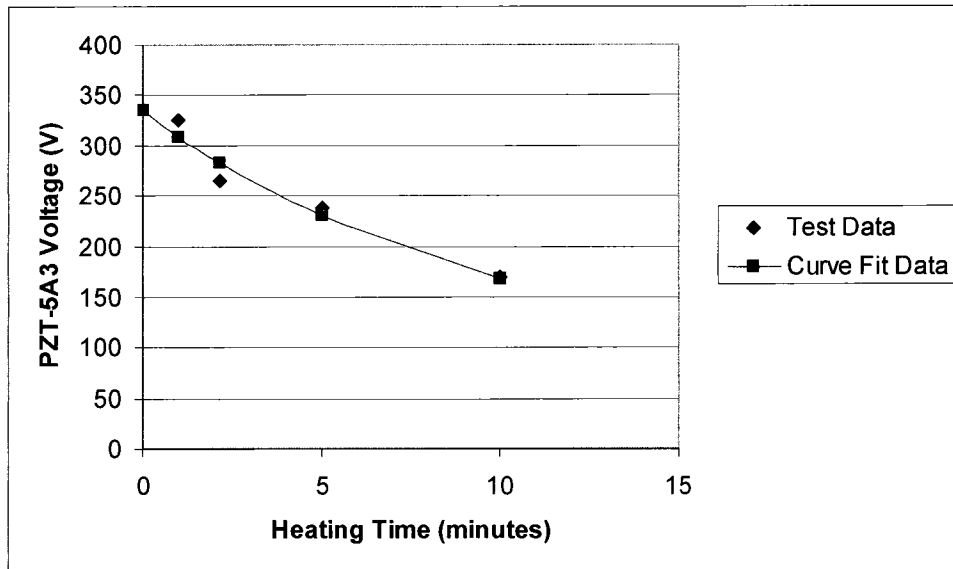
Figure 5-1 – Curve Fit of PZT-5A3/Al Sample RC Circuit Data

To generate the curve fit data points in Figure 5-1, a linear charge growth in the PZT is assumed. This assumption results from an observed linear temperature increase in the PZT during heating. The curve in Figure 5-1 is then extrapolated to time t = 0, resulting in an initial voltage of 335 V in the PZT-5A3 sample due to a 125° F minus 70° F = 55° F (30.6° C) ΔT. In addition, a curve fit of the data in Figure 5-1 results in the following values for the internal resistance (R), and element capacitance (C):

- $R = 2.83 \times 10^9\ \Omega$

- $C = 0.134 \times 10^{-6}\ F$

113

These PZT-5A3 sample curve fit capacitance and resistance values are in good agreement with the measured capacitance and resistance values from the PZT-5A3/Al sample testing in Chapter 4.

Heat Capacity / Heat Energy Estimate

In order to complete a first order system level analysis of the efficiency of the PZT-5A3/Al sample in converting heat to electrical energy, the heat energy (using heat capacity calculations, Reference Equation 3-28) of both the aluminum substrate and the PZT-5A3 sample for a $\Delta T = 55°$ F (30.56° C) is calculated.

Aluminum Heat Capacity / Heat Energy

- Heat Capacity = 900 J/kg·°C

- Volume = 1/8 in · 3 in · 4 in = 1.5 in^3 = 2.4585×10^{-5} m^3

- Density = 2770 kg/m^3

- Mass = V · ρ = 2.4585×10^{-5} m^3 · 2770 kg/m^3 = 6.81×10^{-2} kg

- Heat Energy into Aluminum ($\Delta T = 55°$ F = 30.56° C) = 900 J/kg·°C · 6.81×10^{-2} kg · 30.56° C = 1873 J

In summary, 1873 J of heat energy is required to raise the temperature of the aluminum substrate from 70° F to 125° F ($\Delta T = 55°$ F = 30.56° C). This quantity of

114

energy will later be compared to both the mechanical energy into and the electrical energy out of the PZT-5A3 sample.

PZT-5A3 Heat Capacity / Heat Energy

- Heat Capacity = 420 J/kg·°C

- Volume = 6.145×10^{-7} m^3

- Density = 7700 kg/m^3

- Mass = V · ρ = 6.145×10^{-7} m^3 · 7700 kg/m^3 = 4.732×10^{-3} kg

- Heat Energy into PZT-5A3 Sample (ΔT = 55° F = 30.56° C) = 420 J/kg·°C · 4.732×10^{-3} kg · 30.56° C = 60.7 J

In summary, 60.7 J of heat energy is required to raise the temperature of the PZT-5A3 sample from 70° F to 125° F (ΔT = 55° F = 30.56° C). This quantity of energy will later be compared to both the mechanical energy into and the electrical energy out of the PZT-5A3 sample to arrive at a PZT-5A3 element conversion efficiency.

Strain Energy Estimate

The next step in determining the overall energy balance for the PZT/Al system is to calculate the strain energy in mechanically straining the PZT-5A3 element. This mechanical strain energy is the result of the aluminum substrate heating and expanding at a greater rate than the PZT-5A3, resulting in a 'forced' mechanical straining in the PZT. Referring to Chapter 3, Section "Energy in Deflecting a Piezoelectric Linear Elastic

115

Material", because the initial temperature start point for all testing is room temperature

(70° F / 21.1° C), it is a valid assumption to assume that $\varepsilon_1 = 0$, which simplifies the

strain energy calculations.
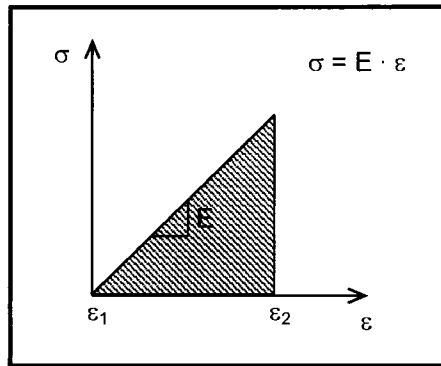
Figure 5-2 – Stress-Strain Plot for PZT-5A3/Al Sample

In Figure 5-2, the strain energy density equals the area under the curve.

Strain Energy Density $= \int \sigma \cdot d\varepsilon$

$$= \int E \cdot \varepsilon \cdot d\varepsilon$$

$$= \frac{1}{2} \cdot (\varepsilon_2 - \varepsilon_1) \cdot E \cdot (\varepsilon_2 - \varepsilon_1)$$

$$= \frac{1}{2} \cdot (\varepsilon_2 - 0) \cdot E \cdot (\varepsilon_2 - 0)$$

$$= \frac{1}{2} \cdot E \cdot \varepsilon_2^2 \qquad\qquad \text{(Equation 5-2)}$$

116

As was stated previously in this section, assuming $\varepsilon_1 = 0$ negligibly impacts the strain energy calculation. From test measurements taken in Chapter 4, $\varepsilon_2 = 605$ με (462 με forced).

In addition, for the PZT-5A3 elements:

- Volume $= 6.145 \times 10^{-7}$ m^3

- Modulus (PZT-5A) $= c_{11}^{D} = 12.6 \times 10^{10}$ N/m^2

Converting Equation 5-2 to express the PZT-5A3 sample strain energy associated with a plane strain loading condition ($S_1 = S_2$, $S_{3,4,5,6} = 0$):

$$\text{PZT-5A3 Element Strain Energy} = 2 \cdot V \cdot \frac{1}{2} \cdot E \cdot \varepsilon_2^2 \qquad \text{(Equation 5-3)}$$

Considering the Total Strain Energy:

$$Energy = 2 \cdot V \cdot \frac{1}{2} \cdot E \cdot \varepsilon_2^2 \qquad \text{(Equation 5-3)}$$

$$= 2 \cdot 6.145 \times 10^{-7} m^3 \cdot \frac{1}{2} \cdot 12.6 \times 10^{10} \, N/m^2 \cdot \left(605 \times 10^{-6} \, m/m\right)^2$$

$$= 2.834 \times 10^{-2} J$$

117

Considering the Forced Strain Energy:

$$Energy = 2 \cdot V \cdot \frac{1}{2} \cdot E \cdot \varepsilon_2^2 \qquad \text{(Equation 5-3)}$$

$$= 2 \cdot 6.145 \times 10^{-7} m^3 \cdot \frac{1}{2} \cdot 12.6 \times 10^{10} \frac{N}{m^2} \cdot \left(462 \times 10^{-6} \frac{m}{m}\right)^2$$

$$= 1.653 \times 10^{-2} J$$

The above energy values represent the total and forced mechanical strain energy into the PZT-5A3 element resulting from a 55° F (30.56° C) ΔT heating.

PZT-5A3 Pyroelectric Term

Next, the theoretical pyroelectric contribution to the PZT-5A3 measured voltage due to a 55° F (30.56° C) ΔT is calculated. From previous capacitance measurements (Chapter 5, Section "Calculation of PZT-5A3 Pyroelectric Coefficient Using Measured Capacitances and Pyroelectric Test Voltage Data"), the PZT-5A3 pyroelectric coefficient is equal to 0.0267×10^{-6} Coul/cm$^2 \cdot$°C. The PZT-5A pyroelectric coefficient as quoted in the literature (Morgan Electro-Ceramics TP-226) is equal to 0.02×10^{-6} Coul/cm$^2 \cdot$°C, which agrees well with the above value based on measured capacitances. The measured PZT-5A3 pyroelectric coefficient value is used to calculate the D_3 term in Equation 3-5a:

118

$$D_3 = 0.0267 \times 10^{-6} \frac{Coul}{cm^2 \cdot {}^\circ C} \cdot \left[\left(125^\circ F - 70^\circ F\right) \cdot \frac{5}{9} \frac{{}^\circ C}{{}^\circ F} \right] = 8.1583 \times 10^{-7} \frac{Coul}{cm^2}$$

$$= 8.1583 \times 10^{-3} \frac{Coul}{m^2}$$

It should be noted that the use of the pyroelectric term to arrive at the D_3 term in Equation 3-5a is perfectly valid, but not the IEEE Std. 176-1987 intended use of Equation 3-5a. Rather than create a whole new set of piezoelectric equations separate from IEEE Std. 176-1987, of which only the D terms are redefined, it is simpler to utilize the IEEE Std. 176-1987 structure. As such, for PZT-5A3:

$$\begin{Bmatrix} E_1 \\ E_2 \\ E_3 \end{Bmatrix} = \begin{bmatrix} \beta_{11} & 0 & 0 \\ 0 & \beta_{22} = \beta_{11} & 0 \\ 0 & 0 & \beta_{33} \end{bmatrix} \cdot \begin{Bmatrix} D_1 \\ D_2 \\ D_3 \end{Bmatrix} \qquad \text{(Equation 3-5a)}$$

Which, for the current configuration reduces to:

$$E_3 = \beta_{33} \cdot D_3$$

Again, considering the measured quantity from testing (i.e. voltage) and β^T:

$$V_3 = E_3 \cdot t = t \cdot \beta_{33}^T \cdot D_3 \qquad \text{(Equation 5-1)}$$

119

Where:

$$t = \text{thickness} = 0.000254 \text{ m}$$

$$\beta_{33}^{T} = 5.4116 \times 10^{7} \text{ m/F}$$

$$D_3 = 8.1583 \times 10^{-3} \text{ Coul/m}^2 \text{ (for } 55^{\circ} \text{ F} = 30.56^{\circ} \text{ C } \Delta T)$$

Substituting the above values into Equation 5-1:

$$V_3 = 0.000254 \text{ m} \cdot 5.4116 \times 10^{7} \text{ m/F} \cdot 8.1583 \times 10^{-3} \text{ Coul/m}^2$$

$$= 112.1 \text{ V}$$

Therefore, the pyroelectrically induced voltage in the PZT-5A3 sample due to a 55° F (30.56° C) ΔT is equal to 112.1 volts.

Strain and Pyroelectric Induced Voltage in the PZT-5A3 Sample

Next, the strain and pyroelectric induced voltages in the PZT-5A3 sample are calculated using IEEE Std. 176-1987.

$$\{E\} = -[h] \cdot \{S\} + [\beta^{S}] \cdot \{D\} \qquad \text{(Equation 3-10b)}$$

Or:

120

$$\begin{Bmatrix} E_1 \\ E_2 \\ E_3 \end{Bmatrix} = -\begin{bmatrix} 0 & 0 & 0 & 0 & h_{15} & 0 \\ 0 & 0 & 0 & h_{15} & 0 & 0 \\ h_{31} & h_{31} & h_{33} & 0 & 0 & 0 \end{bmatrix} \cdot \begin{Bmatrix} S_1 \\ S_2 \\ S_3 \\ S_4 \\ S_5 \\ S_6 \end{Bmatrix} + \begin{bmatrix} \beta_{11}^S & 0 & 0 \\ 0 & \beta_{22}^S = \beta_{11}^S & 0 \\ 0 & 0 & \beta_{33}^S \end{bmatrix} \cdot \begin{Bmatrix} D_1 \\ D_2 \\ D_3 \end{Bmatrix}$$

For the PZT-5A3 test setup, Equation 3-10b simplifies to the following:

$$E_3 = -h_{31} \cdot S_1 - h_{31} \cdot S_2 - h_{33} \cdot S_3 + \beta_{33}^S \cdot D_3 \qquad \text{(Equation 5-4)}$$

As was shown in Chapter 5, Section "Capacitance of PZT-5A3 Samples During Heating and Cooling Phases", the capacitance of the PZT-5A3 element changes significantly during the heating and cooling phases. Because the PZT-5A3 element strain and pyroelectric induced voltage is measured at the peak of the heating phase, Equation 3-10b, and by extension Equation 5-4 above need to be modified to change β^S to β^T to fit the present test configuration, which was not envisioned by IEEE Std. 176-1987. Converting β^S to β^T in Equation 5-4:

$$E_3 = -h_{31} \cdot S_1 - h_{31} \cdot S_2 - h_{33} \cdot S_3 + \beta_{33}^T \cdot D_3 \qquad \text{(Equation 5-5)}$$

Where:

$E_3 \cdot t$ = Measured Voltage (V)

121

$h_{31} = -7.3 \times 10^8$ V/m

$h_{33} = 21.5 \times 10^8$ V/m

$\beta^T_{33} = 5.4116 \times 10^7$ m/F

$D_3 = 8.1583 \times 10^{-3}$ Coul/m^2 (for 55° F / 30.56° C ΔT)

$S_1 = 462$ $\mu\varepsilon$ (Forced)

$S_2 = 462$ $\mu\varepsilon$ (Forced)

$S_3 = -\nu \cdot S_1 - \nu \cdot S_2 + \Delta T \cdot \alpha_{PZT}$

$\quad = 2 \cdot -0.3 \cdot 462$ $\mu\varepsilon + 55°$ F $\cdot 2.603$ $\mu\varepsilon/°$F (30.56° C $\cdot$ 4.685 $\mu\varepsilon/°$C)

$\quad = -134.0$ $\mu\varepsilon$

Converting Equation 5-5 to consider voltage:

$$V_3 = t \cdot E_3 = t \cdot \left(-h_{31} \cdot S_1 - h_{31} \cdot S_2 - h_{33} \cdot S_3 + \beta^T_{33} \cdot D_3 \right) \qquad \text{(Equation 5-6)}$$

$$= 0.000254m \cdot \begin{pmatrix} 7.3 \times 10^8 \,{}^V\!/_m \cdot 462 \times 10^{-6} \,{}^m\!/_m + 7.3 \times 10^8 \,{}^V\!/_m \cdot 462 \times 10^{-6} \,{}^m\!/_m \\ -21.5 \times 10^8 \,{}^V\!/_m \cdot -134 \times 10^{-6} \,{}^m\!/_m \\ +5.4116 \times 10^7 \,{}^m\!/_F \cdot 8.1583 \times 10^{-3} \,{}^{Coul}\!/_{m^2} \end{pmatrix}$$

$= 85.7$ V $+ 85.7$ V $+ 73.2$ V $+ 112.1$ V

$= 356.7$ V

The above calculated theoretical voltage (356.7 V) is higher than the measured value (335 V) resulting from the test data in Chapter 4. However, the error is small

122

(6.5%), and within the allowance of the known test measurement errors (i.e. test scatter,

thermocouple error, etc.)

Energy Stored in a Capacitor

At this point, the above voltages need to be converted into electrical energy

quantities to make a comparison with the heat and mechanical strain energy inputs into

the system. The PZT-5A3 piezoelectric element behaves as a capacitor, so the equation

for electrical energy stored in a capacitor can be used:

$$E = \frac{1}{2} \cdot C \cdot V_0^2 \qquad\qquad\qquad \text{(Equation 5-7)}$$

Where:

$$C = 0.134 \times 10^{-6} \text{ F}$$

$$V = V_0 = 335 \text{ V}$$

Substituting the above values into Equation 5-7:

$$E = \frac{1}{2} \cdot C \cdot V_0^2$$

$$= \frac{1}{2} \cdot 0.134 \times 10^{-6} F \cdot (335V)^2$$

$$= 7.5191 \times 10^{-3} J$$

123

The previous analysis has quantified the various energy inputs and outputs associated with the PZT-5A3/Al test setup. These include the thermal energy input into both the PZT-5A3 element and aluminum substrate, the mechanical strain energy input associated with the thermal expansion of the aluminum substrate relative to the PZT, and the PZT-5A3 pyroelectric and piezoelectric voltage energy terms. The various energy terms will be compared in the next section to obtain the conversion efficiencies associated with the PZT-5A3/Al test setup.

Electromechanical Coupling Factor

The various energy terms associated with the PZT-5A3/Al testing were obtained in the previous section. These terms will be compared in this section to obtain the relevant energy conversion efficiencies for the PZT-5A3/Al test setup. The first comparison (i.e. a plane strain condition, $S_1 = S_2$, $S_{3,4,5,6} = 0$) will be made using the theory developed in IEEE Std. 176-1987 as a baseline. While this comparison is not correct in describing the true energy conversion of the PZT-5A3/Al device in the present research, it does provide a useful check of the test data against an existing theoretical basis. To make this comparison, the pyroelectric and 3 direction terms are ignored, and Equation 3-12a is used to define the energy conversion efficiency:

$$k^2 = \frac{\text{mechanical energy converted to electrical charge}}{\text{mechanical energy input}} \qquad \text{(Equation 3-12a)}$$

Where, from previous analysis, with $S_1 = S_2$:

124

Mechanical Energy Input = Forced Strain Energy $= 2 \cdot \frac{1}{2} \cdot V \cdot c_{11}^{D} \cdot \varepsilon_{2}^{2}$

Thus, the mechanical energy input term in Equation 3-12a, which equals the forced strain energy, can now be calculated:

Forced Strain Energy $= 2 \cdot \frac{1}{2} \cdot V \cdot c_{11}^{D} \cdot \varepsilon_{2}^{2}$

$$= 2 \cdot \frac{1}{2} \cdot 6.145 \times 10^{-7} m^{3} \cdot 12.6 \times 10^{10} \frac{N}{m^{2}} \cdot (462 \times 10^{-6} \frac{m}{m})^{2}$$

$$= 1.653 \times 10^{-2} J$$

Next, consider the numerator in Equation 3-12a ($S_1 = S_2$, $S_{3,4,5,6} = 0$):

Mechanical Energy Converted to Electrical Charge = Strain Induced Voltage in the PZT

$\{E\} = -[h] \cdot \{S\}$

$$\begin{Bmatrix} E_1 \\ E_2 \\ E_3 \end{Bmatrix} = - \begin{bmatrix} 0 & 0 & 0 & 0 & h_{15} & 0 \\ 0 & 0 & 0 & h_{15} & 0 & 0 \\ h_{31} & h_{31} & h_{33} & 0 & 0 & 0 \end{bmatrix} \cdot \begin{Bmatrix} S_1 \\ S_2 \\ S_3 \\ S_4 \\ S_5 \\ S_6 \end{Bmatrix}$$

125

$$E_3 = -h_{31} \cdot S_1 - h_{31} \cdot S_2$$

Where:

$$h_{31} = -7.3 \times 10^8 \text{ V/m}$$

$$S_1 = 462 \text{ } \mu\varepsilon \text{ (Forced)}$$

$$S_2 = 462 \text{ } \mu\varepsilon \text{ (Forced)}$$

$$V_3 = t \cdot E_3 = t \cdot \left(-h_{31} \cdot S_1 - h_{31} \cdot S_2\right)$$

$$= 0.000254m \cdot \left(7.3 \times 10^8 \text{ } V/_m \cdot 462 \times 10^{-6} \text{ } m/_m + 7.3 \times 10^8 \text{ } V/_m \cdot 462 \times 10^{-6} \text{ } m/_m\right)$$

$$= 85.7 \text{ V} + 85.7 \text{ V}$$

$$= 171.4 \text{ V}$$

Converting the above voltage into energy, the energy stored in the PZT-5A3 element capacitor is:

$$E = \frac{1}{2} \cdot C \cdot V_0^2 \qquad\qquad \text{(Equation 5-7)}$$

$$= \frac{1}{2} \cdot 0.176 \times 10^{-6} F \cdot \left(171.4V\right)^2$$

$$= 2.585 \times 10^{-3} J$$

126

Plane Strain Electromechanical Coupling Factor (k_{ps})

The electromechanical coupling factor for the plane strain loading condition (i.e. 2-D strain state $S_1 = S_2$, $S_{3,4,5,6} = 0$) is not defined in the literature (IEEE Std. 176-1987 or elsewhere). As such, a new electromechanical coupling factor will need to be defined, namely (k_{ps}), or the electromechanical coupling factor for a plane strain condition (2-D strain state $S_1 = S_2$, $S_{3,4,5,6} = 0$). Substituting into Equation 3-12a for the plane strain condition, Equation 5-8 is obtained:

$$k_{ps}^2 = \frac{\text{mechanical energy converted to electrical charge}}{\text{mechanical energy input}} \qquad \text{(Equation 5-8)}$$

Substituting values from the test data calculated in the previous section:

$$k_{ps}^2 = \frac{\text{mechanical energy converted to electrical charge}}{\text{mechanical energy input}}$$

$$= \frac{2.585 \times 10^{-3}\, J}{1.653 \times 10^{-2}\, J}$$

$$= 0.156$$

Taking the square root of the above:

$$k_{ps} = 0.395$$

127

The above k_{ps} represents the electromechanical coupling factor for the PZT-5A3/Al test setup, neglecting thermal and piezoelectric element 3 direction effects (i.e. just plane strain loading, $S_1 = S_2$, $S_{3,4,5,6} = 0$). To obtain a theoretical comparison, the electromechanical coupling factors in IEEE Standard 176-1987, "IEEE Standard on Piezoelectricity" are expanded upon to cover the same plane strain loading condition. The most general form of the piezoelectric electromechanical coupling factor is given in Equations 3-12a and 3-12b. Alternatively, the piezoelectric electromechanical coupling factor can be expressed as follows (from "Piezoelectric Ceramics Properties and Applications," Morgan Electro Ceramics):

$$k^2 = \frac{w_{12}^2}{w_1 \cdot w_2} \qquad \text{(Equation 5-9)}$$

Where:

w_{12} = Piezoelectric energy density

w_1 = Mechanical energy density ($\sim \frac{1}{2} \cdot \{S\} \cdot \{T\}$)

w_2 = Electrical energy density ($\sim \frac{1}{2} \cdot \{D\} \cdot \{E\}$)

Utilizing Equations 3-10a and 3-10b, and starting with Equation 3-10a:

$$\{T\} = [c^D] \cdot \{S\} - [h]' \cdot \{D\} \qquad \text{(Equation 3-10a)}$$

Applying the plane strain state $S_1 = S_2$, $S_{3,4,5,6} = 0$, Equation 3-10a reduces to:

128

$$(T_1 + T_2) = 2 \cdot S_1 \cdot \left(c_{11}^D + c_{12}^D\right) - 2 \cdot h_{31} \cdot D_3$$

Next, multiply the above equation by ($\frac{1}{2} \cdot S_1$) to obtain an equation that is expressed in terms of the mechanical and piezoelectric energy components in Equation 5-9:

$$\tfrac{1}{2} \cdot S_1 \cdot (T_1 + T_2) = S_1^2 \cdot \left(c_{11}^D + c_{12}^D\right) - h_{31} \cdot S_1 \cdot D_3 \qquad \text{(Equation 5-10)}$$

Then follow the same process for Equation 3-10b:

$$\{E\} = -[h] \cdot \{S\} + [\beta^S] \cdot \{D\} \qquad \text{(Equation 3-10b)}$$

Applying the plane strain state $S_1 = S_2$, $S_{3,4,5,6} = 0$, Equation 3-10b reduces to:

$$E_3 = -2 \cdot h_{31} \cdot S_1 + D_3 \cdot \beta_{33}^S$$

Next, multiply the above equation by ($\frac{1}{2} \cdot D_3$) to obtain an equation that is expressed in terms of the piezoelectric and electrical energy components in Equation 5-9:

$$\tfrac{1}{2} \cdot D_3 \cdot E_3 = -h_{31} \cdot D_3 \cdot S_1 + \tfrac{1}{2} \cdot D_3^2 \cdot \beta_{33}^S \qquad \text{(Equation 5-11)}$$

129

Equations 5-10 and 5-11 are in a form where the energy components from

Equation 5-9 can be extracted:

$$w_{12} = \text{Piezoelectric energy density} = h_{31} \cdot S_1 \cdot D_3$$

$$w_1 = \text{Mechanical energy density} = S_1^2 \cdot \left(c_{11}^D + c_{12}^D \right)$$

$$w_2 = \text{Electrical energy density} = \frac{1}{2} \cdot D_3^2 \cdot \beta_{33}^S$$

Substituting the above values into Equation 5-9, which gives the piezoelectric

electromechanical coupling factor for a plane strain loading condition:

$$k_{ps}^2 = \frac{w_{12}^2}{w_1 \cdot w_2} \qquad \text{(Equation 5-9)}$$

$$= \frac{\left(h_{31} \cdot D_3 \cdot S_1 \right)^2}{S_1^2 \cdot (c_{11}^D + c_{12}^D) \cdot \frac{1}{2} \cdot D_3^2 \cdot \beta_{33}^S}$$

$$= \frac{2 \cdot h_{31}^2 \cdot D_3^2 \cdot S_1^2}{(c_{11}^D + c_{12}^D) \cdot \beta_{33}^S \cdot D_3^2 \cdot S_1^2}$$

$$= \frac{2 \cdot h_{31}^2}{(c_{11}^D + c_{12}^D) \cdot \beta_{33}^S}$$

Converting from the piezoelectric matrix [h] to the piezoelectric matrix [e]:

$$h = \frac{e}{\varepsilon^S} \qquad \text{(Equation 5-12)}$$

130

Substituting Equation 5-12 into the equation above:

$$k_{ps}^2 = \frac{2 \cdot h_{31}^2}{(c_{11}^D + c_{12}^D) \cdot \beta_{33}^S}$$

$$= \frac{2 \cdot \left(\dfrac{e_{31}}{\varepsilon_{33}^S}\right)^2}{(c_{11}^D + c_{12}^D) \cdot \beta_{33}^S}$$

$$= \frac{2 \cdot e_{31}^2}{(c_{11}^D + c_{12}^D) \cdot \beta_{33}^S \cdot (\varepsilon_{33}^S)^2}$$

And, from Equation 3-6:

$$[\beta] = [\varepsilon]^{-1} \qquad \text{(Equation 3-6)}$$

Substituting Equation 3-6 into the equation above:

$$k_{ps}^2 = \frac{2 \cdot e_{31}^2}{\varepsilon_{33}^S \cdot (c_{11}^D + c_{12}^D)}$$

In summary, the plane strain electromechanical coupling factor (k_{ps}) can be expressed as follows:

$$k_{ps} = \frac{\sqrt{2} \cdot e_{31}}{\sqrt{\varepsilon_{33}^S \cdot (c_{11}^D + c_{12}^D)}} \; ; \; (\text{2D strain state } S_1, S_2, S_{3,4,5,6} = 0) \qquad \text{(Equation 5-13)}$$

131

As with Equation 5-8, Equation 5-13 is a new equation to describe piezoelectric

material behavior which was not envisioned in IEEE Std. 176-1987.

Substituting the values for the PZT-5A3 element:

$$k_{ps} = \frac{\sqrt{2} \cdot e_{31}}{\sqrt{\varepsilon_{33}^{S} \cdot \left(c_{11}^{D} + c_{12}^{D}\right)}}$$

$$= \frac{\sqrt{2} \cdot -5.4 \, Coul/m^2}{\sqrt{7.349 \times 10^{-9} \, F/m \cdot (12.6 \times 10^{10} \, N/m^2 - 8.09 \times 10^{10} \, N/m^2)}}$$

$$= 0.419$$

In summary, a reduction of the test data from the present research to fit a plane

strain condition ($S_1 = S_2$, $S_{3,4,5,6} = 0$) gives an electromechanical coupling factor of 0.395,

while an expansion of the IEEE Std. 176-1987 theory for the same plane strain condition

gives a value of 0.419, a difference of less than 6%. Given the known uncertainties in the

reported piezoelectric quantities (e.g. c^D, ε, etc.), this good correlation gives a high degree

of confidence that the test data and the theoretical basis developed above are accurate.

However, as was stated previously, the electromechanical coupling factors (i.e.

efficiencies) in Equations 5-8 and 5-13 do not represent the true test condition of the

present research, as they neglect thermal factors and 3 direction Poisson effects. The

electromechanical coupling factor which describes the true condition of the present

research is developed in the following section.

132

Thermally Induced Planar Strain Electromechanical Coupling Factor (k_{st})

The piezoelectric electromechanical coupling factor associated with the specific

test configuration in the present research doesn't follow the traditional methodology for

the development of (k) in that it must include the total strain energy and pyroelectric

terms to be accurate. As such, another new electromechanical coupling factor will need

to be defined called (k_{st}), or the electromechanical coupling factor associated with a

thermally induced planar strain loading condition (i.e. thermally induced straining in the

piezoelectric 1 and 2 directions, with associated 3 direction Poisson and thermal effects

included).

$$k_{st}^2 = \frac{\text{total energy converted to electrical charge}}{\text{total energy input}} \qquad \text{(Equation 5-14)}$$

Note that (k_{st}) neglects the thermal energy associated with heating (or cooling)

both the piezoelectric element and the substrate. This energy will be accounted for in the

system level analysis (i.e. satellite application).

In Equation 5-14:

$$\text{Total Energy Input (Strain Energy)} = \tfrac{1}{2} \cdot V \cdot c_{11}^{D} \cdot S_1^2 + \tfrac{1}{2} \cdot V \cdot c_{22}^{D} \cdot S_2^2 + \tfrac{1}{2} \cdot V \cdot c_{33}^{D} \cdot S_3^2$$

For the PZT-5A3 samples:

133

$S_1 = S_2 = 605 \ \mu\varepsilon \ \text{(total)}$

$S_3 = -v \cdot S_1(\text{forced}) - v \cdot S_2(\text{forced}) + \alpha_{PZT} \cdot \Delta T$

$= -0.3 \cdot 462 \ \mu\varepsilon - 0.3 \cdot 462 \ \mu\varepsilon + 2.603 \ \mu\varepsilon/°F \cdot 55° \ F \ (30.56° \ C \cdot 4.685 \ \mu\varepsilon/°C)$

$= -138.6 \ \mu\varepsilon - 138.6 \ \mu\varepsilon + 143.2 \ \mu\varepsilon$

$= -134.0 \ \mu\varepsilon$

Also, the PZT-5A3 samples are isotropic in the 1 and 2 directions, therefore:

$$c_{22}^{D} = c_{11}^{D}; \quad S_2 = S_1$$

The total energy input (i.e. strain energy) in the denominator of Equation 5-14 can now be calculated:

$$\text{Strain Energy} = \tfrac{1}{2} \cdot V \cdot c_{11}^{D} \cdot S_1^2 + \tfrac{1}{2} \cdot V \cdot c_{22}^{D} \cdot S_2^2 + \tfrac{1}{2} \cdot V \cdot c_{33}^{D} \cdot S_3^2$$

$$= 2 \cdot \tfrac{1}{2} \cdot V \cdot c_{11}^{D} \cdot S_1^2 + \tfrac{1}{2} \cdot V \cdot c_{33}^{D} \cdot S_3^2$$

$$= V \cdot c_{11}^{D} \cdot S_1^2 + \tfrac{1}{2} \cdot V \cdot c_{33}^{D} \cdot S_3^2$$

$$= 6.145 \times 10^{-7} m^3 \cdot 12.6 \times 10^{10} \frac{N}{m^2} \cdot (605 \times 10^{-6} \frac{m}{m})^2$$
$$+ \tfrac{1}{2} \cdot 6.145 \times 10^{-7} m^3 \cdot 14.7 \times 10^{10} \frac{N}{m^2} \cdot (-134 \times 10^{-6} \frac{m}{m})^2$$

$$= 2.834 \times 10^{-2} J + 8.11 \times 10^{-4} J$$

$$= 2.915 \times 10^{-2} J$$

134

Next, the numerator in Equation 5-14 is calculated. The total energy converted to electrical charge is the strain induced voltage plus pyroelectric voltage in the PZT-5A3 sample, and is computed using the following equation:

$$\{E\} = -[h] \cdot \{S\} + [\beta^S] \cdot \{D\} \qquad \text{(Equation 3-10b)}$$

$$
\begin{Bmatrix} E_1 \\ E_2 \\ E_3 \end{Bmatrix} = - \begin{bmatrix} 0 & 0 & 0 & 0 & h_{15} & 0 \\ 0 & 0 & 0 & h_{15} & 0 & 0 \\ h_{31} & h_{31} & h_{33} & 0 & 0 & 0 \end{bmatrix} \cdot \begin{Bmatrix} S_1 \\ S_2 \\ S_3 \\ S_4 \\ S_5 \\ S_6 \end{Bmatrix} + \begin{bmatrix} \beta_{11}^S & 0 & 0 \\ 0 & \beta_{22}^S = \beta_{11}^S & 0 \\ 0 & 0 & \beta_{33}^S \end{bmatrix} \cdot \begin{Bmatrix} D_1 \\ D_2 \\ D_3 \end{Bmatrix}
$$

$$E_3 = -h_{31} \cdot S_1 - h_{31} \cdot S_2 - h_{33} \cdot S_3 + \beta_{33}^S \cdot D_3 \qquad \text{(Equation 5-4)}$$

Again, the $\beta \cdot D$ term must be modified to change β^S to β^T, so:

$$E_3 = -h_{31} \cdot S_1 - h_{31} \cdot S_2 - h_{33} \cdot S_3 + \beta_{33}^T \cdot D_3 \qquad \text{(Equation 5-5)}$$

Where:

$E_3 \cdot t = $ Measured Voltage (V)

$h_{31} = -7.3 \times 10^8$ V/m

$h_{33} = 21.5 \times 10^8$ V/m

135

$$\beta^{T}_{33} = 5.4116 \times 10^{7} \text{ m/F}$$

$$D_3 = 8.1583 \times 10^{-3} \text{ Coul/m}^2 \quad (\text{for } 55^\circ \text{ F} / 30.56^\circ \text{ C } \Delta T)$$

$$S_1 = 462 \ \mu\varepsilon \ (\text{Forced})$$

$$S_2 = 462 \ \mu\varepsilon \ (\text{Forced})$$

$$S_3 = -\nu \cdot S_1 - \nu \cdot S_2 + \Delta T \cdot \alpha_{PZT}$$

$$= 2 \cdot -0.3 \cdot 462 \ \mu\varepsilon + 55^\circ \text{ F} \cdot 2.603 \ \mu\varepsilon/^\circ\text{F} \ (30.56^\circ \text{ C} \cdot 4.685 \ \mu\varepsilon/^\circ\text{C})$$

$$= -134.0 \ \mu\varepsilon$$

$$V_3 = t \cdot E_3 = t \cdot \left(-h_{31} \cdot S_1 - h_{31} \cdot S_2 - h_{33} \cdot S_3 + \beta^{T}_{33} \cdot D_3 \right)$$

$$= 0.000254m \cdot \begin{pmatrix} 7.3 \times 10^8 \ V\!/_m \cdot 462 \times 10^{-6} \ m\!/_m + 7.3 \times 10^8 \ V\!/_m \cdot 462 \times 10^{-6} \ m\!/_m \\ -21.5 \times 10^8 \ V\!/_m \cdot -134 \times 10^{-6} \ m\!/_m \\ +5.4116 \times 10^7 \ m\!/_F \cdot 8.1583 \times 10^{-3} \ Coul\!/_{m^2} \end{pmatrix}$$

$$= 85.7 \text{ V} + 85.7 \text{ V} + 73.2 \text{ V} + 112.1 \text{ V}$$

$$= 356.7 \text{ V}$$

The piezoelectric element capacitance is given by the following equation:

$$C = \frac{\varepsilon_0 \cdot \varepsilon_r \cdot A}{t} \qquad \text{(Equation 4-2)}$$

And:

136

$$E = \frac{1}{2} \cdot C \cdot V_0^2 \qquad\qquad\qquad\qquad \text{(Equation 5-7)}$$

Where:

$\quad$ C = 0.176 μF (mechanically free value)

$\quad$ V_0 = 356.7 V (analysis above), or

$\quad$ V_0 = 335 V (measured)

The energy stored in the piezoelectric element capacitor can be calculated for both the measured and calculated V_0:

Measured V_0:

$$E = \frac{1}{2} \cdot C \cdot V_0^2 \qquad\qquad\qquad\qquad \text{(Equation 5-7)}$$

$$= \frac{1}{2} \cdot 0.176 \times 10^{-6} F \cdot (335V)^2$$

$$= 9.876 \times 10^{-3} J$$

Calculated V_0:

$$E = \frac{1}{2} \cdot C \cdot V_0^2 \qquad\qquad\qquad\qquad \text{(Equation 5-7)}$$

137

$$= \frac{1}{2} \cdot 0.176 \times 10^{-6} F \cdot (356.7V)^2$$

$$= 1.120 \times 10^{-2} J$$

The above energies represent the measured and calculated total energy converted to electrical charge in Equation 5-14 (i.e. the numerator). Restating the relationship in Equation 5-14:

$$k_{st}^2 = \frac{\text{total energy converted to electrical charge}}{\text{total energy input}} \qquad \text{(Equation 5-14)}$$

Substituting into Equation 5-14 using the measured V_0:

$$k_{st}^2 = \frac{9.876 \times 10^{-3} J}{2.915 \times 10^{-2} J}$$

$$= 0.339$$

Taking the square root of the above:

$$k_{st} = 0.58 \text{ (Measured } V_0)$$

Substituting into Equation 5-14 using the calculated V_0:

$$k_{st}^2 = \frac{1.120 \times 10^{-2} J}{2.915 \times 10^{-2} J}$$

138

$$= 0.384$$

Taking the square root of the above:

$$k_{st} = 0.62 \text{ (Calculated } V_0)$$

As was noted previously, the above electromechanical coupling factors associated with a thermally induced planar strain loading condition (k_{st}) (i.e. thermally induced straining in the piezoelectric 1 and 2 directions, with associated 3 direction Poisson and thermal effects included) neglect the heat energy input into the piezoelectric and substrate. These terms will be considered in the system level analysis of the satellite application in Chapter 6.

CHAPTER 6 – RESULTS, CONCLUSIONS AND RECOMMENDATIONS

Results

Several significant results were obtained in the course of the present research. In addition, novel piezoelectric theory was developed to describe the unique loading conditions associated with a thermally induced planar strain loading condition on a piezoelectric/substrate. The significant results obtained and novel theory developed in the course of the present research are summarized in the following listing:

1. Demonstration that piezoceramics and piezopolymers are usable in very low frequency (< 0.01 Hz) applications. The time constant associated with element internal resistance dissipation of accumulated electrical charge was shown to be sufficiently large for both piezoceramics (PZT) and piezopolymers (PVDF) such that they can be used effectively to capture mechanical strain energy in very low frequency applications.

2. The challenges and significant variables associated with piezoelectric testing were explored, and to a large extent resolved. These included piezoelectric sample issues such as piezoelectric/substrate bonding trades and electrical lead attachment to the piezoelectric element. In addition, test setup and instrumentation issues such as thermal calibration of the thermometers, thermocouples and strain gages, and recognition of test instrumentation as an integral part of the piezoelectric test measurement circuit were successfully resolved and implemented.

140

3. Quantification of the piezoelectric element capacitance changes from a free state to a bonded state, including development of the applicable theory. In addition, quantification of the bonded piezoelectric element capacitance changes, again including development of the applicable theory, as the element is heated or cooled.

4. Completion of an energy balance for PZT-5A3/Al samples subjected to a temperature change. This balance enables the determination of the component and system level efficiencies associated with the PZT-5A3/Al sample test setup. Energies associated with the relevant terms in the PZT-5A3/Al energy balance are summarized in Table 6-1 below.

Table 6-1 – PZT-5A3/Al Energy Balance (ΔT = 55° F) Term Summary

Term	Energy Conversion / Path	Energy (J)
Al Substrate Heat Energy	Thermal / In	1873
PZT-5A3 Element Heat Energy	Thermal / In	60.7
PZT-5A3 Element Total Strain Energy	Mechanical / In	2.834×10^{-2}
PZT-5A3 Element Forced Strain Energy	Mechanical / In	1.653×10^{-2}
Strain and Pyroelectric Voltage Energy	Electrical / Out	1.120×10^{-2}

Note: comparisons of the values in Table 6-1 are made in the "Conclusions" Section later in this chapter.

141

5. Theoretical development to describe the strain plus pyroelectric induced voltage in a PZT element due to a thermally induced planar strain loading condition.

$$E_3 = -h_{31} \cdot S_1 - h_{31} \cdot S_2 - h_{33} \cdot S_3 + \beta_{33}^T \cdot D_3 \qquad \text{(Equation 5-5)}$$

6. Theoretical development of a plane strain electromechanical coupling factor.

$$k_{ps}^2 = \frac{\text{mechanical energy converted to electrical charge}}{\text{mechanical energy input}} \qquad \text{(Equation 5-8)}$$

$$k_{ps} = \frac{\sqrt{2} \cdot e_{31}}{\sqrt{\varepsilon_{33}^S \cdot \left(c_{11}^D + c_{12}^D\right)}} \ ; \ (\text{2D strain state } S_1, S_2, S_{3,4,5,6} = 0) \qquad \text{(Equation 5-13)}$$

7. Theoretical development of a thermally induced planar strain electromechanical coupling factor.

$$k_{st}^2 = \frac{\text{total energy converted to electrical charge}}{\text{total energy input}} \qquad \text{(Equation 5-14)}$$

142

<u>Discussion</u>

The significant results and novel theory associated with the present research are summarized in the previous section. The results of the present research illuminate several unique attributes of a piezoelectric element bonded to a substrate system worth noting:

1. The heat transfer between the PZT/Al element and the resistor in Figure 2-2 is not dependent on length (at least not in the traditional sense). It is only dependent on length according to electrical losses in the conducting wire, which are significantly less than thermodynamic conduction losses which would be associated with a conducting strip or heat pipe.

2. The heat energy from the component box in Figure 2-2 is converted into a voltage (i.e. electrical energy), which can be utilized (e.g. used to charge a battery).

3. The piezoelectric device bonded to a substrate will generate a voltage due to both a positive and negative temperature change. The result is that the piezoelectric element will attempt to maintain the temperature at which it was applied to the substrate.

Based on the testing, analysis and results presented thus far, the conclusions and recommendations for future research are presented in the following sections.

143

Conclusions

The present research was motivated by two potential applications: a 'satellite' application and a 'bridge' application. The conclusions of the research are presented below in the context of these two potential applications.

Satellite Application

By design, the satellite application corresponds very well to the testing accomplished in the present research. The heating or cooling of the PZT-5A3 samples bonded to the aluminum substrate is an almost exact replication of a potential satellite application configuration and loading condition. As was shown in Chapter 5, the thermally induced planar strain mechanical to electrical conversion efficiency between the PZT-5A3 samples and the aluminum substrate is very good (> 30% with pyroelectric effects included). However, when the thermal portion of the system path is included, the efficiency drops to a vanishingly small value (< 0.01%). This is due almost entirely to the very small thermal to mechanical coefficient of thermal expansion conversion efficiency, which is on the order of 0.01% in the present research (Reference Table 6-1). This value could be improved by substituting a substrate material with a higher ratio of CTE to heat capacity, which would directly improve the overall system level efficiency. However, the system level efficiency would still most likely be too small for use in an energy harvesting application. For this reason, the satellite application as presented in the present research does not show promise. However, as was stated previously, the reason for the low conversion efficiency at the system level is not the piezoelectric/substrate system, but instead the inherently poor conversion of thermal energy to mechanical strain

144

via CTE in aluminum. The satellite application was shown to work if this CTE conversion efficiency were improved. Alternatively, a more efficient path to transfer strain into the piezoelectric/substrate system (e.g. the bridge application that follows) could be utilized to improve the system level energy conversion efficiency.

Bridge Application

The bridge application involves the low frequency behavior of piezoelectric materials bonded to a substrate. In the present research, this is represented by the low frequency planar strain loading of the PZT-5A3/Al samples with the thermal/pyroelectric behavior eliminated from consideration. However, the loading condition in a typical bridge application is more likely going to be either a 1-D in-plane loading (Equation 3-14), or a 1-D out of plane loading (Equation 3-13). Both of these potential loading conditions are illustrated in Figure 2-1. The behavior of piezoelectrics under these loading conditions has been thoroughly researched and is well understood in the literature.

Several of the potential research issues associated with the bridge application have been explored in the present research, including the electrical lead application and the piezoelectric/substrate bonding issues and trades. Most importantly, confirmation that the piezoelectric device is capable of operating in a very low frequency application was verified. Based on the results of the present research, combined with the existing knowledge base in piezoelectric energy harvesting, the bridge application shows great promise for future applications, and should be pursued further.

145

Recommendations for Future Research

Several interesting results were obtained in the course of the present research which warrant further investigation. These are summarized in the following listing:

1. The bridge application shows great promise as a potential energy scavenging application. Further research should be conducted in this area to understand the scalability issues, as well as implementation issues such as bonding, energy storage system interface, environmental effects, etc.

2. The capacitance of a piezoelectric element was shown to change with the external mechanical boundary and loading conditions. It is believed that previous investigations ignored this fact because the frequency of cyclic load application was relatively high, which effectively washed out this effect. However, because of the very low frequency loading, this effect was evident in the present research. From a basic research standpoint, it would be interesting to explore the change of capacitance in a piezoelectric element with load cycle further. This testing was not conducted in the present research as it would require sophisticated test equipment to accurately quantify the resistance and capacitance of the piezoelectric elements during heating and cooling phases. As was noted previously, standard electrical test equipment (which was all that was available in the present research) has electrical circuit properties on the same order as the piezoelectric elements under study, which would make accurate quantification of the piezoelectric element properties difficult/impossible. The piezoelectric element capacitance testing should include, at a minimum, an attempt to

146

understand the mechanism behind the change, and the region of applicability (time, temperature, loading, etc.) of the effect.

3. Exploration of potential applications where the unique attributes of a piezoelectric / substrate system enumerated in the "Discussion" Section of Chapter 5 show promise (beyond the potential bridge application).

SYMBOLS

Symbol	Quantity / Description	Unit
α	Coefficient of Thermal Expansion	$1/°C$
$[\beta]$	Impermeability Matrix	m/F
$[\beta^S]$	Impermeability Matrix – Constant Strain (i.e. Mechanically Clamped)	m/F
$[\beta^T]$	Impermeability Matrix – Constant Stress (i.e. Mechanically Free)	m/F
ε_0	Permittivity of Free Space ($\varepsilon_0 = 8.8542 \times 10^{-12}$ F/m)	F/m
$[\varepsilon]$	Permittivity Matrix	F/m
$[\varepsilon^S]$	Permittivity Matrix – Constant Strain (i.e. Mechanically Clamped)	F/m
$[\varepsilon^T]$	Permittivity Matrix – Constant Stress (i.e. Mechanically Free)	F/m
ρ	Density	Kg/m^3
$[c]$	Stiffness Matrix	$Pa = N/m^2$
$[c^D]$	Stiffness Matrix – Constant Electric Displacement (i.e. Open Circuit)	$Pa = N/m^2$
$[c^E]$	Stiffness Matrix – Constant Electric Field (i.e. Short Circuit)	$Pa = N/m^2$
$[d]$	Piezoelectric Matrix (3x6)	$m/V = C/N$
$\{D\}$	Electric Displacement Tensor	$C/m^2 = N/(m·V)$
$[e]$	Piezoelectric Matrix (3x6)	$C/m^2 = N/(m·V)$
$\{E\}$	Electric Field Tensor	$V/m = N/C$

148

Symbol	Quantity / Description	Unit
[g]	Piezoelectric Matrix (3x6)	$m^2/C = (m \cdot V)/N$
[h]	Piezoelectric Matrix (3x6)	$V/m = N/C$
k	Electromechanical Coupling Factor	unitless
k_{15}	Shear Coupling Factor (Shear Plates)	unitless
k_{31}	Transverse Coupling Factor (Plates)	unitless
k_{33}	Longitudinal Coupling Factor (Rods)	unitless
k_p	Planar Coupling Factor (Thin Disks)	unitless
k_t	Thickness Coupling Factor (Laterally Clamped)	unitless
K	Dielectric Constant, $(K = \varepsilon/\varepsilon_0)$	unitless
[s]	Compliance Matrix	m^2/N
$[s^D]$	Compliance Matrix – Constant Electric Displacement (i.e. Open Circuit)	m^2/N
$[s^E]$	Compliance Matrix – Constant Electric Field (i.e. Short Circuit)	m^2/N
{S}	Strain Tensor	m/m
{T}	Stress Tensor	$Pa = N/m^2$
{x}	n x 1 Matrix (i.e. Vector) x	–
[x]	Matrix x	–
$[x]'$	Matrix Transpose of [x]	–
$[x]^{-1}$	Matrix Inverse of [x]	–
Y	Young's Modulus	$Pa = N/m^2$

149

DEFINITIONS

Word	Definition
Ampere	The constant current which, if maintained in two straight parallel conductors of infinite length, of negligible circular cross section, and placed one meter apart in vacuum, would produce a force between these conductors equal to 2×10^{-7} newtons per meter of length.
Curie Point	A transition temperature marking a change in the magnetic or ferroelectric properties of a substance. Named after its discoverer, Pierre Curie. Also called the Curie Temperature.
Dielectric	Electrical insulator.
Dielectric Constant	The relative permittivity of a dielectric material. Also known as the relative permittivity. Usually given by the symbol K, where $K = \varepsilon/\varepsilon_0$.
Electrostriction	The change in the dimensions of a body as a result of the reorientation of its molecules when it is placed in an electric field; a property of all dielectric materials.
Piezoceramic	An industry term referring to the family of ceramic-based piezoelectric materials, most notably PZT.
Piezoelectric	Relating to or involving piezoelectricity.
Piezoelectricity	The generation of electricity or of electric polarity in dielectric crystals subjected to mechanical stress, or the generation of stress in such crystals subjected to an applied voltage.
Piezopolymer	An industry term referring to the family of polymer-based piezoelectric materials, most notably PVDF.

150

Word	Definition
Poling	The process of heating a piezoelectric material above its Curie Point, then cooling it in the presence of a strong electric field.
Pyroelectric	Relating to or exhibiting pyroelectricity.
Pyroelectricity	Generation of an electric charge on certain crystals (e.g. tourmaline) as a result of a temperature change.
Volume Resistivity	The electrical resistance between the opposite faces of a solid volume of insulating material. Usually measured on a 1cm cube of material per ASTM D257-61, and generally expressed in $\Omega \cdot cm$.
Weiss Domain	Microscopic electric or magnetic dipoles that form in certain crystal structures and piezoelectric and ferroelectric materials.

151

ACRONYMS / ABBREVIATIONS

Acronym / Abbreviation	Title
AC	Alternating Current
AFRL	Air Force Research Laboratory
AFRL/VS	Air Force Research Laboratory / Space Vehicles Directorate
Al	Aluminum
COTS	Commercial Off The Shelf
CTE	Coefficient of Thermal Expansion
DARPA	Defense Advanced Research Projects Agency
DC	Direct Current
DMM	Digital Multi-Meter
ESD	Electrostatic Discharge
HP	Hewlett Packard
IEEE	Institute of Electrical and Electronics Engineers
LED	Light Emitting Diode
Li-Ion	Lithium Ion
MEMS	Micro-Electro-Mechanical Systems
MIT	Massachusetts Institute of Technology
Ni-Cd	Nickel Cadmium
PMN-PT	Lead-Magnesium-Niobate – Lead-Titanate
PVDF	Polyvinylidine-Fluoride
PZT	Lead-Zirconate-Titanate

152

Acronym / Abbreviation	Title
RT	Room Temperature
SG	Strain Gage
SoNaR	Sound Navagation and Ranging
TC	Thermocouple

153

APPENDIX A – PIEZOELECTRIC SUPPLIERS

The following is a listing of piezoelectric suppliers obtained through a comprehensive web search.

1. Piezo Kinetics (http://www.piezo-kinetics.com)

2. Mide (http://www.mide.com)

3. Smart Material Corporation (http://www.smart-material.com)

4. International Components Corporation (http://icc107.com)

5. Physik Instrumente, LP (http://www.pi-usa.us)

6. CeramTec North America (http://www2.ceramtec.com)

7. MSI Sensors (http://www.meas-spec.com)

8. Omega Piezo Technologies (http://www.omegapiezo.com)

9. American Piezo Ceramics, Inc. (http://www.americanpiezo.com)

10. CTS (http://www.ctscorp.com)

11. Face International Corporation (http://www.faceinternational.com)

12. Kinetic Ceramics, Inc. (http://www.kineticceramics.com)

13. Morgan Electro Ceramics (http://www.morganelectroceramics.com)

14. Piezo Solutions (http://www.piezosolutions.net)

15. Piezo Systems Inc. (http://www.piezo.com)

16. Piezosystem Jena (http://www.piezojena.com)

17. Sensor Technology Limited (http://www.sensortech.ca)

APPENDIX B – VISHAY 2310 STRAIN GAGE AMPLIFIER SETUP

PROCEDURE

Equipment:

-Vishay Measurements Group 2310 Signal Conditioning Amplifier

-Vishay CEA-13-250UW-350 (Lot A59AF815, Batch VF335022) Strain Gages

    -350 Ω Gages

    -Gage Factor = 2.110 ± 0.5%

-4 Strain Gages input (typical)

2310 Shunt Calibration:

    $\mu\varepsilon_{CAL}$ = Simulated Strain (με)

    R_a = Shunt Leg Resistance (Ω) = 350.2 Ω – 350.6 Ω

    k = Gage Factor = 2.110

    R_{CAL} = Resistance of Calibration Resistor (Ω), (2310 Resistor B = 174.8 kΩ)

$$\mu\varepsilon_{CAL} = \frac{R_a}{k \cdot (R_{CAL} + R_a)} \times 10^6$$

$$= \frac{350.6\Omega}{2.11 \cdot (174.8k\Omega + 350.6\Omega)} \times 10^6$$

$$= 948 \ \mu\varepsilon$$

**Shunt the 2310 to channel B and set the output to 948 to calibrate such that 1 on the

Vishay 2310 channel output screen = 1 με.

155

Vishay Measurements Group 2310 Signal Conditioning Amplifier Setup Procedure:

1. Hook strain gage leads up to the 2310 breakout box.

2. Verify strain gage resistance is 350 Ω. Flip break out box toggles to '350 Ω'.

3. Power on the Vishay 2310 Signal Conditioning Amplifier.

4. Set 'Excitation' (all channels) to '3.5 V'.

5. Set 'Gain' (all channels) to '×100'.

6. Toggle and hold 'Auto Balance Reset' for 2 seconds (all channels) (+/- red lights on each channel should go out in turn).

7. Toggle and hold 'Cal B' (all channels) both + and -. Set 2310 output using 'Gain' knob to ±948. Release 'Cal B'.

8. Adjust 'Trim Adjust' knob to get 0 output (all channels).

*Note – Channel 4 on the breakout box is broken – do not use. All channels on the 2310 are functional.

**Note – On the 2310 (+ is tensile strain / - is compressive strain) regardless of lead orientation (i.e. always).

156

REFERENCES

Ayers, Joshua P., Greve, David W., Oppenheim, Irving J., "Energy Scavenging for Sensor Applications using Structural Strains," *Smart Structures and Materials 2003: Smart Systems and Nondestructive Evaluation for Civil Infrastructures*, Proceedings of SPIE, Vol. 5057 (2003), pp. 364-375.

Ballato, Arthur, "Piezoelectricity: Old Effect, New Thrusts," *IEEE Transactions on Ultrasonics, Ferroelectrics, and Frequency Control*, Vol. 42, No. 5, September 1995, pp. 916-926.

Berlincourt, D., Krueger, H. H. A., Near, C., "Properties of Piezoelectricity Ceramics," *Morgan Electro-Ceramics Technical Publication TP-226*.

Boresi, Arthur P., Schmidt, Richard J., Sidebottom, Omar M., *Advanced Mechanics of Materials*, 5th Edition, John Wiley and Sons, New York, NY, 1993.

Dorf, Richard C., *Introduction to Electric Circuits*, 2nd Edition, John Wiley and Sons, New York, NY, 1993.

Goldfarb, Michael, Jones, Lowell D., "On the Efficiency of Electric Power Generation with Piezoelectric Ceramic," *Journal of Dynamic Systems, Measurement and Control*, Vol. 121, September 1999, pp. 566-571.

157

Grossman, Stanley I., *Multivariable Calculus, Linear Algebra, and Differential Equations*, 2nd Edition, Harcourt Brace Jovanovich, San Diego, CA, 1986.

Guan, Mingjie, Liao, Wei-Hsin, "Studies on the Circuit Models of Piezoelectric Ceramics," *Proceedings of 2004 International Conference on Information Acquisition*, IEEE, 2004, pp. 26-31.

IEEE Standard 176-1987, "IEEE Standard on Piezoelectricity", Published by IEEE, 29 January 1988.

Keawboonchuay, Chok, and Engel, Thomas G., "Electrical Power Generation Characteristics of Piezoelectric Generator Under Quasi-Static and Dynamic Stress Conditions," *IEEE Transactions on Ultrasonics, Ferroelectrics, and Frequency Control*, Vol. 50, No. 10, October 2003, pp. 1377-1382.

Keawboonchuay, Chok, and Engel, Thomas G., "Scaling Relationships and Maximum Peak Power Generation in a Piezoelectric Pulse Generator," *IEEE Transactions on Plasma Science*, Vol. 32, No. 5, October 2004, pp. 1879-1885.

Le, Triet, Han, Jifeng, von Jouanne, Annette, Mayaram, Karti, Fiez, Terri S., "Piezoelectric Power Generation Interface Circuits," *IEEE Custom Integrated Circuits Conference*, 2003, pp. 489-492.

158

Lesieutre, G.A., Ottman, G.K., Hofmann, H.F., "Damping as a Result of Piezoelectric Energy Harvesting," *Journal of Sound and Vibration*, Vol. 269 (2004), pp. 991-1001.

Luck, Rogelio, Agba, Emmanuel I., "On the Design of Piezoelectric Sensors and Actuators," *ISA Transactions*, Vol. 37, 1998, pp. 65-72.

Mezheritsky, Alex V., "Elastic, Dialectric, and Piezoelectric Losses in Piezoceramics: How it Works All Together," *IEEE Transactions on Ultrasonics, Ferroelectrics, and Frequency Control*, Vol. 51, No. 6, June 2004, pp. 695-707.

MIL-HDBK-5H, "Metallic Materials and Elements for Aerospace Vehicle Structures," United States Department of Defense, 1 December 1998.

Ohanian, Hans C., *Physics*, 2nd Edition, W. W. Norton & Co., New York, NY, 1989.

Park, Chul H., "On the Circuit Model of Piezoceramics," *Journal of Intelligent Material Systems and Structures*, Vol. 12, July 2001, pp. 515-522.

"Piezoelectric Ceramics Properties and Applications," Morgan Electro Ceramics, http://www.morganelectroceramics.com.

Richards, Cecilia D., Anderson, Michael J., Bahr, David F., "Efficiency of Energy Conversion for Devices Containing a Piezoelectric Component," *Journal of Micromechanics and Microengineering*, Vol. 14 (2004), pp. 717-721.

Roundy, S., Wright, P.K., "A Piezoelectric Vibration Based Generator for Wireless Electronics," *Smart Materials and Structures*, Vol. 13 (2004), pp. 1131-1142.

Shenck, Nathan S., Paradiso, Joseph A., "Energy Scavenging with Shoe-Mounted Piezoelectrics," *IEEE Micro*, May-June 2001, pp. 30-42.

Sodano, Henry A., Inman, Daniel J., Park, Gyuhae, "A Review of Power Harvesting from Vibration using Piezoelectric Materials," *The Shock and Vibration Digest*, Vol. 36, No. 3, May 2004, pp. 197-205.

Sodano, Henry A., Park, Gyuhae, Leo, Donald J., Inman, Daniel J., "Use of Piezoelectric Energy Harvesting Devices for Charging Batteries," *Smart Structures and Materials 2003: Smart Sensor Technology and Measurement Systems*, Proceedings of SPIE, Vol. 5050 (2003), pp. 101-108.

Starner, Thad E, "Piezoelectric Materials," *The MIT Media Lab*, http://web.media.mit.edu/~testarne/TR328/node7.html, November 1996.

Steyn, J.L., Hagood IV, N.W., "Development of a Solid State Microhydraulic Energy Harvesting Mechanism for Heel Strike Power Harvesting," DARPA Contract DAAG55-98-1-0361 Final Report, Distribution Unlimited, 10 April 2003.

Taylor, George W., Burns, Joseph R., Kammann, Sean M., Powers, William B., Welsh, Thomas R., "The Energy Harvesting Eel: A Small Subsurface Ocean/River Power Generator," *IEEE Journal of Oceanic Engineering*, Vol. 26, No. 4, October 2001, pp. 539-547.

Vishay Measurements Group Tech Note, "Measurement of Thermal Expansion Coefficient Using Strain Gages," *TN-513-1 – Thermal Expansion Measurement*, October 1999.

Vishay Measurements Group Tech Note, "Strain Gage Thermal Output and Gage Factor Variation with Temperature," *TN-504-1 - Strain Gage Temperature Effects*, April 1999.

Vujic, Nikola, Leo, Donald J., Lindner, Douglas K., Griffin, Steven F., "Power Flow Analysis for Amplifier Design and Energy Harvesting," *Proceedings of SPIE's 2002 North American Symposium on Smart Structures and Materials: Damping and Isolation*, San Diego, CA, Vol. 4697, March 2002, pp. 109-120.

Wertz, James R. and Larson, Wiley J., *Space Mission Analysis and Design*, 3rd Edition, Microcosm Press, El Segundo, CA, 1999.